THESIS ON NATURAL AND EXACT SCIENCES B102

Chemical Composition of Sprayed Copper Indium Disulfide Films for Nanostructured Solar Cells

ATANAS KATERSKI

TUT PRESS

TALLINN UNIVERSITY OF TECHNOLOGY
Faculty of Chemical and Materials Technology
Department of Materials Science

Dissertation was accepted for the defense of the degree of Doctor of Philosophy in Chemistry and Materials Technology on February 7th, 2011

Supervisor: Leading research scientist Dr. Malle Krunks, Department of Materials Science, Tallinn University of Technology

Opponents: Professor Dr. Rositza Yakimova, Department of Physics, Chemistry and Biology (IFM), Linköping University, Linköping, Sweden

Professor Dr. Väino Sammelselg, Faculty of Science and Technology, Institute of Chemistry, University of Tartu, Tartu, Estonia

Defense: March 28th, 2011 at 14.00
Lecture hall: VII-226
Tallinn University of Technology, Ehitajate tee 5, Tallinn

Declaration: Hereby I declare that this doctoral thesis, my original investigation and achievement, submitted for the doctoral degree at Tallinn University of Technology has not been submitted for any academic degree.

Atanas Katerski

ISSN 1406-4723
ISBN 978-9949-23-062-4

LOODUS-JA TÄPPISTEADUSED B102

Pihustatud vaskindiumdisulfiid-kilede keemiline koostis ja rakendus nanostruktuursetes päikesepatareides

ATANAS KATERSKI

TTÜ
KIRJASTUS

Table of Contents

LIST OF PUBLICATIONS

The present doctoral thesis is based on the following papers, which are referred to in the text by their Roman numerals **I-V**:

I. M. Krunks, A. Mere, **A. Katerski**, V. Mikli, J. Krustok, Characterization of sprayed $CuInS_2$ films annealed in hydrogen sulphide atmosphere, *Thin Solid Films*, 511-512 (2006) 434-438.

II. **A. Katerski**, A. Mere, V. Kazlauskiene, J. Miskinis, A. Saar, L. Matisen, A. Kikas, M. Krunks, Surface analysis of spray deposited copper indium disulfide films, *Thin Solid Films* 516 (2008) 7110-7115.

III. **A. Katerski**, M. Danilson, A. Mere, M. Krunks, Effect of the growth temperature on chemical composition of spray-deposited $CuInS_2$ films, *Energy Procedia,* 2 (2010) 103-107.

IV. M. Krunks, **A. Katerski**, T. Dedova, I. Oja Acik, A. Mere, Nanostructured solar cell based on spray pyrolysis deposited ZnO nanorod array, *Sol. Energy Mater. Sol. Cells* 92 (2008) 1016-1019.

V. M. Krunks, **A. Katerski**, T. Dedova, A. Mere, I. Oja Acik, Photovoltaic cell based on zinc oxide nanorods and the method for making the same, International patent application WO2009/006910A2 (Priority No. US60/948508, priority date 09.07.2007).

In Appendix A, copies of these papers are included.

Author's own contribution

The contribution by the author to the papers included in the thesis is as follows:

I. Deposition of $CuInS_2$ films by chemical spray pyrolysis (CSP), post-deposition thermal treatment of $CuInS_2$ films in H_2S atmosphere, characterization of optical and electrical properties of thin films, discussion of the results, minor part of writing.

II. Deposition of $CuInS_2$ films by CSP, chemical etching, thermal treatment in H_2S atmosphere; preparation of thin film solar cell; XPS measurements of $CuInS_2$ films and data processing, characterization of electrical properties of thin films and output properties of solar cells, analysis of the results, major part of writing.

III. Deposition of $CuInS_2$ films, post-deposition thermal treatment of $CuInS_2$ films in H_2S atmosphere, characterization of optical and structural properties (XRD and Raman spectroscopy), and elemental composition (XPS) of thin films, analysis of the results, major part of writing.

IV. Deposition of In_2S_3 and $CuInS_2$ thin films as component layers of solar cells. Characterization of component layers, flat and nanostructured solar cells, analysis of the results, minor part of writing.

V. Deposition of In_2S_3 and $CuInS_2$ thin films as component layers of solar cells. Characterization of thin films and of flat and nanostructured solar cells, analysis of the results, preparation of materials for patent application.

List of abbreviations

A	area of the current channel
AES	Auger Electron Spectroscopy
AFM	Atomic Force Microscopy
Ar^+	Argon ion
BE	Binding Energy
CA	Cu-Au
CBD	Chemical Bath Deposition
CH	Chalcopyrite
CIGS	$Cu(In,Ga)S_2$
CIS	Copper Indium Disulfide, $CuInS_2$
CIS-1.0	$CuInS_2$ film prepared by CSP using the precursor molar ratio [Cu]/[In]=1.0 in solution
CIS-1.1	$CuInS_2$ film prepared by CSP using the precursor molar ratio [Cu]/[In]=1.1 in solution
CISCuT	$CuInS_2$ on Cu tape
CSP	Chemical Spray Pyrolysis
Cu^+	copper in the first valence state
Cu^{2+}	copper in the second valence state
DTA	Differential Thermal Analysis
EBIC	Electron Beam Induced Current
EDS	Energy Dispersive X-ray Spectroscopy
E_g	Optical bandgap
ETA	Extremely Thin Absorber
eV	electron volt
FF	Fill Factor
FWHM	Full With at Half Maximum
I_i	integrated area of a core level peak of a certain element
ILGAR	Ion Layer Gas Reaction
ITO	Indium Tin Oxide
j_{eff}	current density at maximum power output
j_{sc}	short-circuit current density
k	number of the elements in the film
KCN	potassium cyanide
KE	Kinetic Energy
l	length of the current path between the contacts
Me-O	oxygen bonded to a metal
P_{st}	power of the standard illumination of AM1.5 (100 mW/cm^2)
PV	Photovoltaic
QF	quality factor

R	electrical resistance
RBS	Rutherford Backscattering Spectrometry
RTP	Rapid Thermal Process
SC	solar cell
SEM	Scanning Electron Microscopy
SILAR	Successive Ionic Layer Adsorption and Reaction
S_i	sensitivity factor
TG	Thermo-Gravimetry
tu	Thiocarbamide, Thiourea, $(CS(NH_2)_2)$
UV-VIS	Ultraviolet-Visible (Spectroscopy)
V_{eff}	voltage at maximum power output
V_{oc}	open circuit voltage
XPS	X-ray Photoelectron Spectroscopy
XRD	X-ray Diffraction
XRF	X-ray Fluorescence
ZnO_{rod}	zinc oxide nanorods
η	light to electricity conversion efficiency
ρ	electrical resistivity
φ_s	work function

INTRODUCTION

Electricity production with solar cells is promising for it is a renewable energy source and zero harmful emissions are discharged to the Earth's atmosphere. The most expensive part of photovoltaic generators is solar cells, therefore researchers are focused on reductions in their cost. Historically, crystalline silicon (c-Si) has been used as the light-absorbing semiconductor in the "first generation" solar cells which have had a major share on the market (about 80 %) during last 20 years [1]. Due to complexity of the growing technology and its high energy consumption, the present solar cell technologies need to be replaced by cheaper and more effective ones in the near future. The price of the produced renewable electricity may be reduced by the use of new materials with better properties and thin films as active component layers. In the "second generation" of the solar cell technology, typically semiconductor materials with thicknesses up to some micrometers are required, being 100-1000 times less than the thickness of a silicon wafer solar cell [1], thereby minimizing the material costs. The highly effective thin-films solar cells have light-to-electricity conversion efficiencies close to 20 % for CIGS [2], close to 17 % for CdTe [3], less than 15 % for amorphous or polycrystalline silicon [1] and more than 12 % for $CuInS_2$ [4] based absorbers. The thin film solar cells represent the market share in an increasing volume [5].

The development of materials in the nanometer scale has generated new photovoltaic materials and devices. In this area a revolutionary development has been introduced by Grätzel and co-workers in the form of an electrochemical dye-sensitized solar cell (DSSC) [6]. In this type of SC, nanostructured TiO_2 is sensitized by a monolayer of an organic dye. A concept of an extremely thin absorber (ETA) layer solar cell has been developed on the basis of DSSC. In an ETA cell a very thin semiconductor layer with thickness up to some tens of nm will be used to replace a dye which often is non-stable.

The chemical spray pyrolysis (CSP) is an attractive technique to manufacture thin films as it is a low-cost, large-area scalable and non-vacuum deposition method. $CuInS_2$ is a promising absorber material due to its direct bandgap of about 1.5 eV [7]. The deposition of $CuInS_2$ thin films by the low-cost CSP method attracted researchers' interest already ca 20-25 years ago [8]. As the light-to–electricity conversion efficiencies of 2 % were obtained with solar cells based on sprayed $CuInS_2$ in this stage [9], the interest disappeared. The studies on the deposition of $CuInS_2$ films by CSP were newly initiated about ten years ago when material cost became an important topic. Now main focus was shifted to the studies of material properties. Most of the studies were devoted to the development of the structure, morphology, optical and electrical properties of the films [10-14]. Much less attention has been paid to the chemical composition

of spray-deposited films, although chemical composition of the films largely determines the film quality. Particularly, surface-sensitive analytical tools are rarely applied to study the $CuInS_2$ films prepared by advanced preparation methods [15-20], and very occasionally to characterize the surface of sprayed $CuInS_2$ films [10-12, 21, 22]. A systematic study on the effect of technology parameters on the chemical composition of sprayed $CuInS_2$ films and relationship with the film other properties was practically missing.

The present doctoral thesis is a continuation of the studies on the deposition of $CuInS_2$ films by the CSP method at the Department of Materials Science. The aim of my doctoral thesis was to study the effect of the CSP process variables and post-deposition treatments on the chemical composition of sprayed $CuInS_2$ films to develop the absorber preparation process. CSP-$CuInS_2$ thin film absorber layer was used in a nanostructured solar cell, technology and design of that was invented (with application for a patent) in the Laboratory of Thin Film Technologies at the Department of Materials Science of Tallinn University of Technology.

The thesis is divided into four Chapters. Following the introduction, main properties of $CuInS_2$ and deposition methods of $CuInS_2$ thin films, properties of CSP deposited $CuInS_2$ films, and solar cells based on CSP-$CuInS_2$ absorber are summarized in Chapter 1. Chapter 2 reviews the preparation of $CuInS_2$ films by the CSP method and a nanostructured solar cell using CSP-$CuInS_2$ as an absorber layer as well as characterization methods. Chapter 3, divided into five sections, presents the results of the study. Sections 3.1 and 3.2 summarize the results of the studies of as-deposited $CuInS_2$ films prepared by CSP, published in papers II and III. Results on the effect of post-deposition treatment on properties of $CuInS_2$ films, published in papers I and II, are outlined in sections 3.3 and 3.4. Application of the sprayed $CuInS_2$ thin film as an absorber layer in a nanostructured solar cell, discussed in paper IV and presented in the patent application V, is summarized in section 3.5. The main conclusions are given in Chapter 4.

The work is financially supported by the Estonian Ministry of Education and Research (SF0142515s03, SF0140092s08), Estonian Science Foundation (grants ETF6954, ETF5612), Estonian Doctoral School of Materials Science and Materials Technology and funding from Estonian Graduate School of ”Functional Materials and Processes“ received from the European Social Fund under project 1.2.0401.09-0079.

1. LITERATURE REVIEW AND AIM OF THE THESIS

1.1. Main properties of $CuInS_2$

Copper indium disulfide ($CuInS_2$) is a promising wide-gap chalcopyrite absorber for photovoltaic applications due to its direct bandgap of 1.55 eV [7]. Hence, it does not necessarily require alloying with other materials for bandgap adjustment as $CuInSe_2$ with lower bandgap (1.04 eV) does [23]. $CuInS_2$ has a number of additional potential advantages, such as high absorption coefficient $\alpha \approx 10^5$ cm^{-1} [15], p-type of conductivity [24, 25], and as it does not contain any toxic components, it is a perspective absorber layer for thin film solar cells.

The Gibbs' phase triangle of the Cu-In-S system at room temperature and atmospheric pressure [26] is presented in Fig. 1.1a. The equilibrium in the Cu-In-S system is only partially known due to its complexity. The homogeneity region of $CuInS_2$ appears to cover a small deviation from the ideal stoichiometric composition [27, 28]. The homogeneity range for $CuInS_2$ extends up to 2 mole % of In_2S_3 and up to 1.5 mole% of Cu_2S in the Cu_2S-In_2S_3 pseudo-binary system [29]. In the CuS-InS system, the homogeneity region is narrower, up to 0.1 mole% of InS [29].

The phase diagram of the Cu-In-S system along the Cu_2S-In_2S_3 tie line in the Gibbs phase triangle is presented in Fig. 1.1b [29]. The interaction between the binary sulfides gives rise to two ternary sulfides, $CuInS_2$ and $CuIn_5S_8$. $CuInS_2$ exists in three modifications: up to 980 °C in chalcopyrite structure, between 980 °C and 1045 °C in the zinc-blende structure, and above 1045 °C up to the melting point (1090 °C) in the wurtzite structure [29]. The $CuIn_5S_8$ semiconductor has the spinel structure over the whole temperature range, from room temperature up to the melting point (1085 °C). Formation of $CuIn_5S_8$ is non-wanted when a p-type absorber is planned to synthesize as $CuIn_5S_8$ is an n-type material [30].

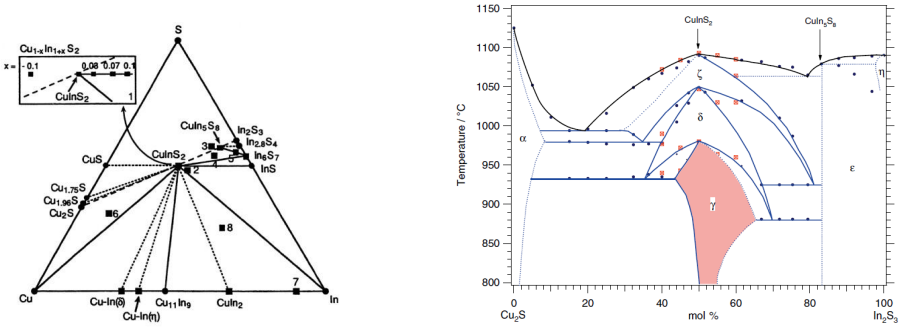

a) b)

Fig. 1.1. *a) Gibbs phase triangle for the Cu–In–S system at room temperature and atmospheric pressure [26] and b) phase diagram of the Cu-In-S system along the Cu_2S-In_2S_3 tie line [29].*

$CuInS_2$ crystallizes in the chalcopyrite structure, which is thermodynamically stable. The lattice type is primitive tetragonal, the corresponding space group is $I\bar{4}2d$, its mineral name is roquesite, and lattice parameters are: a=0.5523 nm, c=1.1141 nm (JCPDS 027-0159) [31]. Besides chalcopyrite (CH) structure, $CuInS_2$ can also crystallize in the form where the stacking sequence of cations (Cu, In) is changed compared to that in the CH ordered structure. The structure with changed stacking sequence of cations in the [102] and [111] directions results in so-called Cu-Au ordered structure (space group $P\bar{4}m2$) [32-34]. As the formation energies of those cation orderings (CH or Cu-Au) are very similar, CH and Cu-Au ordered structures can co-exist [34].

However, presence of Cu-Au ordered $CuInS_2$ in an absorber leads to an inferior quality of a solar cell, thus being unwanted [24, 26, 35]. Presence of Cu-Au ordered phase cannot be verified by a conventional XRD study due to overlapping of almost all XRD peaks [36]. The Raman spectroscopy is a proved technique to determine the content of CH and Cu-Au ordered phases of $CuInS_2$ [33-36].

1.2. Methods for deposition of $CuInS_2$ thin films

$CuInS_2$ layers with chalcopyrite structure and p-type conductivity can be grown by several deposition techniques.

The most successful absorber preparation methods are multi-source evaporation and two-step (sulfurization of metal precursor films) processes [16-20]. The two-step process is developed due to its potential for industrial production. Rapid thermal processing (RTP) was introduced shortly after that, leading to reduction of typical annealing times from 1 h to 3 min [17-18]. Cells based on RTP-$CuInS_2$ absorbers have reached a confirmed total area efficiency of 11.4 % [18]. The RTP-process is a basic method for manufacturing of $CuInS_2$-based solar cell modules at SULFURCELL, the company was first to commercialize the solar cell based on the $CuInS_2$ absorber layer [37]. A specific feature for multi-source and two-step processes is that the best absorber material is grown under the high excess of Cu compared to In, resulting in Cu-S phases, which eliminates kinetic limitations of the compound formation, makes the very fast RTP process feasible and stabilizes the p-type conductivity [17-20].

Due to needs for reducing production costs of solar cells, also wet chemical deposition methods, such as chemical spray pyrolysis (CSP) [38-45], electrodeposition [46-47], chemical bath deposition (CBD) [48-49], solvothermal deposition [50], ion layer gas reaction (ILGAR) [51, 52], etc. have been applied to prepare $CuInS_2$ films. Up to date, $CuInS_2$ films prepared by solution based techniques have not reached the properties obtained by the RTP or CISCuT technique [17, 53] and solar cells based on wet chemically deposited

$CuInS_2$ absorber layer show low conversion efficiencies (2-3 %) in thin film solar cells. On the other hand, significant progress recently achieved with an alternative In_2S_3 buffer layer deposited by CBD, CSP and ILGAR methods in CIGS and $CuInS_2$ absorber thin film solar cells [54] still makes these methods promising also for ternary compounds.

1.3. $CuInS_2$ thin films deposited by chemical spray pyrolysis

1.3.1. Chemical spray pyrolysis method

Chemical spray pyrolysis (CSP) is a low cost, large-area scalable, non-vacuum thin film deposition technique first described by Chamberlin and Skarman in 1966 for the preparation of CdS films [55]. With this method, the precursor solution, usually containing the salts of the constituent elements of the desired compound dissolved in a solvent, is pulverised in the form of micron dimension droplets onto the preheated substrate where the thermal decomposition of the precursor salt or a new precursor formed in the spray solution takes place, and adherent film of thermally more stable compound forms [56].

According to the method of generation of fine droplets ('atomization') of the precursor solution, CSP could be classified as pneumatic, ultrasonic, and electrostatic spray (electrical field is applied between the spray nozzle and substrate), respectively (See Fig. 1.2) [57-59].

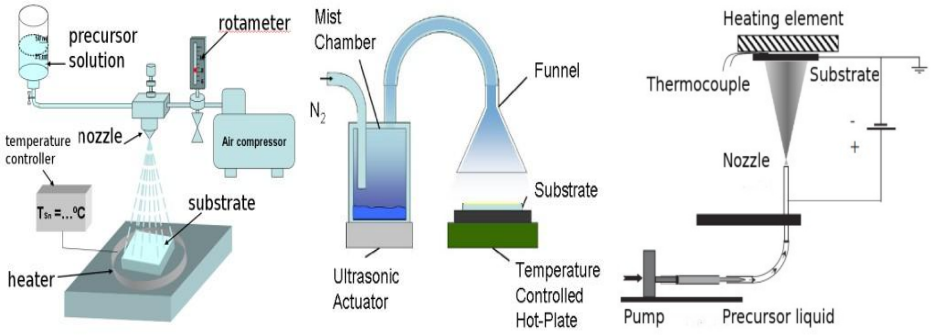

a) b) c)

Fig. 1.2. *Diagrams of a) pneumatic [57], b) ultrasonic [58], and c) electrostatic spray [59] systems.*

For successful film deposition by the CSP method, the precursor salts must be soluble in a solvent (water, alcohol, alcohol-water mixture). It is highly important that a precursor or an intermediate formed in spray solution would not

volatilize before its thermal decomposition [60].

In the spray pyrolysis process, the substrate temperature is the key parameter that determines the final compound morphology and properties. By increasing the temperature, the morphology of the final product can change from a well adherent thin film to a cracked layer, or a porous film [61]. Other important parameters which influence the deposition process and thus the final product quality are: the carrier gas and solution flow, deposition time, nature of the substrate [59], the volatility and viscosity of the solution used, the distance between spray nozzle and substrate, solution amount and concentration of the precursor in solution [61].
Finally, the properties of the layer and the morphology can be modified by use of the various additives in the precursor solution.

In general, the CSP technique is a simple, low-cost and relatively rapid method for deposition of metal oxide, metal sulfide and selenide thin films with a large area [61-63]. In addition to its simplicity, CSP has a number of other advantages: 1) easy way to dope with any element in a ratio of required proportion through the solution medium; 2) deposition at moderate temperatures of 100-500 °C and technological ability to mass production [61, 64, 65]; 3) the film thickness is easily controlled by an amount and concentration of sprayed precursor solution [57].

However, as any other method, CSP has some disadvantages that can be listed as follows: 1) possible oxidation of sulfides/selenides when processed in the air atmosphere; 2) three-dimensional growth mechanism [66, 67]; 3) the growth of temperature is difficult to control directly during the film growth; 4) limited number of precursors, especially for metal sulfide and selenide films; 5) no industrial set-up available up to now. Only very recently the production of spray pyrolysis equipment has been launched by the SPD Laboratory Inc in Japan [68].

1.3.2. Properties of as-sprayed $CuInS_2$ films

Formation of $CuInS_2$ in CSP process

In general, the formation of a metal sulfide (Me=Cd, Zn, Cu) film in the CSP process using metal halogenide and thiourea (tu) as starting chemicals in an aqueous solution, passes through the formation of a complex compound – an intermediate from the point of view a film formation. Complex compound could be presented with a general formula $[Me(tu)_n]X_m yH_2O$, where X is a halogen, and n, m and y are parameters depending on the metal and metal halogenide to the thiourea ligand molar ratio [69-71].

For the deposition of $CuInS_2$ films usually $CuCl_2$, $InCl_3$ and $SC(NH_2)_2$ (tu)

have been used as starting chemicals [62]. Cu-chloride-thiourea complexes, such as $[Cu(tu)Cl]\cdot 0.5H_2O$ [69] and $Cu(tu)_3Cl\cdot H_2O$ [70] could be formed in an aqueous solution containing $CuCl_2$ and $SC(NH_2)_2$. Interaction of $InCl_3$ and $SC(NH_2)_2$ in an aqueous solution is not yet known, studies are initiated and are in progress in our laboratory.

According to the thermogravimetric (TG) and differential thermal analysis (DTA), the complexes $[Me(tu)_n]X_m yH_2O$ formed in the spray solution are thermally stable up to ~200 °C. The thermal decomposition of $[Me(tu)_n]X_m yH_2O$ is a complicated multistage process, MeS forms at temperatures above 200 °C independent of the cation and atmosphere [61, 72].

Thermal behavior of a solid precursor for $CuInS_2$ films obtained by drying of spray solution containing $CuCl_2$, $InCl_3$ and tu at a molar ratio of 1:1:3 is studied by M. Krunks et al. [72] and O. Kijatkina [73].

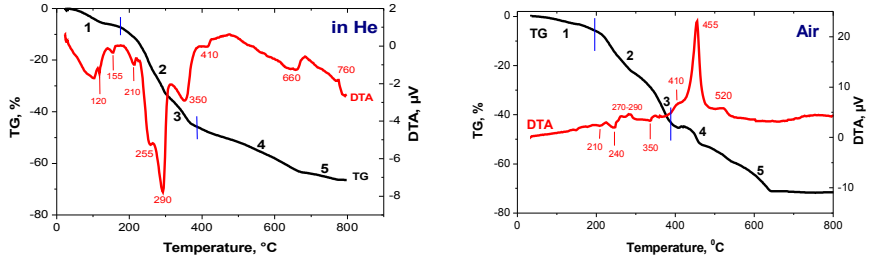

a) b)

Fig. 1.3. *TG/DTA curves of the dried precursor for $CuInS_2$. TG/DTA curves are recorded in flowing a) He and b) air at the heating rate of 10 °C min^{-1} [73, 74].*

TG and DTA curves of a $CuInS_2$-precursor material, which contains a Cu-tu complex compound [73, 74] and may contain an In-tu complex compound [75], are presented in Fig. 1.3. As can be seen, thermal degradation of the precursor for $CuInS_2$ is a complicated multi-step process, where $CuInS_2$ forms at temperatures close to 210 °C independent of the atmosphere. All decomposition steps in an inert atmosphere are endothermic processes and $CuInS_2$ is the final decomposition product. In an oxidative atmosphere, endothermic decomposition reactions in the temperature region of 200-300 °C are less pronounced due to overlapping with simultaneously running oxidation reactions [73]. Oxidation becomes very strong at temperatures > 400°C (Fig. 1.3b) and the mixture of CuO and In_2O_3 phases is the final decomposition product [73].

Results of the thermal analysis studies show that the deposition of $CuInS_2$ films in air could be performed in a quite narrow temperature region of about 230-380 °C, whereat oxidation of a condensed matter is not excluded [71, 72,

74]. Higher deposition temperatures could be used only in an inert atmosphere.

The formation of $CuInS_2$ in the CSP process could be compared with the formation of ternary compound in a different vacuum based technologies where the reaction between binaries, such as $Cu_{2-x}S$ and In_2S_3 yields $CuInS_2$ [76, 77]. When using copper and indium chlorides and thiourea as precursor materials in an aqueous solution sprayed onto the preheated substrate, the formation of the $CuInS_2$ in the CSP process could be divided into the next stages [73]:

1) formation of intermediate metal chloride thiourea complexes in an aqueous solution;
2) spraying of the solution, evaporation of the solvent;
3) thermal decomposition of individual complex(es) with the formation of copper and indium sulfide (formation of binaries) and by-products;
4) ternary compound formation from binaries.

According to the literature not only copper and indium salts such as Cu and In sources, and thiourea (or its analogues) as a sulfur source have been used as starting materials to deposit $CuInS_2$ films by the CSP method. In the early 1990s, Hirpo et al. reported the synthesis of a new family of single source molecular precursors for $CuInS_2$ [78]. Two compounds of the type $[(P(i\text{-}But)'_3)_2CuIn(SEt)_4]$ (where P- phosphorus, S- sulfur, Et- ethyl and i-But- isobutyl) were structurally characterized, and it was observed that these compounds decomposed at temperatures below 300 °C yield $CuInS_2$. More recently, Hollingsworth et al. and J. Harris et al. demonstrated that $[(P(i\text{-}But)_3)_2CuIn(SEt)_4]$ could be used to deposit $CuInS_2$ films by a spray method [78-81]. When using these molecular precursors, one cannot change the [Cu]/[In] molar ratio to tune the film properties and the deposition should be made in a closed system in an inert atmosphere [81]. It should be pointed out that properties of the $CuInS_2$ film (as well as properties of corresponding solar cells) are not superior compared to those manufactured in air using metal chlorides and thiourea as starting materials.

Next, the properties of $CuInS_2$ films obtained by spray of solutions containing copper chloride, indium chloride and thiourea are outlined.

Properties of sprayed $CuInS_2$ films controlled by the growth temperature

According to XRD, the films deposited at temperatures below 400 °C do not contain secondary phases independent of the precursors molar ratio in solution, spray set-up and carrier gas (compressed air, N_2) used [44, 62, 73]. Deposition at temperatures above 400 °C result in an additional crystalline In_2O_3 phase in the sprayed $CuInS_2$ films (see Fig. 1.4) [44, 72, 82]. It has been reported that the film deposition temperature has an effect on the preferred orientation and size of

crystallites. Increase in the film deposition temperature enhances the preferential orientation along the (112) direction and increases the mean crystallite size [10, 33, 73, 82]. Deposition temperature has also an effect on the optical bandgap value as Eg of 1.44 eV is measured for the films deposited at ca 320 °C, while deposition at ca 380 °C results in Eg of 1.46 eV [44]. Electrical resistivity of sprayed $CuInS_2$ films ([Cu]/[In]=1.0 in solution) decreases with an increase in the deposition temperature from 320 to 380 °C (see Fig. 1.5) [35, 83]. It is explained by the recrystallization processes resulting in larger crystallite size [34, 35, 82]. When the film is deposited from the Cu-rich solution ([Cu]/[In]≈1.2 in solution], the electrical resistivity is independent of the deposition temperature.

Chemical purity of the films was found to increase by increasing the deposition temperature. According to Energy Dispersive X-ray Spectroscopy (EDS) study

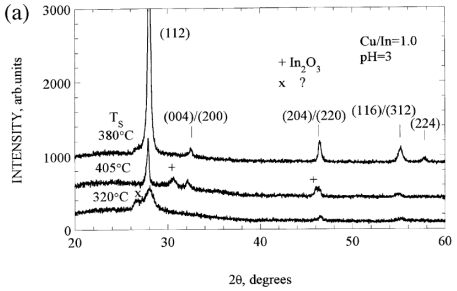

Fig. 1.4. *XRD patterns of sprayed $CuInS_2$ films prepared at a) Ts=320 °C and b) Ts= 380 °C using $CuCl_2$:$InCl_3$ = 1:1 (molar ratio) in an aqueous spray solution [44]. Deposition of the films was made in air.*

(see Fig. 1.6), the content of chlorine in the films is decreased increasing the deposition temperature [82]. Also, the content of C, N containing residues originated from thiourea as a sulfur source, is lower in the films grown at higher temperatures [82, 83].

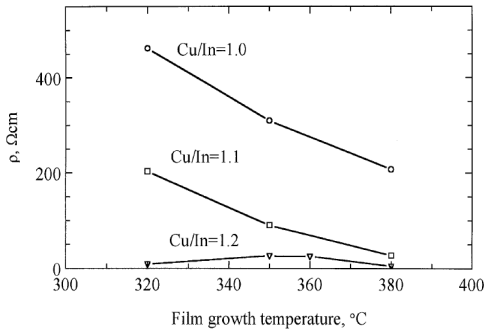

Fig. 1.5. The electrical resistivity of as-sprayed films depend on the film deposition temperature using spray solutions with [Cu]/[In]=1.0-1.2, [S]/[Cu]=3 [83].

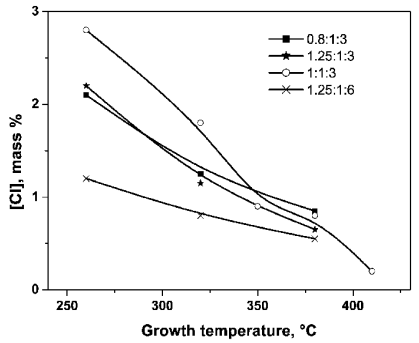

Fig. 1.6. Concentrations of chlorine in sprayed $CuInS_2$ films grown at different temperatures and solution compositions [82].

Thus, the content of residues originated from the precursor materials is decreasing with the deposition temperature. Much less attention has been paid to the determination of the oxygen content in the film, nevertheless its high content in the film could be expected according to the process chemistry studies [43, 44] and as confirmed by XRD in the films prepared at temperatures above 400 °C [82].

Contamination of sprayed $CuInS_2$ films with oxygen has been studied in few papers. Oxygen content as high as 16.7 at.% was detected by RBS [82]. The XPS technique as a sensitive tool to investigate the composition of sprayed $CuInS_2$ films is infrequently applied. T.T. John et al. investigated sprayed $CuInS_2$ films deposited at 300 °C in air ([Cu]/[In]=1.0 in spray solution) and detected oxygen only as a surface contamination [22]. Marsillac et al. recorded oxygen bonded to metal (O1s with BE of 530.0 eV [11]) in sprayed $CuInS_2$ films deposited in the temperature interval of 317-377 °C ([Cu]/[In]=1.1 in solution) after Ar^+ ion cleaning for 1 minute [10]. Thus, metal oxide was present in the film at the depth corresponding to the Ar^+ etching time 1 minute. Based on these data, the authors speculate that a metal oxide phase may be placed on the grain boundaries and could also control the transport of charge carriers in the sprayed $CuInS_2$ film [11, 16].

Properties of sprayed $CuInS_2$ films controlled by the precursor molar ratio in spray solution

XRD analysis of the films deposited from In-rich solutions shows that films are multiphase consisting of $CuInS_2$ and of an extra phase. For example, the XRD pattern of the film deposited from In-rich solution with [Cu]/[In] molar

ratio of 0.8 at 370 °C (Fig. 1.7) shows only one strong replica at 2θ=46.5° belonging to the (220)/(204) plane of $CuInS_2$ [34, 73] and an extra reflection at 2θ=26.5° (marked by 'x' in Fig. 1.7) which does not belong to the $CuInS_2$ phase [34, 73]. Increase in [Cu]/[In] molar ratio in spray solution from 0.8 to 1.0 decreases the relative intensity of 'x' peak and increases the intensity of the (112) peak of $CuInS_2$ (Fig. 1.7).

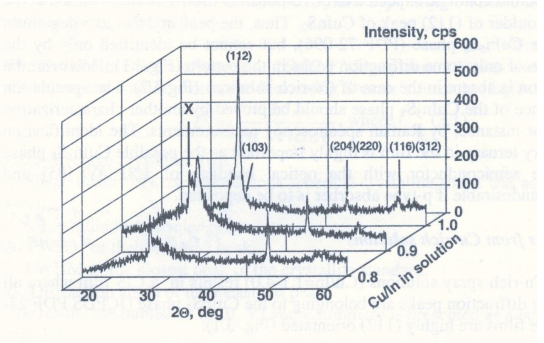

Fig. 1.7. *XRD patterns of as-deposited $CuInS_2$ films prepared at 370 °C using the [Cu]/[In]≤1 in spray solution [35].*

This extra reflection at 2θ=26.5° on the XRD pattern ('x' peak) has been assigned belonging to an indium sulfide phase [84], organic residues [65], or $CuIn_5S_8$ phase [34]. Raman spectroscopic study of the films from In-rich solutions shows Raman bands characteristic of $CuInS_2$ and a band at 348 cm^{-1}, which could belong to $CuIn_5S_8$ [34]. The films deposited from solutions with [Cu]/[In]=0.8-1.0 have a crystallite size less than 10 nm [35], but these films show a smooth surface (Fig. 1.8a). According to hot probe measurements, films from In-rich solutions show the n-type of conductivity [73].

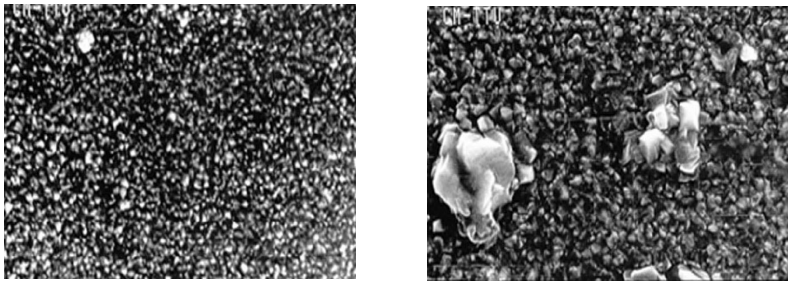

a) b)

Fig. 1.8. *SEM micrographs of KCN etched sprayed $CuInS_2$ films deposited at 380 °C from stock solution with different [Cu]/[In] molar ratios: a) [Cu]/[In] = 1.0 [44]; b) [Cu]/[In] = 1.25 [44].*

Using the solution with [Cu]/[In]=1.0, the film surface is still smooth and homogeneous (Fig. 1.8a), but the films show p-type conductivity [73] in spite of the fact that the film may contain the crystalline 'x' phase using growth temperatures up to 370°C (Fig. 1.7).

Contrarily, the deposition of Cu-rich solutions ([Cu]/[In]>1) results in single phase $CuInS_2$ films with significantly increased crystallite size according to XRD [35, 43, 85]. For example, the films grown from the solution with the [Cu]/[In] ratio of 1.1 showed the mean crystallite size of ca 44 nm (see Fig.1.10 in section 1.3.3), and the films deposited from the solution with [Cu]/[In]=2.0 had the crystallite size of about 120 nm [35, 73, 85]. Further increase of the [Cu]/[In] molar ratio in the spray solution has an insignificant effect on the mean crystallite size [35, 44, 73, 85]. According to SEM studies, the deposition of Cu-rich solutions leads to the films with un-homogeneous, rough surfaces (Fig. 1.8b). The films show two different surface areas - flat area and area with large grains (Fig. 1.8b). Area of large grain domains increases with increasing the [Cu]/[In] molar ratio in spray solution [73, 85]. The mechanism of the formation of large grain domains in a sprayed $CuInS_2$ film was thoroughly studied by M. Krunks et al. by use of EDS analysis and electrical resistivity measurements before and after the KCN treatment of the films [83, 85]. It has been shown that the Cu_xS phase formed in addition to the $CuInS_2$ when Cu-rich solutions are sprayed is responsible for increased mean crystallite size and formation of large grain domains. Films from Cu-rich solutions show lower optical transmittance due to light scattering from rough surfaces [35]. Although the spray of highly Cu-rich solutions results in the films showing closely single-phase composition and p-type conductivity after KCN etching [73, 85], the large grain areas show In-rich elemental composition and are not dense after KCN etching [85]. The latter makes the films out-of-use for solar cells [35]. Thus, non-uniform morphology and elemental composition of the films deposited from Cu-rich solutions ([Cu]/[In]>1.1) is the reason why most of the studies on the deposition of $CuInS_2$ films by the CSP method are made using slightly Cu-rich solutions (up to [Cu]/[In]=1.1 in the spray solution).

Raman spectroscopy studies showed that the share of chalcopyrite (CH) and Cu-Au (CA) ordered $CuInS_2$ phases in as-deposited films are almost independent of the [Cu]/[In] ratio in the spray solution [34, 35].

The optical bandgap values in the range of 1.40-1.45 eV are characteristic of sprayed $CuInS_2$ films [8, 34, 42-44, 85]. There is no direct evidence on the effect of the [Cu]/[In] molar ratio in solution on the bandgap although some authors report that bandgap decreases increasing the [Cu]/[In] ratio in spray solution [22, 86].

In brief, the precursor molar ratio in spray solution is an important technological parameter controlling the phase composition, crystallite size,

morphology, optical properties, conductivity type and electrical resistivity of the sprayed $CuInS_2$ film.

1.3.3. Post-deposition treatment of sprayed $CuInS_2$ films

Chemical treatment

Post-deposition treatments have been applied with the aim to improve the film properties.

Cu_xS phase present on the surface of as-deposited films from Cu-rich solutions with [Cu]/[In]>1 is usually removed by etching in the KCN solution, which is a strong selective etchant for copper sulfides and does not affect the underlying $CuInS_2$ [85]. It has been observed that the resistivity of initially Cu-rich films is increasing by two orders of magnitude after the chemical treatment in the KCN solution [83]. Due to toxicity of KCN, some authors try to replace the KCN etching procedure by electro-chemical treatment to remove of the Cu_xS phases [77].

Thermal treatments

Post-deposition treatment of sprayed $CuInS_2$ films deposited from solutions with the precursors molar ratio of [Cu]:[In]:[S]=1:1:3 and 1:1:6 in vacuum or in an inert atmosphere at temperatures above 400 °C leads to significant improvement in the film crystallinity [10, 82], and also reduces the chlorine content in the films according to EDS [10, 82]. The treatment of $CuInS_2$ films grown from In-rich solutions at 500 °C in vacuum does not result in any structural improvement [44, 83]. Nevertheless the extra reflection at 2θ=26.5 ° disappears, a new XRD peak appears at 2θ = 30.6 deg in the XRD pattern corresponding to In_2O_3 [44] and as a result, the film conductivity type changes from p-type to n-type [35, 73]. Observed phenomenon is explained by the decomposition of an oxygen containing indium compound into In_2O_3 [73]. It is also possible that the crystallization of an amorphous In_2O_3, initially present in as-deposited film prepared by spray of In-rich solutions at temperatures close to 380 °C, takes place during the thermal treatment.

The thermal treatment of sprayed $CuInS_2$ films deposited from the solution with [Cu]/[In]=1 in H_2 atmosphere at temperatures above 400 °C removes extra reflection at 2θ=26.5 ° in the XRD pattern [101] and increases the crystallite size from 7.8 nm (as-deposited film) to 32.6 nm (H_2 treated film). The sprayed $CuInS_2$ films deposited at 380 °C using a solution with precursors molar ratio [Cu]/[In]=1.25 demonstrate the crystallite size of 20.1 and 41.6 nm before and after the H_2 treatment, respectively [83]. But thermal treatments of sprayed

$CuInS_2$ films from In-rich solutions ([Cu]/[In]<1) do not show any structural improvement by annealing in H_2 at temperatures up to 500 °C [82, 83].

Thermal treatment of sprayed films in sulfur containing atmosphere was found to be effective to reach the composition close to the stoichiometric $CuInS_2$ [11]. Deficiency of sulfur in as-deposited $CuInS_2$ films is a characteristic feature for sprayed films [10, 11, 35]. Annealing in sulfur vapour significantly improves the film stoichiometry as [S]/ ([Cu]+[In]) in the films increases from 0.85 (as-sprayed) to 1.0 (after annealing) [11]. In addition, chlorine and metal-bonded oxygen (O1s with BE=530 eV) were removed from the film surface (Fig. 1.9) [11].

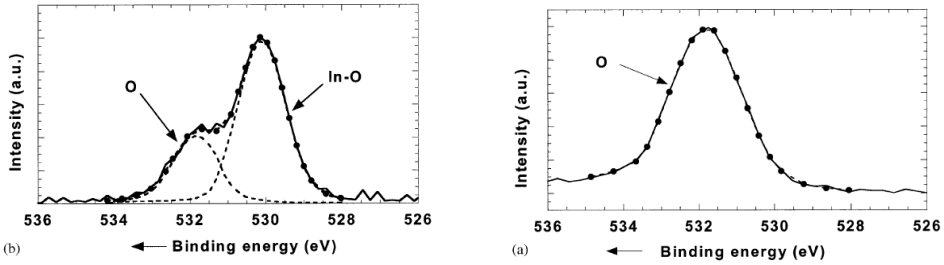

a) b)

Fig. 1.9. *XPS spectra of O1s core level of a) as-sprayed $CuInS_2$ films and b) after the thermal treatment in S vapour atmosphere [11].*

It has been reported that H_2S treatment temperature of 450 °C is not sufficient to improve the structural properties of $CuInS_2$ films deposited from the solutions with [Cu]/[In]≤1.0 [34, 35] (Fig. 1.10a). The treatment temperature above 500 °C should be applied to obtain well-crystallized films [34] (Fig. 1.10a). For example, annealing of the film deposited from In-rich solution in H_2S atmosphere at 525 °C for 120 minutes leads to a well-crystallized film with crystallite size of about 98 nm (Fig. 1.10b) [34].

Post-deposition thermal treatments in different atmospheres have been found to be effective to increase the film purity, removing chlorine residues from the film [10, 11, 82].

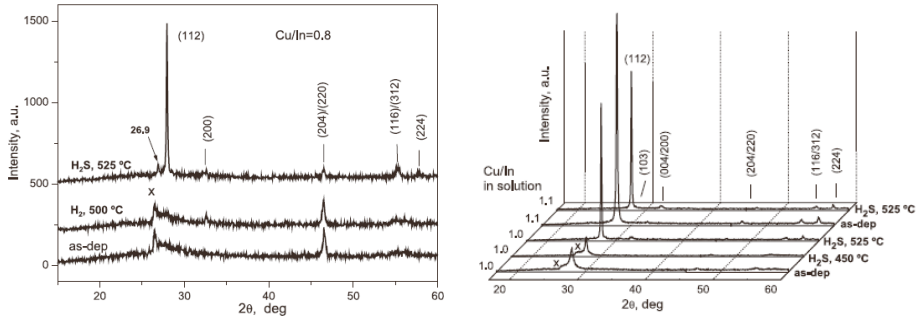

a) *b)*

Fig. 1.10. *XRD patterns of a) as-sprayed $CuInS_2$ films using the precursor molar ratio [Cu]/[In]=0.8 in solution and annealed in H_2 at 500 °C and in H_2S at 525 °C [34] b) as-sprayed $CuInS_2$ films using the precursor molar ratio [Cu]/[In]=1.0 and 1.1 in solution and treated in H_2S at 450 °C and 525 °C [34].*

According to Raman spectroscopic studies, the treatment in the H_2S atmosphere at 525 °C for 120 minutes has been found to increase also the $CuInS_2$ chalcopyrite ordering. The film quality factor (QF), expressed as QF=I(CH)/{(I(CH) +I(CA)}, where I(CH) is the peak intensity of A_1 mode of the CH structure and I(CA) is the peak intensity of A_1* mode of the Cu-Au ordered structure [34, 35] increased from 40 % to 62 % for the film deposited from the solution with precursors molar ratio [Cu]/[In]=1.0 [34]. In the case of the films deposited from In-rich or Cu-rich solutions the structure improvement was found less pronounced [34].

1.4. Solar cells based on sprayed $CuInS_2$ thin films

Interest in thin film solar cells based on sprayed $CuInS_2$ absorber was aroused more than 20 years ago due to the fact that the spray method allows preparation of all layers for solar cell at extremely low cost. Tiwari et al. [9] was the first who prepared all-layers-sprayed solar cell based on $CuInS_2$ as an absorber with an efficiency of about 2 % in 1987. In this stage of development, the properties of a sprayed absorber were poorly studied, and due to low light-to-electricity conversion efficiencies interests in the spray technology for an absorber material disappeared. The CSP deposition method emerged again at the end of 1990s when the production cost of a solar cell became an important issue. In parallel with studies on material properties, CSP-deposited $CuInS_2$ was also tested in solar cells. Table 1.1 summarizes the results for solar cells based on a sprayed $CuInS_2$ thin film.

Thin film solar cells with efficiencies close to 3% were prepared in our laboratory [87]. This solar cell is built up in a superstrate configuration (row 4 in

Table 1.1). It has been shown that indium sulfide is an appropriate buffer layer for solar cells with CSP deposited $CuInS_2$ absorber [88].

To date the conversion efficiency of about 1 % is the maximum obtained with a sprayed $CuInS_2$ absorber based solar cell in the substrate configuration (row 5 in Table 1.1). Interestingly, the solar cells based on the $CuInS_2$ absorber layer prepared from a single molecular precursor solution in an inert atmosphere show lower conversion efficiencies (up to 1 %) [89] than those prepared by CSP in air [87, 88].

The research group at Cochin University has reported a conversion efficiency of 5.87 %, which is the highest efficiency for thin film solar cells based on sprayed $CuInS_2$ absorber [90]. It is noteworthy that the presented current density j_{sc} = 44.03 mA/cm^2 (Table 1.1) overcomes the theoretical limit (43 mA/cm^2) for the $CuInS_2$ thin film solar cell [92].

Table 1.1. *Output parameters of solar cells based on sprayed $CuInS_2$ absorber.*

		Structure	Cell output parameters	Year	Ref.
1		ITO/ZnO/$CuInS_2$(Cu-rich)/Al	V_{oc} = 280 mV, j_{sc} = 13.3 mA/cm^2, FF = 38 %, η = 2 %	1987	[9]
2		Mo/$CuInS_2$/CdS/ZnO/Al	V_{oc} = 304 mV, j_{sc} = 5.25 mA/cm^2, FF = 29 %, η = 0.68 %	2003	[81]
3		TiO_2/$In(OH)_xS_y$/$CuInS_2$*	V_{oc} = 450 mV, j_{sc} = 10.7 mA/cm^2, FF = 43 %, η = 2.1 %	2004	[88]
4	**Thin film solar cells**	TiO_2/In-O-S/$CuInS_2$*	V_{oc} = 456 mV, j_{sc} = 14.6 mA/cm^2, FF = 43 %, η = 2.9 %	2004	[87]
5		Mo/$CuInS_2$/CdS/ZnO:F/Al	V_{oc} = 309 mV, j_{sc} = 4.6 mA/cm^2, FF = 36.8 %, η =1.03 %	2005	[89]
6		ITO/CdS/$CuInS_2$	η = 0.65 %	2005	[86]
7		ITO/$CuInS_2$/In_2S_3/Ag	V_{oc} = 450 mV, j_{sc} = 44.03 mA/cm^2, FF = 29.5 %, η =5.87 %	2006	[90]
8	**Structured solar cells**	TiO_2porous/In_2S_3/$CuInS_2$**	V_{oc} = 710 mV, j_{sc} = 23 mA/cm^2, FF = 43 %, η = 7 %	2008	[91]

* Solar cell made at TUT, ** 3D solar cell.

The results of the solar cells based on the as-sprayed $CuInS_2$ absorber (Table 1.1) clearly show that materials with lower quality cannot be effectively used in classical thin film devices. Fortunately, the development of materials in the nanometer scale has generated new photovoltaic (PV) materials and devices that could potentially lead to the realization of high-efficient low-cost solar cells (SC) in the future [93].

In this area a revolutionary development has been introduced by Grätzel and

co-workers in the form of an electrochemical dye-sensitized solar cell (DSSC) [6]. In this type of SC, nanostructured TiO_2 is sensitized by a monolayer of an organic dye. DSSC has reached an efficiency of 11% [7] and commercial production of such devices commenced in 2007.

A concept of an extremely thin absorber (ETA) layer SC has been developed on the basis of DSSC (Fig. 1.11a) [94, 95]. In an ETA cell a very thin semiconductor layer with a thickness up to some tens of nm will be used to replace a dye which often is non-stable. The electrons photogenerated in a semiconductor have to travel a very short distance before being abstracted by the TiO_2. Therefore an absorber with much lower quality than required for a thin film cell may still result in good conversion efficiencies. Thus, absorbers for ETA cells could be manufactured using low-cost chemical methods, such as chemical bath deposition (CBD), chemical spray pyrolysis (CSP), successive-ion-layer-adsorption–and-reaction (SILAR), etc. According to the theoretical model, efficiencies of 10-15 % are predicted for ETA cells [96].

Absorber materials, such as PbS, CdSe, CdS, In_2S_3 made by CBD or SILAR are commonly used in ETA cells on TiO_2 nanoparticle layer [99, 100, 101, 125], the highest efficiency of 3.4 % was obtained with CBD-Sb_2S_3 [97]. In the 3D solar cell, the highest efficiency of 7 % was obtained with CSP-$CuInS_2$ (Fig. 1.11b) [91]. High recombination losses during electrons path through a large number of TiO_2 nanoparticles to the electrode strictly limit this type of the SC. Replacing TiO_2 particles by vertically aligned nanorod arrays will exclude this disadvantage [126].

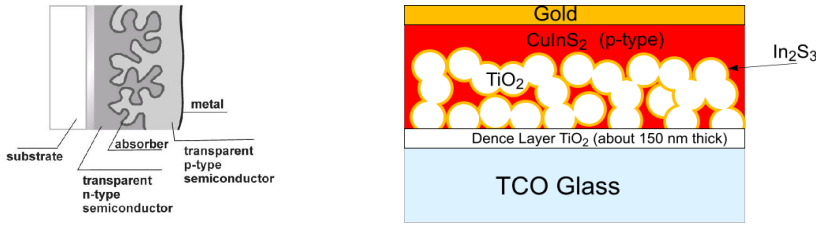

a) b)

Fig. 1.11. *Sketches of a) "extremely thin absorber" (ETA) solar cell based on $CuInS_2$ absorber [95], and b) 3D solar cell based on meso-porous TiO_2 and sprayed $CuInS_2$ absorber layer [91].*

In the first ZnO nanorod ETA cells absorber materials like CBD-CdTe [98] and CBD-CdSe [99] have been used, and a conversion efficiency of 2.3% has been achieved with CdSe [99]. Applying a In_2S_3 layer by the ion-layer-gas-reaction (ILGAR) technique onto ZnO nanorods (ZnO_{rod}) and using CuSCN as a p-conductor, ETA cells with efficiencies of 2.5-3.4 % have been prepared recently [100, 101].

1.5. Analytical methods for the determination of the film elemental composition

1.5.1. Energy dispersive x-ray spectroscopy

Energy Dispersive X-ray Spectroscopy (EDS) is an analytical technique which utilizes X-rays that are emitted from the sample when it is excited by an electron beam to identify the elemental composition of the sample [102-104]. When the sample is bombarded by an electron beam, electrons are ejected from the atoms on the sample surface (photoelectric effect). A resulting electron vacancy is filled by an electron from an outer shell, resulting in the emission of an Auger electron or X-radiation to balance the energy difference between the two electrons and to fulfil the momentum conservation law (see Fig. 1.12a) [105]. The EDS X-ray detector registers the energy and the intensity of the emitted X-rays. The energy of the X-ray quantum is characteristic of the chemical element from which the X-rays were emitted. The intensity of the X-rays, characteristic of a chemical element, is proportional to the abundance of the element atoms in the excited volume.

Spatial resolution on a lateral and depth scale of approximately 1 μm to 3 μm can be achieved, depending on the energy of the exciting beam and sample composition (see Fig. 1.12b) [102-104].

If there is an inhomogeneous distribution of elements in the specimen depth, the composition measured by EDS represents an average composition. Uncertainties in the quantitative determination of elements could arise if for some of the elements the L-lines and for others K-lines are used. Modern SEM is equipped with an EDS analyzer, a combined tool widely used to characterize PV materials and thin films [103-104].

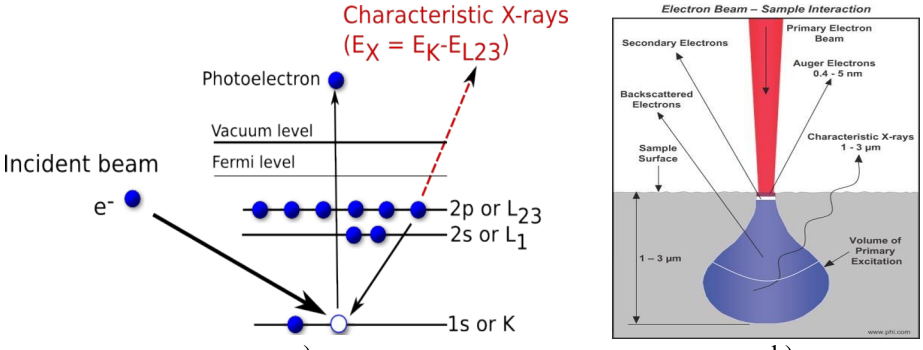

a) b)

Fig. 1.12 *a) Energy diagram of EDS signal formation [102], b) Schematic representation of the interaction of an electron beam with a sample [102].*

1.5.2. X-ray photoelectron spectroscopy

X-ray photoelectron spectroscopy (XPS), also known as electron spectroscopy for chemical analysis (ESCA), is a surface-sensitive method for the characterization of the chemical composition of materials with a depth resolution of approximately 2 nm to 7 nm [105]. Surface analysis by XPS is carried out by

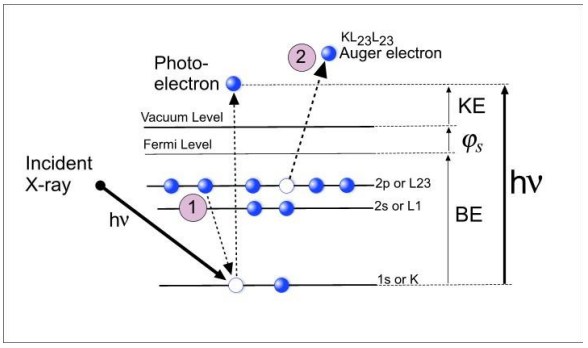

Fig. 1.13. *Energy diagram illustrating the generation of a photo-electron and an Auger electron [106].*

irradiating a sample in ultra-high vacuum (UHV) with soft X-ray radiation (usually from achromatic Mg Kα, hν=1253.6 eV or from monochromatic Al Kα, hν=1486.6 eV) [105, 106].

The energy diagram of the allowed electron states in an atom is presented in Fig. 1.13. The photoelectron excited by an incident X-ray beam with an energy of hν, is ejected from the material surface with a kinetic energy of KE from an occupied state (1s) with a potential energy of BE (Binding Energy). The kinetic energy (KE) of the emitted photoelectrons is given by the formula [105]:

$$KE = h\nu - BE - \varphi_s \,, \tag{1.1}$$

where hν is the energy of the X-ray photon, BE is the binding energy of the electron, φ_s is the work function of the detector.

The chemical shifts, i.e. the variations in the elemental binding energies, caused by differences in the chemical potential and polarizability of the elements in compounds, can be used to identify the chemical state of the elements [105].

The Auger process, characteristic of both XPS and EDS, can be understood by considering the ionization process of an isolated atom. The vacancy of the inner shell can be generated by irradiation with electrons or X-rays.

During XPS measurements X-rays cause the ejection of photoelectrons,

ionizing the core level (e.g. the K level). The vacancy thus produced is immediately filled by another electron from L_2 level (Fig. 1.13 process (1)). The energy ($E_K - E_{L2}$) released from this transition will be transferred to another electron in the L_3 level and as a result, this electron could eject as an Auger electron (Fig. 1.13 process (2)). The kinetic energy (KE) of the Auger electron is given by the formula [105]:

$$KE = E_K - E_{L2} - E_{L3}, \quad (1.2)$$

where E_K is the energy of K level, E_{L2} is the energy of L_2 level and E_{L3} is the energy of L_3 level, respectively. This excitation process is denoted as a KL_2L_3 Auger transition. It is obvious that at least two energy states must exist and two electrons must take part in an Auger process. Therefore, H and He atoms cannot eject Auger electrons. Several transitions (KL_1L_1, KL_1L_2, LM_1M_2, etc.) exist, with different probabilities for the transition to occur. The kinetic energy of the Auger electrons is characteristic of the element and is independent of the incident beam energy [106].

The XPS technique provides qualitative information about the elements and their chemical valence states by obtaining the binding energies of core levels and changes in the signal peak shape. Therefore we have a possibility to distinguish different elements with different oxidation states or elements with the same valence state, but in a different environment.

The possibility to distinguish elements by their chemical valence state is the main advantage of XPS compared to the EDS technique.

1.6. Summary of the literature overview and aim of the study

The studies reported in the literature of chemical spray $CuInS_2$ thin films and solar cells based on the sprayed $CuInS_2$ absorber layer can be summarized as follows:

1. $CuInS_2$ thin films by CSP are usually deposited using aqueous or alcoholic solutions containing Cu and In chloride and thiourea (or its analogue N, N, dimetylthiourea) in an appropriate molar ratio. $CuInS_2$ films could also be prepared using a single molecular source $[(P(i\text{-}But)_3)_2CuIn(SEt)_4]$ dissolved in toluene.
2. When Cu and In chlorides and thiourea are used as starting materials, a metal chloride and thiourea form a complex compound in an aqueous solution, $CuCl_2$ and thiourea form $[Cu(tu)Cl]\cdot 0.5H_2O$ and/or $Cu(tu)_3Cl\cdot H_2O$ depend on the precursors molar ratio. $InCl_3$ may also form a complex with thiourea, but the composition of the complex it not yet determined. It is expected that $CuInS_2$ forms from binary sulfides, binary sulfides aroused from the thermal

decomposition of complexes formed in spray solution.

3. $CuInS_2$ films by spray of aqueous solutions containing Cu and In chloride and thiourea were deposited in the temperature range of 230-400 °C using compressed air or nitrogen as carrier gas in air. The lowest growth temperature is determined by the decomposition temperature of metal-chloride-thiourea complexes. The highest growth temperature used is close to 400 °C as at higher temperatures the In_2O_3 phase was present in sprayed $CuInS_2$ films according to XRD. The content of residues originated from precursors is decreased by increasing the film deposition temperature. It could be expected that oxygen content increases with an increase in the deposition temperature, but has not been systematically studied.
4. The phase composition, crystallinity and morphology of sprayed $CuInS_2$ films are controlled by the [Cu]/[In] in spray solution. Deposition of In-rich solutions results in the films with smooth surface and small crystallite size (<10 nm), films contain a secondary phase (In-S or the second ternary). Films grown by spray of Cu-rich solutions ([Cu]/[In]>1) compromise well-crystallized $CuInS_2$ due to the presence of Cu_xS phase acting as a crystallization agent. Cu_xS segregates on the film surface and could be easily removed by the KCN etching. Films from Cu-rich solutions show a rough surface with large crystals irregularly placed on the film flat area. After KCN etching areas with large crystals with a size of some tens microns leave behind a sparse structure.
5. The post-deposition thermal treatment of as-sprayed films in an inert or reducing atmosphere at temperatures up to 500 °C leads to the purification as well as to the improvement of the film structural properties. Thermal treatment in sulfur containing atmospheres decreases the sulfur deficiency, the treatment in H_2S was found to increase the chalcopyrite ordering.
6. Elemental composition of sprayed $CuInS_2$ films had been mainly characterized by the EDS method, which is limited in terms of detection of light elements. The surface-analysis technique of XPS, giving information on both the elements and their chemical valence state, has been rarely applied.
7. Thin solar cells based on sprayed $CuInS_2$ absorber layer show conversion efficiencies close to 3 %. 3D solar cells on nanoporous TiO_2 using CSP-deposited $CuInS_2$ absorber show a conversion efficiency of 7 %, indicating the sprayed absorber potential for nanostructured cells.

Aim of the study

On the basis of the studies made on sprayed $CuInS_2$ films and from an application point of view to develop solar cell materials and solar cells by low-cost deposition techniques, the aims of the doctoral thesis were:

- to study the chemical composition of $CuInS_2$ films deposited by CSP at different growth temperatures using aqueous spray solutions containing $CuCl_2$, $InCl_3$ and $SC(NH_2)_2$ with the $[CuCl_2]/[InCl_3]$ molar ratio of 1.0 and 1.1;
- to study the effect of post-deposition thermal treatment in hydrogen disulfide atmosphere on the structure, optical properties and chemical composition of sprayed $CuInS_2$ films;
- to study the elemental composition of sprayed $CuInS_2$ films;
- to study the distribution of the elements in depth of sprayed $CuInS_2$ films;
- to prepare and characterize flat and nanostructured solar cells where $CuInS_2$ prepared by CSP is used as an absorber layer.

2. EXPERIMENTAL

2.1. Spray pyrolysis deposition and post-deposition treatment of $CuInS_2$ films

2.1.1. Deposition

$CuInS_2$ films were deposited by chemical spray pyrolysis method using a pneumatic spray mode and N_2 or compressed air as a carrier gas. Aqueous solutions containing $CuCl_2$, $InCl_3$ and $SC(NH_2)_2$ in the molar ratio of 1:1:3 ([Cu]/[In]=1.0) or 1.1:1:3.1 ([Cu]/[In]=1.1) were sprayed onto the preheated bare or ITO covered glass sheets both with a thickness of ca 1 mm. The stock solution of $InCl_3$ with the concentration of $[In^{3+}]$=0.1 mol/l was made, dissolving Indium (Indium wire, 2.0 mm diameter, purity 99.99%, Alfa Aesar) in HCl (purity p.a., 37%, Merck). $CuCl_2 \cdot 2H_2O$ (purity p.a., >99.0%, Merck) and $CS(NH_2)_2$ (purity for synthesis, >98%, Merck) were used as copper and sulfur sources, respectively. The films were grown in the temperature region of 250 - 370 ºC, the deposition temperature was kept with an accuracy of ±5 °C with the help of the feedback control system for the heater supply. The film deposition temperature was measured from the glass surface under the spray of the deionized water. Details of the deposition conditions for $CuInS_2$ films prepared in this thesis are summarized in Table 2.1.

Table 2.1. *Spray deposition conditions for $CuInS_2$ thin films in the papers included in the thesis.*

Film deposition conditions						Annealing in H_2S			
$[Cu^{2+}]$, mmol/l	[Cu]/[In] molar ratio in sol.	Solution volume, ml	Dep. Temp., °C	Carrier gas	Spray rate, ml/min	Temp., °C	Time, min	Cooling	Paper
2	1.1	100	370	N_2	2.5	530	60, 120	R*, S**	I
2	1.0	100	370	N_2	2.5	530	60, 120	R*, S**	I
2	1.1	100	350	N_2	2.5	530	60	S**	II
2	1.0	50	350	air	1	-	-	-	III
2	1.0	50	250	air	1	-	-	-	III
2	1.0	35	270	air	1	-	-	-	IV,V

*-rapid cooling, **-slow cooling

2.1.2. Post-deposition treatment

Chemical etching of sprayed films was performed in a 5 % KCN aqueous solution for 5 min at room temperature to remove a copper sulfide from the film surface. After etching the samples were cleaned by rinsing in deionized water and dried **[I, II].**

Post-deposition heat treatments were performed in a flowing H_2S atmosphere at 530 °C for 1 and 2 h, followed by rapid or slow cooling with the cooling rates of about 25 °C/min and 2 °C/min, respectively [**I**, **II**]. Hydrogen sulfide (purity 99.999 %) was purchased from Linde Gas (Linde AG).

2.2 Characterization of $CuInS_2$ thin films

2.2.1. Crystal structure

The crystal structure of the films was characterized by the X-ray diffraction (XRD) patterns recorded on a Bruker AXS D5005 [**I**] and Rigaku Ultima IV [**III**] diffractometers using monochromatic Cu Kα radiation (λ=1.540560 Å), anode voltage 40 kV, anode current 40 mA. The average crystallite size was calculated from the FWHM of the (112) diffraction peak of $CuInS_2$ (JCPDS card 00-027-0159) using Scherrer's formula [35].

Raman spectroscopy was used to determine the short-range ordering of sprayed $CuInS_2$ films [**III**]. Raman spectra of the films were recorded in the backscattering nonpolarized mode at room temperature using micro-Raman spectrometer HORIBA Jobin Yvon Model HR 800. The excitation radiation wavelength was 532.0 nm and the power density was ca 2.5 ±0.5 10^4 W/cm^2.

2.2.2. Elemental composition

The elemental composition of the films was studied by the energy dispersive x-ray spectroscopy (EDS) on a Link Analytical AN 10000 spectrometer using an accelerating voltage of 7 kV and a beam current of 3 nA. EDS measurements were made from the surface area of 2 x 2 μm^2 at four different characteristic points on each sample [**I**]. EDS study was performed by Dr. V. Mikli.

X-ray photoelectron spectroscopy (XPS) experiments in the present study were carried out using a LAS-3000 ISA-Riber (University of Vilnius) and SCIENTA SES 100 (University of Tartu) with the photon energy of Mg Kα (hν=1253.6 eV) radiation [**II**], and on Kratos AXIS Ultra DLD with monochromatic Al Kα radiation (hν=1486.0 eV) [**III**] at a base pressure of about 2×10^{-8} Torr [**II, III**]. The Ar^+ ion sputtering was used for the depth profiling to obtain information of the film bulk composition. Energy calibration was

performed using the C1s line at 284.6 eV for LAS-3000 ISA-Riber and SCIENTA SES 100 [**II**] and at 285.0 eV for Kratos AXIS Ultra DLD [**III**] as a reference. The atomic concentrations of the elements (x_i) were calculated from the Cu2p, In3$d_{5/2}$, S2p, O1s and Na1s core level peak areas using the following formula:

$$x_i = \frac{\frac{I_i}{S_i}}{\sum_k \frac{I_k}{S_k}}, \qquad (2.1)$$

where

I_i – is the integrated area of a core level peak of a certain element (proportional to the number of emitted photoelectrons for a certain element);

S_i – is the sensitivity factor of the element. In the case of XPS study on LAS-3000 ISA-Riber [**II**], S_i is the Scofield's ionization cross-section [105] with no corrections for both λ (mean free path of photoelectrons) and analyzer transmission function. In the case the XPS measurements were performed on Kratos AXIS Ultra DLD [**III**], the sensitivity factors provided by the Vision 2.2.6 analysis software were used;

k – is the number of the elements in the film.

More detailed description of the XPS experiments is given in papers **II** and **III**.

2.2.3. Morphology

Scanning Electron Microscopy

Morphology and cross-sectional views of the films and solar cells were studied by scanning electron microscopy (SEM) on Leo Supra 35 [**I**] and Zeiss HR FESEM Ultra 55 [**IV**], respectively. The image of the p-n junction [**IV**] was investigated with the help of an electron beam induced current (EBIC) detector. The SEM and EBIC studies were made by Dr. O. Volobujeva.

Atomic Force Microscopy

Atomic force microscopy (AFM) images were obtained using NT-MDT scanning head Smena, Scanning Probe Image Processor SPIP V3.2.4.0 and MicroMasch cantilevers CSC 21 with silicon probe tip in a contact mode. The AFM study in [**II**] was made by Mrs. R. Nisumaa.

2.2.4. Optical properties

The optical bandgap (E_G) of sprayed $CuInS_2$ films was determined from the absorbance spectra (measured on a Varian Techtron 635 model UV-VIS-NIR spectrophotometer [**I**]), applying an analysis model presented by Davis and Mott [107], using the formula:

$$\alpha = \frac{A \cdot \left(h\nu - E_G \right)^n}{h\nu}, \qquad (2.2)$$

where
A – parameter depending on the transition probability;
α – absorption coefficient;
h – Plank's coefficient;
ν – frequency of the radiation;
E_G – optical bandgap;
n – coefficient depending on the transition type, n=1/2 for direct allowed transition.

The Eg is found from the plot $(\alpha \cdot h \cdot \nu)^2$ versus the photon energy $h \cdot \nu$ by the extrapolation of the linear portion of the plot up to α=0.

2.2.5. Electrical properties

The electrical resistivity of the films was calculated using the following conventional equation:

$$\rho = \frac{R \cdot A}{l}, \qquad (2.3)$$

where
ρ – resistivity;
R – resistance of the film (resistance was calculated from the I-V curve measured on the Keithley-616 electrometer [**I**] and the AUTOLAB PGSTAT 30 set-up [**II**]);
l – length of the current path between the contacts;
A – area of the current channel.

To characterize non-homogeneity of the films, the electrical resistance of sprayed $CuInS_2$ films was measured by two routes – across the film thickness ("perpendicular" resistance) and along the surface ("longitudinal" resistance) using the films sprayed in the same deposition process onto ITO/glass substrate and glass substrate, respectively **[II].**

To perform the electrical conductivity measurements, the Pt-Au contacts with an area of 1.83 mm^2 were made by sputtering on the top of the films. The ITO was used as a back contact.

2.3. Preparation and characterization of solar cells

CSP deposited $CuInS_2$ films were used as an absorber layer in the thin film **[II, IV]** as well as in nanostructured solar cells based on the CSP deposited ZnO nanorod array [**IV**, **V**].
The thin film solar cells had the following structures:
a) superstrate configuration: glass/ITO/ZnO/CdS /$CuInS_2$/Contact [**II**].
b) substrate configuration: glass/ITO/$CuInS_2$/CdS/ZnO/Contact [**II**].
c) glass/ITO/ZnO/blocking layer/buffer layer/$CuInS_2$/Contact [**IV, V**].

The nanostructured solar cells had the following structure [**IV, V**]: glass/ITO/ZnO_{rod}/blocking layer/buffer layer/$CuInS_2$/Contact. Preparation conditions of the component layers of a nanostructured solar cell and a flat thin film cell in brief are presented in Table 2.2. Preparation details are provided in [**IV**] and [**V**].

Table 2.2. *Deposition conditions of component layers for nanostructured solar cells using $CuInS_2$ as an absorber layer. Glass/ITO sheets were used as a substrate.*

Layer function	Layer	Method	Starting chemical(s)	Molar ratio of starting chemicals in solution	Acidity of solution	Spray rate, ml/min	Deposition temp., °C
Window	ZnO_{rod}	CSP	$ZnCl_2$	-		2.5	550
Buffer	In_2S_3	CSP	$InCl_3$, $SC(NH_2)_2$	In:S=1:3	pH≈3	2.5	300
Blocking	In_2S_3	CSP	$InCl_3$, $SC(NH_2)_2$	In:S=1:3	pH≈5	1	270
	TiO_2	sol-gel dip coating	$Ti(OC_3H_{7)4}$	-		-	-
Absorber	$CuInS_2$	CSP	$CuCl_2$, $InCl_3$, $SC(NH_2)_2$	Cu:In:S= 1:1:3	pH≈3	1	270

Output characteristics of solar cells based on the sprayed $CuInS_2$ thin film absorber were characterized by I-V characteristics measured in the dark and

under halogen lamp illumination (intensity 100 mW/cm^2). I-V curves were recorded on AUTOLAB PGSTAT 30 set-up.
The solar cell efficiency was calculated by the formula:

$$\eta = \frac{j_{sc} \cdot V_{oc} \cdot FF}{P_{st}} \cdot 100\,\%, \qquad (2.4)$$

where
η – efficiency;
j_{sc} – short circuit current density;
V_{oc} – open circuit voltage;
FF – fill factor;
P_{st} – power of the halogen lamp illumination (100 mW/cm^2).

The fill factor of the solar cell was calculated by the formula:

$$FF = \frac{j_{eff} \cdot V_{eff}}{j_{sc} \cdot V_{oc}}, \qquad (2.5)$$

where
j_{eff} – current density at maximum power output;
V_{eff} – voltage at maximum power output.

3. RESULTS AND DISCUSSION

3.1. Properties of $CuInS_2$ films deposited by CSP using the precursor molar ratio [Cu]/[In]=1.1 in solution

The properties of as-sprayed films were studied in order to investigate the influence of the deposition temperature and the [Cu]/[In] molar ratio in the solution on the phase and elemental composition of sprayed $CuInS_2$ films.

This part of the thesis summarizes the studies on the phase and chemical composition of sprayed films prepared by spray of slightly Cu-rich solutions with precursor molar ratio $CuCl_2$:$InCl_3$= 1.1:1 ([Cu]/[In]=1.1) using a growth temperature of 370 °C. The films are labelled CIS-1.1. Details of the deposition are presented in section 2.1.1. Spray solution composition with [Cu]/[In]=1.1 was chosen according to the literature data and to the results previously obtained in our research group [65, 82]. Using the [Cu]/[In]=1.1 in a spray solution, the films are composed of a well-crystallized $CuInS_2$ phase and show relatively smooth surface compared to the films deposited from the solutions with [Cu]/[In]>1.1 [85].

Results are published in papers [**I**] and [**II**].

3.1.1. Structure of as-sprayed films

XRD pattern of a CIS-1.1 film deposited at 370 °C is presented in Fig. 3.1,

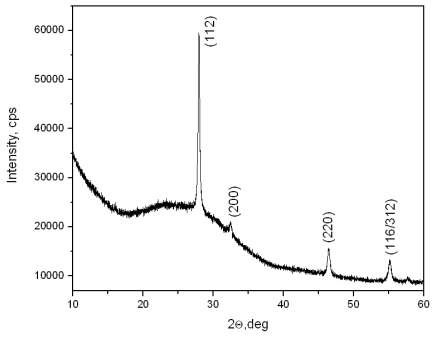

Fig. 3.1. *XRD pattern of KCN etched CIS-1.1 film on the glass substrate, Ts=370 °C.*

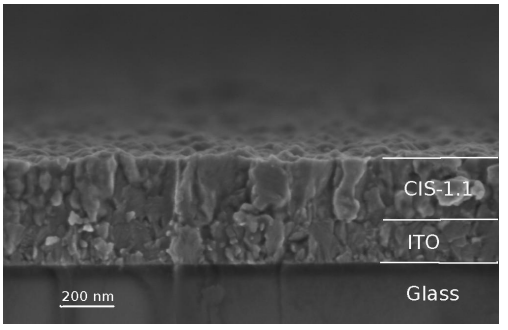

Fig. 3.2. *SEM image of KCN etched CIS-1.1 film on the glass/ITO substrate, Ts=370 °C.*

SEM image is exhibited in Fig. 3.2. According to XRD, the film is composed of the tetragonal chalcopyrite $CuInS_2$ phase (JCPDS card 00-027-0159) showing preferred orientation along the (112) plane, no additional crystalline phases were

detected. The crystallite size was about 44 nm, as calculated from the FWHM of the (112) diffraction peak. XRD pattern of the film and size of crystallites is close to that reported in literature [10, 11]. The film has smooth surface with some 'spot-like' areas (Fig. 3.2) which are characteristic of CIS-1.1 films prepared by spray [10, 11, 43, 44, 81]. The as-sprayed CIS-1.1 film shows the optical energy gap of 1.44 eV.

3.1.2. Surface analysis of as-sprayed films

XPS spectra

According to the XPS survey scan from the as-sprayed surface, signals from Cu, In, S, O and C were detected (Fig. 3.3). The signal characteristic of chlorine with binding energy (BE) around 198-200 eV that often is present in the XPS spectra of sprayed $CuInS_2$ films [10] was not detected. The peak positions of $Cu2p_{3/2}$, $In3d_{5/2}$, S2p core levels were at BE 932.7 eV, 444.6 eV, 161.5 eV, respectively (See Fig. 3.4). The BE values of copper, indium and sulfur core levels were close to those reported for sprayed $CuInS_2$ films [10, 108].

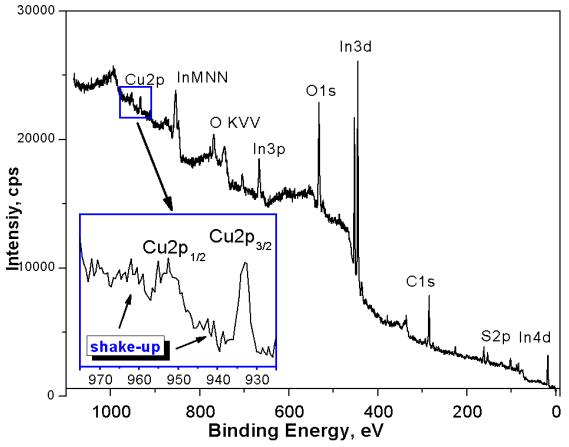

Fig. 3.3. *XPS wide scan spectrum of the as-sprayed CIS-1.1 film. Spectra were recorded on LAS-3000 ISA-Riber.*

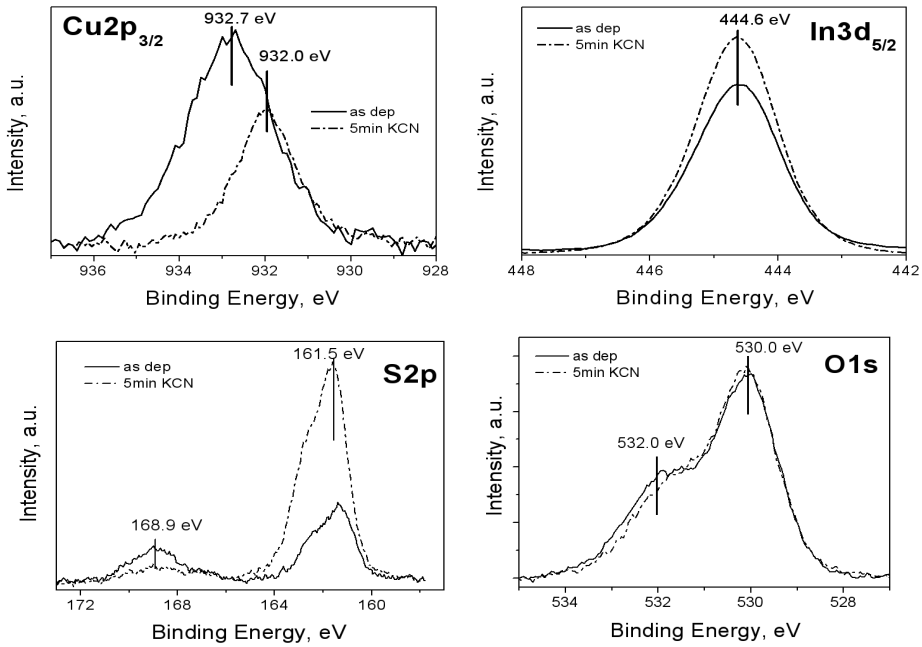

Fig. 3.4. *$Cu2p_{3/2}$, $In3d_{5/2}$, O1s and S2p core levels spectra of as-sprayed (solid line) and 5min-KCN-etched (dashed line) CIS-1.1 films. Spectra were recorded on SCIENTA SES 100.*

The $Cu2p_{3/2}$ core level peak at BE=932.7 eV has FWHM of 2.1 eV. The binding energies characteristic of Cu^{+} and Cu^{2+} states are in the interval of 932.0 – 932.8 eV and 932.7 – 934.1 eV, respectively [110]. Thus, the existence of Cu in both oxidation states is possible [111]. Weak copper shake-up peaks at around BE of 940 and 944 eV were observed in the wide-scan XPS spectrum (see inset in Fig. 3.3), indicating the existence of phases containing copper in the Cu^{2+} state [111].

The O1s spectrum from the as-sprayed surface shows two peaks: at BE=532.0 eV and BE=530.0 eV corresponding to the oxygen in $(OH)^{-}$ groups adsorbed on the surface and oxygen bonded to the metal (Me-O), respectively [109].

The detected S2p core level peak at BE=161.5 eV (Fig. 3.4) is characteristic of sulfides [109]. In addition, the sulfur signal at 168.9 eV, characteristic of sulfates [109], can be clearly seen on the S2p core level spectrum (Fig. 3.4).

After KCN etching, the $Cu2p_{3/2}$ peak is located at BE=932.0 eV, also characteristic of $Cu2p_{3/2}$ peak position in $CuInS_2$ prepared by 2-stage process [112]. The FWHM of the peak is decreased from 2.1 eV to 1.65 eV (Fig. 3.4). KCN etching decreases the intensity of the S2p peak characteristic of sulfate

(168.9 eV) and increases the intensity of sulfide peak (161.5 eV), whereas no significant changes were observed in the binding energies and intensities of $In3d_{5/2}$ and O1s peaks.

Changes in the film surface composition resulting from KCN etching could be characterized using the $Cu2p_{3/2}$, $In3d_{5/2}$, S2p and O1s (BE=530.0 eV) integrated area ratios. By KCN etching, the [Cu]/[In] ratio is decreased from 0.5 to 0.2, Cu/S from 3.8 to 0.9, whereas no significant changes were observed in the In/O ratios. Observed changes in the composition support the EDS results on removal of Cu–S phases by KCN etching [73] according to the chemical reaction:

$$CuS+4KCN+H_2O \rightarrow K_2[Cu(CN)_4]+KHS+KOH \qquad (3.1)$$

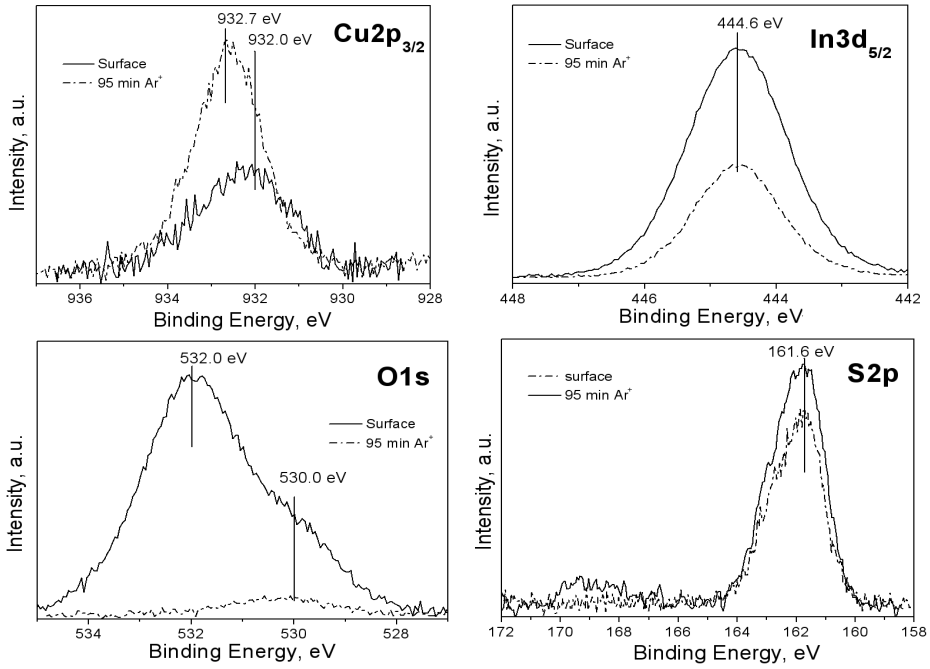

Fig. 3.5. *$Cu2p_{3/2}$, $In3d_{5/2}$, O1s and S2p core level spectra of the KCN-etched (solid line) CIS-1.1 film and of this film after Ar^+ sputtering for 95 minutes (dashed line). Spectra were recorded on LAS-3000 ISA-Riber.*

XPS spectra of the $Cu2p_{3/2}$, $In3d_{5/2}$, O1s and S2p core levels of KCN-etched CIS-1.1 films and KCN-etched films after Ar^+ sputtering for 95 minutes are presented in Fig. 3.5. It can be seen that the spectra are different. After Ar^+ sputtering the intensity of the copper signal is increased, however, the position of

the $Cu2p_{3/2}$ core level peak (BE=932.7 eV) is similar to that of the $Cu2p_{3/2}$ core level peak for as-sprayed CIS-1.1 with no KCN treatment (Fig. 3.4). It indicates that phases similar to those on the surface of the as-sprayed CIS-1.1 film could also be present in the film bulk. As shake-ups around BE=940 eV and 944 eV, characteristic of Cu^{2+} containing pieces [111], were not detected in the spectra after Ar^+ treatment, the presence of Cu^{2+} containing phases is not proved. It is possible that two different Cu-containing phases are present in the film bulk. Auger spectra are discussed below to clarify this speculation.

After Ar^+ sputtering for 95 minutes, the signal from oxygen in metal oxide (BE=530 eV) is still present but the peak intensity is significantly decreased compared to that on the film surface. It allows a conclusion to be made that metal oxide phase is present in the bulk of the film.

Auger spectra

In every XPS measurement not only photoelectrons but also Auger electrons are detected. In $M_{45}N_{45}N_{45}$ and Cu $L_{23}VV$ spectra of as-deposited and KCN-etched CIS-1.1 films are presented in Figs 3.6 and 3.7, respectively. Spectra were recorded for both samples from the surface and from the bulk, in depth that responds to the Ar^+ sputtering for 15 minutes.

In $M_{45}N_{45}N_{45}$ Auger maxima on the surfaces of as-deposited and KCN-etched films have similar energies (KE=406.6 eV) (curve 1 in Fig. 3.6a and 3.7a). Ar^+ bombardment of both as-deposited and KCN-etched films causes indium Auger maxima shift of ~0.7 eV to lower binding energies (curve 2 in Fig. 3.6a and 3.7a), indicating lower impact of In-oxides in the film bulk compared to that on top [113].

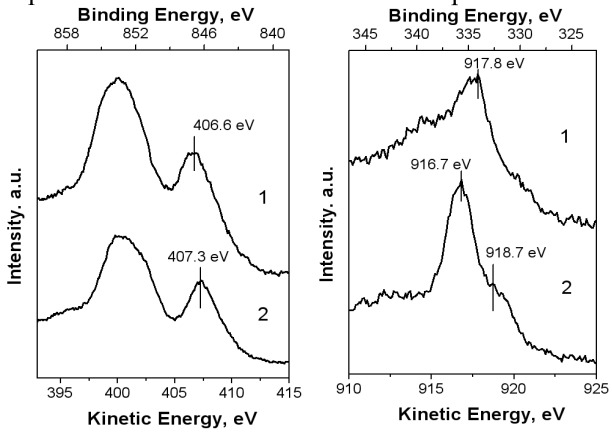

Fig. 3.6. *a) In $M_{45}N_{45}N_{45}$ and b) Cu $L_{23}VV$ Auger spectra of the as-deposited CIS-1.1 film recorded from the surface (curve 1 in graphs a and b) and from the depth after Ar^+-sputtering for 15 minutes (curve 2 in graphs a and b). Spectra recorded on SCIENTA SES 100.*

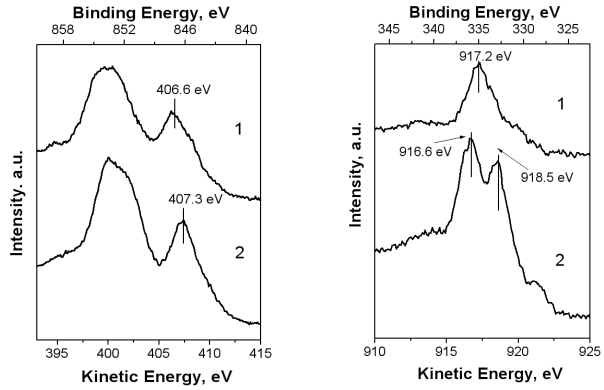

a) b)

Fig. 3.7. *a) In $M_{45}N_{45}N_{45}$ and b) Cu $L_{23}VV$ Auger spectra of the KCN-etched CIS-1.1 film recorded from the surface (curve 1 in graphs a and b) and from the depth after Ar^+-sputtering for 15 minutes (curve 2 in graphs a and b). Spectra recorded on SCIENTA SES 100.*

KCN etching causes a shift of the Cu $L_{23}VV$ Auger peak from KE=917.8 eV (as-sprayed) to 917.2 eV (See curve 1 in Figs 3.6b and 3.7b). Ar^+ sputtering of KCN-etched results in the shift of the Cu Auger peak towards lower KE values (see curve 2 in Figs 3.6b and 3.7b), indicating the presence of the Cu^+ containing phases [114]. Cu $L_{23}VV$ Auger peak at KE=916.6 eV is very close to that reported for RTP-$CuInS_2$ [52]. Interestingly, there appears an additional peak at KE around 918 eV (Fig. 3.7b, curve 2), which could be originated from the Cu^{2+} based pieces [111] or due to Cu^+ in octahedral coordination [111]. As shake-ups were not detected in the XPS spectrum, there is no confirmation of the presence of Cu^{2+} containing pieces. Cu Auger peak at KE close to 918 eV coincides with the peak position observed for the Spray ILGAR deposited Cu_xS film [52].

3.1.3. Elemental composition of as-sprayed films

XPS analysis

The atomic concentrations of the detected elements on the film surface and at the depth after Ar^+ etching for 95 minutes were calculated from integrated areas of $Cu2p_{3/2}$, $In3d_{5/2}$, O1s and S2p core levels peak using Scofield's cross-sections. Content of oxygen was calculated from the O1s core level peak at BE=530.0 eV. The calculated atomic concentrations of elements are presented in Table 3.1.

According to the results of XPS, the surface of the KCN-etched $CuInS_2$ film is highly indium and oxygen rich, probably with a high amount of In-oxide on the surface. Contents of In and O are decreasing while copper concentration is

increasing from the surface to the film bulk. Content of oxygen as high as 17 at. % in the film bulk (Table 3.1) is close to the oxygen concentration (16.7 at.%) determined by RBS in $CuInS_2$ films deposited at 380 °C [82]. Our XPS results indicate that the surface of KCN-etched CIS-1.1 film is Cu-deficient (Cu - 3 at. %, In - 32 at.%, S - 32 at.%, O - 31 at.%, Na - 2 at.%) which is in agreement with XPS results reported by Zouaghi et al. for sprayed $CuInS_2$ films deposited from a Cu-rich solution (Cu - 7 at.%, In - 48 at.%, S - 45 at.%) [10]. In spite of the fact that Zouaghi et al. in their study [10] detected oxygen on the surface, they did not take it into account in quantitative calculations.

According to quantitative analysis, composition of the KCN-etched surface is quite different from that after Ar^+ ion etching. Thus, it is likely that the elemental composition throughout $CuInS_2$ film is graded.

Table 3.1. *Elemental composition of as-deposited CIS-1.1 films calculated from the data of the XPS analysis*.*

Treatment	In, at.%	Cu, at.%	S, at.%	O (MeO), at.%	Na, at.%	In/Cu	S/(Cu+In)
KCN etching	32	3	32	31	2	10.7	0.9
Ar^+ etching for 95 min.	28	11	44	17	0	2.5	1.1
Etching in $(NH_4)_2S_2O_8$ for 6 min.	28	23	49	0	0	1.2	1.0

* Atomic concentrations of the elements presented in Table 3.1 are not absolute values due to absence of the reference sample.

According to XPS, the spray-deposited CIS-1.1 film grown at 370 °C in our experiment has differences in its chemical, and consequently, phase composition on the film surface and in the bulk.

The film graded composition is also reflected in the electrical resistivity (ρ) of the step-by-step chemically etched CIS-1.1 film measured in “longitudinal” and “perpendicula” modes. Chemical etching was made in peroxydisulfuric acid diammonium salt ($(NH_4)_2S_2O_8$, ammonium persulfate) aqueous solution. For acceleration of the chemical etching reaction, some drops of H_2SO_4 was added into the solution [115]. Etching depth was controlled via etching time. Chemical dissolution of In_2O_3 and $CuInS_2$ in the ammonium persulfate solution could be described as follows:

$$In_2O_3 + 3(NH_4)_2S_2O_8 \xrightarrow{6H^+} In_2(SO_4)_3 + 3(NH_4)_2SO_4 + 3H_2O \qquad (3.2)$$

$$2CuInS_2 + 3(NH_4)_2S_2O_8 \xrightarrow{H^+} 2CuSO_4 + In_2(SO_4)_3 + (NH_4)_2SO_4 + 4(NH_4)HS \quad (3.3)$$

$$(NH_4)HS \rightarrow NH_3\uparrow(g) + H_2S\uparrow(g) \quad (3.4)$$

AFM image of the CIS-1.1 film after etching for 6 minutes is presented in Fig. 3.8. Elemental composition according to XPS at the similar depth obtained by etching for 6 minutes (ca. 150 nm as evaluated from the AFM image) is given in Table 3.1.

Electrical resistivity (ρ) of the chemically etched CIS-1.1 film depends on the etching depth controlled by the etching time, as presented in Fig. 3.9.

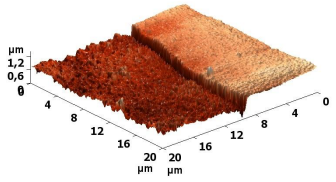

Fig. 3.8. *AFM image of the CIS-1.1 film etched in 0.01 M $(NH_4)_2S_2O_8$ solution. Etching time was 6 minutes.*

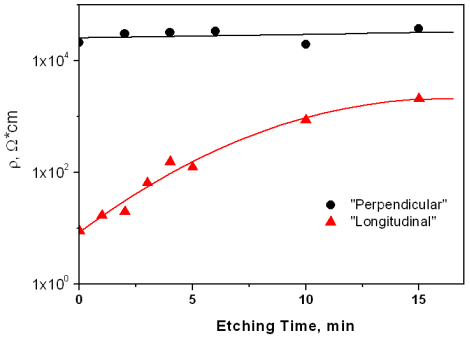

Fig. 3.9. *Electrical resistivity (ρ) of CIS-1.1 films vs. etching time in $(NH_4)_2S_2O_8$ solution. Electrical resistance was measured across the film ("perpendicular") and along the film surface ("longitudinal").*

It can be seen that the electrical resistivity of the un-etched sample measured by two modes, in "longitudinal" or "perpendicular" modes, respectively, differs more than three orders of magnitude ($\rho=1x10^1$ Ω.cm vs. $\rho>1x10^4$ Ω.cm). The value of the "perpendicular" resistivity of 2.5 $x10^4$ Ω.cm was measured for CIS-1.1 films in [**I**]. Phenomenon that the resistivity of sprayed $CuInS_2$ films depends on the measurement mode was reported earlier [35]. "Perpendicular" resistivity is much higher than "longitudinal" one independent of the etching time. By increasing the etching time, "longitudinal" resistivity increases, obviously due to removal of the more conductive (In and O-rich) upper layer.

I-V curves of solar cells in a substrate (ITO/$CuInS_2$/CdS/ZnO) and superstrate (ITO/ZnO/buffer/$CuInS_2$) configurations, using sprayed CIS-1.1 as an absorber layer, are presented in Fig. 3.10. It can be seen that the preparation of the solar

cell in the substrate configuration (buffer and window layers are deposited onto the absorber layer) was not successful. It could be speculated that the more conductive upper layer of CIS-1.1 is also responsible for the unsuccessful heterojunction preparation in substrate configuration.

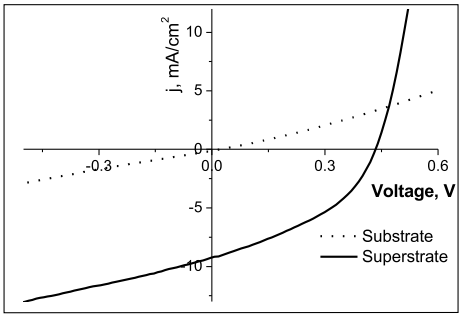

Fig. 3.10. *Current-voltage characteristics of a superstrate (ITO/ZnO/CdS/$CuInS_2$, solid line) and a substrate (ITO/$CuInS_2$/CdS/ZnO, dashed line) configuration solar cell based on the sprayed CIS-1.1 absorber layer under the halogen lamp illumination of 100 mW/cm^2.*

In conclusion, both resistivity measurements of step-by-step etched CIS-1.1 films and I-V characteristics of substrate and superstrate configuration solar cells support the results of the XPS study on the film's graded composition in thickness.

Polarographic and EDS analyses

According to polarographic analysis, the [Cu]/[In]=1.06 in the as-deposited CIS-1.1 film (no KCN etching) is close to the precursor molar ratio in a spray solution ([Cu]/[In]=1.1). KCN etching turns the film slightly In-rich ([Cu]/[In]=0.9) [**II**].

Elemental composition of the as-deposited KCN-etched CIS-1.1 film according to EDS is as follows: Cu- 26.4 at.%, In- 26.6 at.%, and S- 44.4 at.%, with [Cu]/[In]=0.99 and S/(Cu+In)=0.83 [**I**]. Composition of sprayed CIS-1.1 films as determined by EDS in this study is different to that reported by M.C. Zouaghi et al. [10], S. Marsillac et al. [11] and O. Kijatkina [73] for sprayed $CuInS_2$ films deposited from slightly Cu-rich solutions. Differences in the results of our EDS investigations and the literature are explained by the KCN treatment applied before the measurement.

Differences in the elemental composition of the sprayed $CuInS_2$ films studied by EDS and XPS can be explained by the differences of those techniques (see chapter 1.5). In addition, the concentrations calculated from the XPS data are not

absolute values due to missing of a calibrated reference sample.

Summary

The as-sprayed CIS-1.1 films prepared at 370 °C from the solution with the precursor molar ratio [Cu]/[In]=1.1 are composed of relatively well-crystallized $CuInS_2$ with crystallite size of about 44 nm, and no other crystalline phases in the film according to XRD. These findings correspond to the results reported by different authors [10, 35, 73, 85].
Results of the XPS study could be summarized as follows:

- Cu and S containing secondary phases such as Cu sulfide and sulfate are present on the surface of the as-deposited film. Thus, the XPS study confirms the results of previous studies where the presence of the Cu-sulfide phase on the surface has been proved by other direct or indirect methods. Chemical etching in the KCN solution is necessary to remove copper-sulfide phase(s) from the film surface.
- An additional copper containing phase could be present in the bulk of the film according to the XPS and Auger spectra.
- Oxygen bonded to metal, probably in the form of In_2O_3, is present on the film surface and in the film bulk. The content of oxide on the surface is much higher than in the film bulk. Presence of In_2O_3 phase on the surface of the as-sprayed CIS-1.1 film has been reported earlier [10, 11], in this study we showed that oxide phase could be present in a high amount in the bulk of the film deposited at 370 °C.
- The elemental composition of the film is given also quantitatively. We showed that the film has un-uniform composition through the film (from the film surface to the bottom), as it is also reflected in the differences of the film's electrical resistivity measured from the film surface or across the film ("longitudinal" and "perpendicular" resistivity, respectively).

3.2. Properties of $CuInS_2$ films deposited by CSP using the precursor molar ratio [Cu]/[In]=1.0 in solution

$CuInS_2$ films obtained by spray using [Cu]/[In]=1.0 solution have been investigated less than those obtained from Cu-rich solutions as the films were low-crystalline and may contain secondary phases [35, 65, 73, 101]. In this study $CuInS_2$ films using [Cu]/[In]=1.0 solution were deposited at two different temperatures 250 and 350 °C. Films were characterized to their phase composition and structure by the XRD and Raman spectroscopy. XPS was applied to study the elemental composition. The films sprayed from the solution

with [Cu]/[In]=1.0 are labelled CIS-1.0.
The studies of as-deposited CIS-1.0 films are published in paper [**III**].

3.2.1. Structure of as-sprayed films

Fig. 3.11 presents the XRD and Raman spectra of the films deposited at 250 and 350 °C. According to XRD (Fig. 3.11a), the film grown at 250 °C has poor crystallinity, the main reflections belong to the $CuInS_2$ phase (JCPDS card-00-027-0159). An additional reflection at 2θ=26.4° (marked by 'x' in Fig. 3.11a) is recorded and it could belong to In_xS_y or $CuIn_5S_8$ phases [34]. The results for the 'x' phase are in good correspondence with the earlier results on spray-deposited $CuInS_2$ films [34, 65]. Deposition at 350 °C leads to narrowing of the reflections indicating an increase in the crystal size. The crystallite sizes of about 8 and about 20 nm have been calculated from the XRD patterns of sprayed films deposited at 250 and 350 °C, respectively. The XRD pattern of the film grown at 350 °C shows an additional diffraction peak at 2θ=30.5° belonging to the (222) reflection of the In_2O_3 phase (JCPDS card-00-006-0416). In_2O_3 phase has not been earlier detected by XRD in the sprayed $CuInS_2$ films deposited at temperatures T<400 °C. Appearance of the peaks belonging to In_2O_3 in the XRD pattern could be explained by better resolution of an advanced XRD apparatus and low deposition rate (Table 2.1).

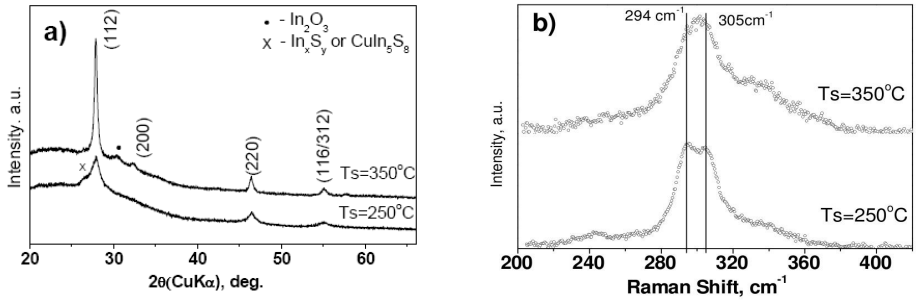

a) b)

Fig. 3.11. *a) XRD patterns and b) Raman spectra of as-sprayed at 250 ºC and 350 ºC CIS-1.0 films.*

Figure 3.11b shows the Raman spectra of as-deposited $CuInS_2$ films grown at 250 and 350 ºC. The obtained results show that the most intensive Raman band consists of two bands, A_1 band of chalcopyrite (CH) ordered compound at 294 cm^{-1} and A_1* band of Cu–Au (CA) ordered phase at 305 cm^{-1} [34]. Although the phase composition and crystallinity of CIS-1.0 films was strongly affected by the deposition temperature (Fig. 3.11a), the short-range ordering of sprayed

$CuInS_2$ films is similar and is almost independent of the deposition temperature in the temperature region of 250-350 °C (Fig. 3.11b).

3.2.2. Surface analysis of as-sprayed films

The XPS spectra of as-sprayed CIS-1.0 films deposited at 250 and 350 °C were recorded. The binding energies (BE) of $Cu2p_{3/2}$, $In3d_{5/2}$, S2p core levels located at 932.5 eV, 445.0 eV, 162.0 eV, respectively, were detected for both samples. These binding energies correspond to those of copper, indium and sulfur in spray deposited $CuInS_2$ films [10, **II**].

For the CIS-1.0 film deposited at 350 °C, the second $Cu2p_{3/2}$ core level peak at 935.0 eV and shake-up satellites in the BE region of 940-944 eV both characteristic of Cu^{2+} state [111], were recorded from the as-sprayed film surface (Fig. 3.12). Also, the second observed peak of S2p core level at BE=168.9 eV, corresponding to sulfur in the form of sulfates, was detected on the surface (Fig. 3.12). The O1s core level peaks at 532.0 and 530.0 eV BE, characteristic of oxygen in the form of adsorbed $(OH)^-$ groups and oxygen bonded to metal (Me-O) [109], respectively, were present in the XPS spectra recorded from the film surface (Fig. 3.12). The Cu2p peak at BE of 935 eV, S2p peak at 168.9 eV and O1s peak at 532.0 eV were not detected in the XPS spectra of the film after their Ar^+ sputtering.

In the case of the CIS-1.0 film deposited at 250 ºC, the secondary peaks of $Cu2p_{3/2}$ and S2p core levels with BE of 935.0 eV and 168.9 eV, respectively, were not detected on the film surface (XPS spectra of the films deposited at 250 °C are not presented). The O1s peak at BE=532.0 eV was present in the spectrum recorded from the as-sprayed film surface and refers to the surface contamination from the ambient. The O1s core level peak at BE=530.0 eV was on the noise level.

Also, weak response from Cl2p at BE=198.7 eV has been detected in the XPS spectra due to contamination originated from the metal chloride precursors. Content of chlorine impurity on the surface was about 1.0-1.5 at.% in the film deposited at 250 °C, its content dropped below 1 at.% in the film prepared at a higher temperature.

3.2.3. Elemental composition of as-sprayed films: XPS depth-profiling

Figure 3.12 presents the XPS spectra of $Cu2p_{3/2}$, O1s and S2p core levels of the CIS-1.0 film deposited at 350 °C after different Ar^+ ion etching cycles. The number of the Ar^+ sputtering cycles is given in the graphs: the upper spectrum is recorded from the as-sprayed surface, by increasing the number of etching cycles the signal is recorded from the film bulk region down to the substrate.

Due to similarity of In3d binding energies in $CuInS_2$ and in possible secondary phases, such as In_2O_3, In_2S_3 etc., the chemical shift of the In3d core level peak was not observed. Independent of the deposition temperature and profiling depth, the BE of $In3d_{5/2}$ is located at 445.0 eV.

There is no shift in the positions of $Cu2p_{3/2}$, $In3d_{5/2}$ (not shown) and S2p core level peaks in the film depth.

The intensity of O1s core level peak at BE=530.0 eV (Me-O) is decreasing from the film surface to the bulk. It can be observed that the Me-O peak intensity increases before the signal at BE=533.6 eV, characteristic of oxygen in silicates (in glass) [109], becomes apparent.

The positions as well as the intensities of $Cu2p_{3/2}$, $In3d_{5/2}$ and S2p core level peaks were close throughout the CIS-1.0 film deposited at 250 ºC.

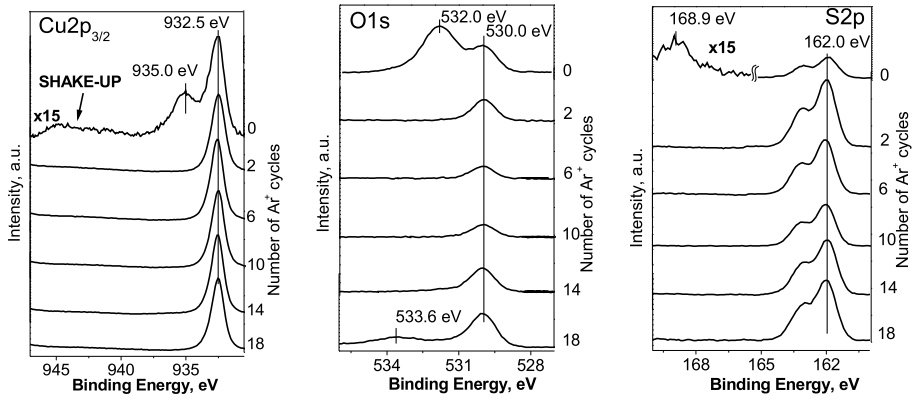

Fig. 3.12. *Cu2p, O1s and S2p core level spectra of the spray deposited CIS-1.0 film taken from the film surface and after different Ar^+ sputtering cycles. CIS-1.0 film was deposited at 350ºC. Spectra recorded on Kratos AXIS Ultra DLD.*

The atomic concentrations of detected elements were calculated from the integrated peak areas of $Cu2p_{3/2}$, $In3d_{5/2}$, O1s and S2p core level spectra using the formula 2.1. Content of oxygen was calculated from the O1s core level with BE=530.0 eV. The atomic concentrations of the elements vs. the number of Ar^+ ion sputtering cycles of CIS-1.0 films deposited at 250 and 350 ºC are presented in Fig. 3.13.

Atomic concentrations of the elements presented in Fig. 3.13a and b are not absolute values, as already mentioned in section 3.3 due to the absence of appropriate reference samples. Fig. 3.13a shows the results of the depth profiling analysis of the CIS-1.0 film deposited at 350 ºC. It can be seen that the distribution of the elements throughout the film could be divided into three regions. Non-uniform distribution of In and Cu is characteristic of the first

region, whereat [Cu]/[In] is much lower than 1. In the second region, the overall composition is still In-rich, but concentrations of In, Cu and O are almost constant and the concentration of sulfur starts to decrease. In the third region, the concentration of sulfur is decreasing from about 44 at.% to 30 at.% and is accompanied by an increase in the amount of oxygen (Me-O). The presence of the In_2O_3 phase was confirmed by XRD (Fig. 3.11a). The XPS depth profiling shows that the In_2O_3 phase is present throughout the film thickness. Furthermore, the amount of Me-O oxygen is increasing (and sulfur concentration is decreasing) before the signal from a glass substrate (Si) becomes apparent at about 15 Ar^+ sputtering cycles (Fig. 3.13a). Probably the In_2O_3 phase is easily formed in an initial stage of the film growth at this deposition temperature.

Concentration depth profiling of the CIS-1.0 film deposited at 250 ºC (Fig. 3.13b) shows homogeneous distribution of the Cu, In and S throughout the film. Content of oxygen (Me-O) in the film is about 1 at.%. Concentration of sulfur is

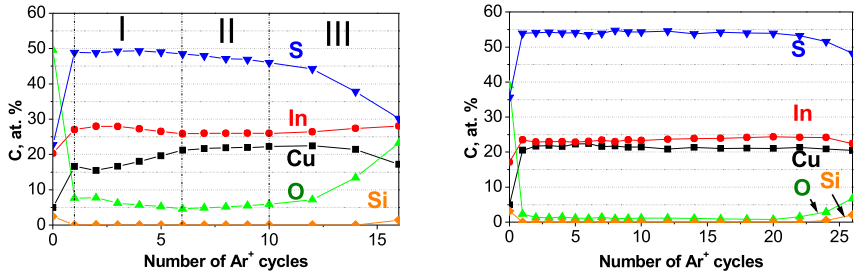

a) b)

Fig. 3.13. *The element concentration depth profiling in CIS-1.0 films deposited at a) 350°C and b) 250 °C onto glass substrates.*

above 50 at.% and refers to a sulfur-rich film compared to the stoichiometric $CuInS_2$. Obviously, secondary phases such as In_xS_y or $CuIn_5S_8$ could be present in the film deposited at 250 °C. This assumption is supported by the XRD pattern of the film (Fig. 3.11a) and literature data on $CuInS_2$ films deposited at low temperatures [10, 11, 108].

Summary

The as-sprayed CIS-1.0 films deposited from the solution with the precursor molar ratio [Cu]/[In]=1.0 at 350 °C are consisting of polycrystalline $CuInS_2$ with the crystallite size of about 20 nm. XRD pattern recorded on an advanced X-ray diffractometer indicate presence of In_2O_3 phase. Films grown at 250 °C are composed of low-crystalline $CuInS_2$ with the crystallite size below 10 nm and contain a secondary phase which could be an In_xS_y or the second Cu-In-S-ternary

compound. According to Raman spectroscopy studies, both the chalcopyrite (CH) and Cu-Au (CA) ordered $CuInS_2$ phases are present in the film, and the short-range ordering is almost independent of the growth temperature.
The results of the film composition study could be summarized following:

- According to the XPS results of the film deposited at 350 °C, the Cu^{2+} containing pieces are present only on the film surface, the film elemental composition in the film bulk region is graded as shown by depth profiling. The film contains oxygen (Me-O) ca 5-8 at.%. Oxygen is present in the form of In_2O_3, as also confirmed by XRD.
- XPS study showed that the $CuInS_2$ films with low amount of oxygen (1 at.% or less) and uniform distribution of Cu, In and S throughout the film thickness can be produced by the CSP method in air using the deposition temperature close to 250 °C.

3.3. Properties of H_2S treated $CuInS_2$ films deposited by CSP using the precursor molar ratio [Cu]/[In]=1.1 in solution

Results are published in papers [**I**] and [**II**].

3.3.1. Structure and optical properties of H_2S treated films

Figure 3.14 presents the XRD spectra of the films deposited from solutions with precursor molar ratio [Cu]/[In]=1.1 at 370 °C (CIS-1.1) after the heat treatment at 530 °C in an H_2S atmosphere. According to XRD, the main reflections belong to the $CuInS_2$ phase (JCPDS card 00-027-0159). The film is well-crystallized and shows preferred orientation of crystals along (112) plane. By annealing the mean crystallite size is increased from about 44 nm, characteristic of as-deposited film, to ca 90 nm, as calculated from the FWHM of the (112) diffraction peak.

H_2S treatment was found to increase the bandgap of the film. The as-sprayed CIS-1.1 film shows the optical energy gap of 1.44 eV (Section 3.1). After the

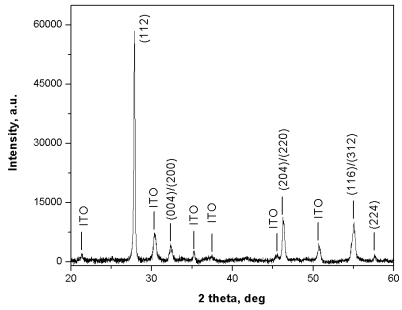

Fig. 3.14. *XRD pattern of CIS-1.1 films on the glass/ITO substrate annealed for 60 min at 530 °C in a flowing H_2S atmosphere, slow cooling to room temperature.*

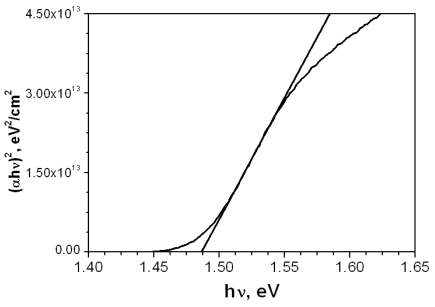

Fig. 3.15. *The plot of $(\alpha h\nu)^2$ vs. energy of CIS-1.1 film after treatment for 60 minutes at 530 °C in a flowing H_2S atmosphere, slow cooling.*

heat treatment in an H_2S atmosphere followed by slow cooling, the bandgap energy is 1.49 eV (Fig. 3.15).

In summary, post-deposition treatment at 530 °C in an H_2S atmosphere improves the crystal quality of the films, as also has been shown in the previous studies in our laboratory [34, 35] and by other research groups [11, 116].

3.3.2. Surface analysis of H_2S treated films

XPS measurements were performed for KCN-etched CIS-1.1 films (grown at 350 °C) after their annealing in an H_2S atmosphere.

$Cu2p_{3/2}$, $In3d_{5/2}$, S2p and Na1s core level spectra recorded from the film surface and after Ar^+ sputtering are presented in Fig. 3.16. The binding energies (BE) of $Cu2p_{3/2}$, $In3d_{5/2}$, S2p and Na1s core levels measured from the as-sprayed surface and after Ar^+ sputtering (35 min) are placed at 932.7 eV, 444.6 eV, 161.6 eV and 1072.7 eV, respectively. The presence of sodium could be explained by diffusion of sodium atoms from the substrate (soda-lime glass sheets) during the heat treatment at temperatures above 500 °C.

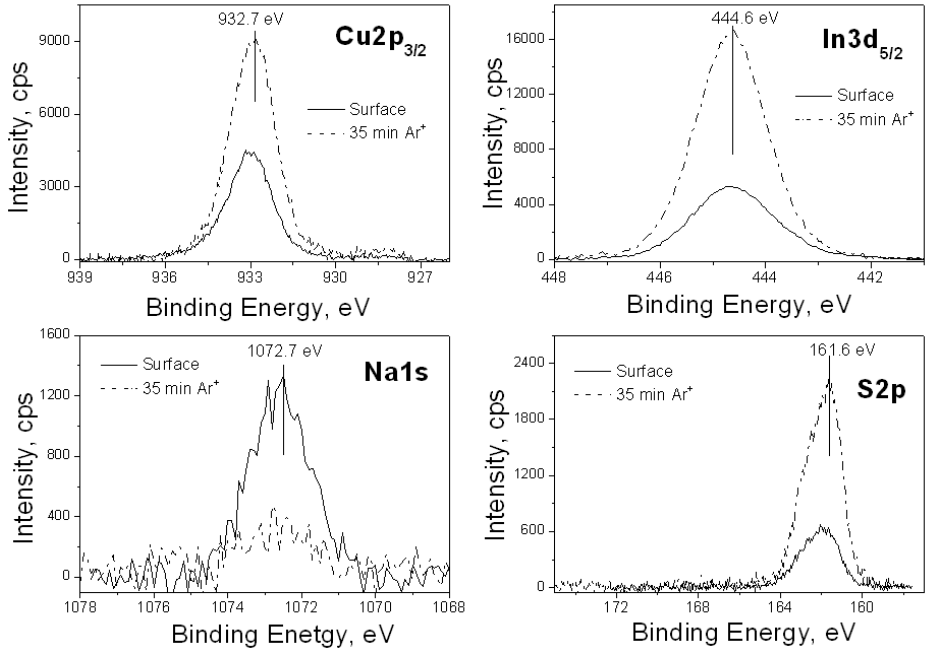

Fig. 3.16. *Cu2p$_{3/2}$, In3d$_{5/2}$, Na1s and S2p core levels spectra of CIS-1.1 film annealed in the H_2S atmosphere. $CuInS_2$ film was grown on glass substrate.*

This explanation is supported by an experiment using quartz substrates, as Na was not detected on the surface of the annealed $CuInS_2$ film grown on a quartz slide. After Ar^+ etching the intensities of the Cu, In and S peaks were increased due to removal of the highly Na-contaminated surface layer (Fig. 3.16). The position of Cu2p$_{3/2}$ core level peak (BE=932.7 eV) is independent of the depth profiling and is similar to that recorded in the depth of the as-deposited sample (See Fig. 3.5). BE of 932.7 eV for Cu2p$_{3/2}$ core level allows a speculation that a H_2S treated film is contaminated with some Cu^{2+} containing pieces [111]. The observation that prolonged etching in KCN solution detaches the film from the substrate, obviously due to the presence of the Cu_XS phase, is an indirect proof to the speculation made.

There is also no shift in In and S core level binding energies compared to as-sprayed films (Fig. 3.5). No signal from oxygen was detected. Therefore, indium oxide, present on the surface and bulk of the CIS-1.1 film prepared at 370 °C, was converted into In-sulfide during the H_2S treatment. Similar conclusion on the effect of post-deposition annealing in sulfur-containing atmosphere was made by Marsillac et al. for spray deposited $CuInS_2$ films [11], and later by Camus et al. for spray-ILGAR deposited $CuInS_2$ films [52]. Marsillac et al.

suggested that the In-sulfide phase is located on grain boundaries [11].

3.3.3. Elemental composition of H_2S treated $CuInS_2$ films

According to the EDS measurements of the CIS-1.1 sample after the H_2S treatment at 530 °C for 60 minutes, followed by a rapid cooling procedure, shows slightly In-rich composition (Cu=24.8 at.%, In=26.0 at.%, S=49.1 at.%) [**I**]. The sample treated at similar conditions, but slowly cooled down shows similar elemental composition (Cu=24.3 at.%, In=26.1 at.%, S=49.5 at.%) [**I**]. H_2S treatment increases sulfur concentration from 44.4 at.% (as-sprayed film) up to 49.3±0.2 at.%. The [S]/([In]+[Cu])=0.83 characteristic of as-deposited films is increased up to 0.97 after rapid cooling and 0.98 after slow cooling. Therefore, H_2S treatment independent of the cooling rate results in the films with improved stoichiometry.

According to the XRF measurements, also ILGAR-spray deposited $CuInS_2$ films show In-rich composition (Cu=24 at.%, In=26 at.%, S=50 at.%) after treatment in the H_2S atmosphere at 550 °C for 45 min [52]. Thus, elemental compositions of both of our CIS-1.1 films and ILGAR-spray deposited $CuInS_2$ films after the H_2S treatment at temperatures above 500 °C are very similar, as proved by EDS and XRF, respectively.

Elemental composition of the H_2S treated CIS-1.1 on the surface and at depth after 35 min of Ar^+ sputtering is given in Table 3.2.

The composition of the as-sprayed surface is highly In and S rich. As-sprayed CIS-1.1 film shows In/Cu=10.7 on the surface and In/Cu=2.5 at the depth after Ar^+ sputtering for 95 minutes (Table 3.1). After the H_2S treatment In/Cu=6.0 on the surface and In/Cu=1.6 at the depth obtained by Ar^+ sputtering for 35 minutes (Table 3.2). Higher values of In/Cu on the surface of the as-sprayed film compared to the H_2S treated film could be explained with sulfurization of the In-oxide phase into In_2S_3 during the heat treatment and its partial evolution due to relatively high vapor pressure at temperatures close to 500 °C [117]. According to XPS, the content of Na is higher on the surface than in the region below the surface. Very high content of Na in the H_2S treated film indicates diffusion of Na from the glass substrate into the film. Thus, soda-lime glass sheet is not a proper substrate material if sodium contamination should be avoided.

Nevertheless the atomic concentrations calculated from the XPS data are not absolute values due to missing of calibrated reference samples, it clearly shows that surface composition differs from that in the bulk and the film has graded elemental composition in film thickness, as it also was characteristic of as-sprayed films deposited at temperatures above 300 °C.

Table 3.2. *Elemental composition of CIS-1.1 films annealed at 530 °C in H_2S atmosphere for 60 minutes and slowly cooled to room temperature according to the XPS analysis*.*

	In, at.%	Cu, at.%	S, at.%	Na, at.%	In/Cu	S/(Cu+In)
Surface	18	3	60	19	6.0	2.9
After Ar^+ sputtering for 35 min	30	19	45	6	1.6	0.9

* Atomic concentrations of the elements presented in Table 3.2 are not absolute values due to absence of the reference sample

To summarize, the thermal treatment of CIS-1.1 films in H_2S atmosphere at 530 ºC has the following effects:

- increases the crystallite size from ca 44 nm, characteristic of as-deposited film, up to ca 90 nm according to XRD, and increases the optical bandgap from 1.44 eV (characteristic of as-deposited films) up to 1.49 eV as calculated from the optical transmittance spectra;
- removes oxygen from the film - indium oxide, originally present in as-deposited films grown at 370 °C, is converted into the indium sulfide;
- increase in sulfur content makes the film composition closer to the stoichiometric $CuInS_2$ - according to EDS results the [S]/([In]+[Cu]) in the film is increased from 0.83 (as-deposited CIS-1.1 film) to 0.98 after the H_2S treatment. Increase in [S]/([In]+[Cu]) ratio is also confirmed by XPS;
- causes diffusion of Na atoms from a glass substrate into the film;
- no effect on a secondary Cu-containing phase present in bulk of sprayed CIS-1.1 film, graded elemental composition in film thickness preserved.

3.4. Properties of H_2S treated $CuInS_2$ films deposited by CSP using the precursor molar ratio [Cu]/[In]=1.0 in solution

Results are published in paper [**I**].

3.4.1. Structure and optical properties of H_2S treated films

Figure 3.17 shows that the main reflections of the H_2S treated CIS-1.0 film belong to the $CuInS_2$ phase (JCPDS card 00-027-0159). The film is well-crystallized and shows preferred orientation along (112) plane. By annealing in

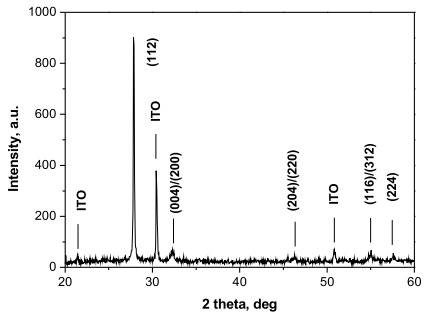

Fig. 3.17. *XRD pattern of the CIS-1.0 film on the glass/ITO substrate annealed for 60 min at 530 °C in a flowing H_2S atmosphere, slow cooling.*

an H_2S atmosphere at 530 °C for about 120 min with rapid cooling, the mean size of crystallites is increased from about 20 nm, characteristic of as-deposited films, to ca 90 nm as calculated from the FWHM of the (112) diffraction peak.

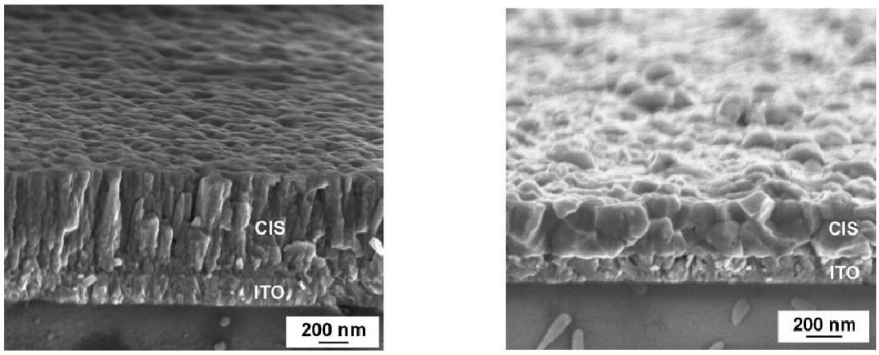

a) b)

Fig. 3.18. *SEM cross-sectional micrographs of CIS-1.0 films on glass/ITO substrate, a) as-deposited CIS-1.0 film; b) CIS-1.0 film annealed for 60 minutes at 530 °C in a flowing H_2S atmosphere, slow cooling.*

The crystallite size calculated from the XRD pattern is similar to that of annealed CIS-1.1 films (see section 3.3). The development of grains is characterized by the SEM cross-sectional micrographs (Fig. 3.18). It could be seen that H_2S treated films at 530 °C for 60 min with slow cooling composed of grains with sizes up to 300 nm. Thus, post-deposition treatment at 530 °C in an H_2S atmosphere improves the crystal quality of the films, as was shown in section 3.3. The H_2S treatment was found to increase the bandgap energy from 1.41 eV to 1.47 eV. The increase in the energy gap is reported for $CuInS_2$ films

obtained by the vacuum thermal evaporation method and subjected to annealing in sulfur atmosphere [118].

3.4.2. Elemental composition of H_2S treated films

Elemental composition of H_2S treated CIS-1.0 films was determined by EDS. Results are presented in Table 3.3.

Table 3.3. *Elemental composition of the CIS-1.0 films annealed at 530 °C in an H_2S atmosphere according to EDS. CIS-1.0 films were deposited at 370 °C.*

Cooling	Type of surface	Cu, at.%	In, at.%	S, at.%	Na, at.%	Cu/In	S/(Cu+In)
Rapid	Flat	23.1	24.1	48.3	4.5	0.96	1.02
	Crystals	0.5	24.8	49.2	25.5	0.02	1.94
Slow	Flat	25.6	24.5	46.3	3.6	1.04	0.92

According to EDS, the CIS-1.0 and CIS-1.1 films deposited at 370 °C show comparatively similar elemental composition after the H_2S treatment at 530 °C for 60 minutes [**I,** unpublished data]. H_2S treatment increases sulfur concentration from 44.5 at.% (as-sprayed film) to 48.3 at.% and to 46.3 at.% using rapid or slow cooling, respectively. The [S]/([In]+[Cu])=0.83 characteristic of as-deposited films is increased to 1.02 (flat surface) by H_2S treatment using rapid cooling and to 0.92 using slow cooling (Table 3.3) [**I**, unpublished data]. Interestingly, the cooling rate has an influence on the composition of CIS-1.0 films. The use of rapid cooling from the heating temperature to the room temperature results in a flake-like crystals, mainly composed of Na, In and S, on the film surface (Table 3.3). Such crystals were not detected on the surface of H_2S-treated CIS-1.1 films.

It could be speculated that another In-rich ternary ($Cu_xIn_yS_z$) or an In-S phase could be present in as-deposited CIS-1.0 films (Fig. 3.11), as also discussed in literature [110, 116]. Sodium diffuses from the glass substrate and reacts with an In-S compound, and as a result, a Na-In-S compound is formed. Interestingly, flake-like crystals were not observed on the surface of H_2S treated CIS-1.0 films when slow cooling rate was used.

According to the XPS study of as-deposited CIS-1.0 films grown at 350 °C, high content of oxygen bonded to metal ([O]>5 at.%), In/Cu>1, and grading of the elements concentration through the film thickness (section 3.2) is similar to that recorded for as-deposited CIS-1.1 films (section 3.1). Probably, the indium

oxide phase present in the CIS-1.0 film deposited at temperatures above 300 °C is converted into an indium sulfide phase as proved for H_2S treated CIS-1.1 films.

The fact that the electrical resistivity of H_2S treated films ($\rho \approx 10^5$ Ωcm) is higher than that of as-deposited films ($\rho \approx 10^4$ Ωcm) despite larger crystallites and slightly higher concentration of charge carriers, supports the speculation that the sulfurized phase on grain boundaries [11] is responsible for increased electrical resistivity.

It was shown in section 3.2 that CIS-1.0 films deposited at 250 °C contain low amount of oxygen ([O]<1 at.%) and show uniform distribution of the elements through the film thickness. It could be expected that the post-deposition treatment of $CuInS_2$ films deposited at low temperature will result in proper thin film absorber material.

Summary

To summarize, thermal treatment of CIS-1.0 films in an H_2S atmosphere at 530 ºC has the following effects:

- increases crystallite size from ca 20 nm, characteristic of as-deposited film, up to ca 90 nm according to XRD, and increases the optical bandgap from 1.44 eV (characteristic of as-deposited films) up to 1.47 eV as calculated from the optical transmittance spectra;
- increase in sulfur content makes the film composition closer to the stoichiometric $CuInS_2$ - according to EDS results the [S]/([In]+[Cu]) in the film is increased from 0.83 (as-deposited CIS-1.0 film) to 1.02 (flat surface) after the H_2S treatment;
- causes diffusion of Na atoms from a glass substrate into the film. The formation of flake-like crystals with the composition of Na:In:S=1:1:2 on the surface of an annealed film shows that probably the as-deposited CIS-1.0 film contains a secondary phase which forms a Na-In-S compound as a result of Na diffusion.

In brief, it was shown that the post-deposition thermal treatment in an H_2S atmosphere has potential to improve the structural and optical properties, increase the purity and sulfur content in sprayed $CuInS_2$ films. Contrarily, electrical resistivity of the films obtained by spray at temperatures above 300 °C in air is increasing by the H_2S treatment. XPS study confirms that an oxide phase is present in as-deposited films. Post-deposition treatment in H_2S atmosphere turns the oxide into the sulfide while non-uniform distribution of the elements in the thickness of as-deposited films is preserved over the H_2S treatment. Thus, the spray procedure should be carried out using preparation conditions where the formation of an oxide phase is suppressed. We believe that the post-deposition

thermal treatment in H_2S atmosphere of low oxygen content CIS-1.0 will lead to better film quality and properties, respectively.

3.5. Sprayed $CuInS_2$ absorber based nanostructured solar cell

In the thesis, we describe the possibility for using of sprayed $CuInS_2$ films in structured solar cells as an absorber layer.
Results are published in paper [**IV**], preparation of the solar cell is described in [**V**].

3.5.1. Structure of nanostructured solar cell on ZnO nanorod layer

A nanostructured cell on the spray-deposited ZnO nanorod layer using a thin layer of sprayed $CuInS_2$ as an absorber layer has been developed in our group. Figure 3.19 presents a sketch of the preparation of a structured solar cell.

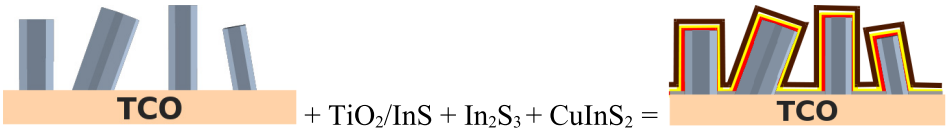

Fig. 3.19. *Sketch of the preparation of a nanostructured solar cell based on sprayed $CuInS_2$ absorber.*

A provisional US patent application "Photovoltaic Cell based on ZnO nanorods" was submitted 09.07.2007 [119]. Thereupon, international patent application was submitted 09.07.2008 [**V**]. Currently patent pending is running in the USA (US12/668443, 11.01.2010), in Europe (EP08773333.3, 01.02.2010), in the People Republic of China (CN101861654A, 22.02.2010) and in the Republic of India (IN 500/KOLNP/2010, 08.02.2010) [120].

In the structured solar cell developed, the component layers, such as ZnO nanorod layer, In_2S_3 buffer layer and $CuInS_2$ absorber layer, are prepared by the CSP technique. Both In_2S_3 and $CuInS_2$ in the spray process are obtained by spray of acidic solutions. Acidic solutions are also used when deposited by another solution based method, for example, by CBD [48]. Thus, chemical instability of ZnO in an acidic medium should be taken into consideration as ZnO nanocrystals could be dissolved. To protect ZnO nanorods from chemical dissolution, a thin layer of TiO_2 or 'In-S' should be deposited onto ZnO nanorods as a chemical barrier layer. TiO_2 barrier layer was deposited by different methods, such as sol-gel dip-coating [**IV, V**], sol-gel spray or ALD [121]. Thickness of the TiO_2 layer is a critical parameter controlling the cell

efficiencies, since starting from some thickness it starts to impede the transport of carriers resulting in s-shaped I-V curves [121]. TiO_2 film thickness could be controlled by the number of dipping cycles [**V**], the number of spray pulses or the number of ALD deposition cycles [121]. Instead of TiO_2 we proposed to use a very thin layer of indium sulfide ('In-S') deposited from the spray solution with low acidity [**IV, V**]. For that purpose diluted $InCl_3$ solutions with $[In^{3+}] > 10^{-4}$ mol/l should be used.

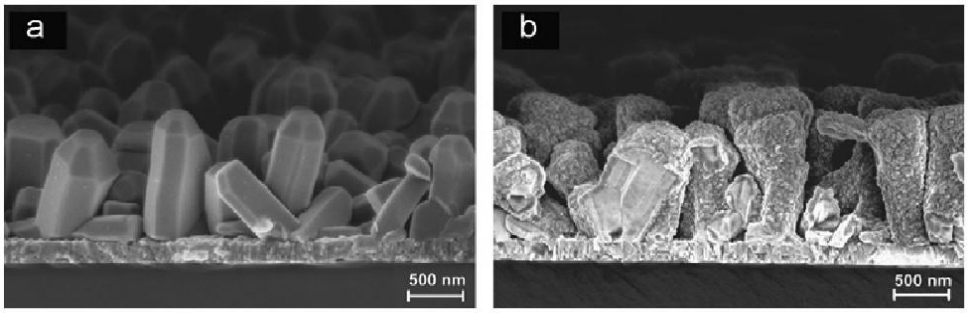

Fig. 3.20. *SEM cross-sections of a) a spray deposited ZnO nanostructured layer on an indium tin oxide (ITO) covered glass substrate, and b) the solar cell structure ($ITO/ZnO_R/TiO_2/In_2S_3/CuInS_2$) before conducting.*

SEM cross-sectional micrographs in Figs 3.20a and 3.20b present the ZnO nanorod layer and complete solar cell structure before applying the contact to the absorber layer, respectively. As can be seen, ZnO crystals in the solar cell structure are covered with a $CuInS_2$ layer with a thickness lower than 50 nm. Thus, the solar cell formed could be classified as an ETA solar cell. $CuInS_2$ layer thickness is almost uniform on top and side planes of the ZnO crystals, as shown by the cross-section of one broken crystal (Fig. 3.20b).

3.5.2. Solar cell output characteristics

I–V curves of a flat and nanostructured cells are presented in Fig. 3.21, solar cell output parameters of flat and structured solar cells with different blocking layers are summarized in Table 3.3.

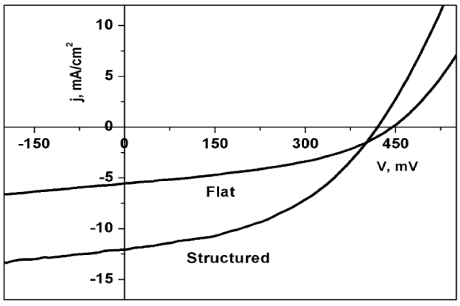

Fig. 3.21. *Current-voltage characteristics of a flat cell (ITO/TiO_2/In_2S_3/$CuInS_2$) and a nanostructured cell (ITO/ZnO_{rod}/TiO_2/In_2S_3/$CuInS_2$) under halogen lamp illumination of 100 mW/cm^2.*

Solar cell output parameters show that the current density (jsc) of the cell built on ZnO nanorods is at least two times higher than that of the flat cell prepared simultaneously with the structured one (Fig. 3.21, Table 3.3). Open

Table 3.3. *Output characteristics of flat and nanostructured solar cells under the halogen lamp illumination intensity of 100 mW/cm^2.*

Cell no.	Cell structure	Blocking layer	Voc, mV	J , mA/cm^2	FF, %	Eff., %
1	Flat	TiO_2	445	5.5	41	1.0
2	Structured		425	12	43	2.2
3	Flat	'In-S'	485	4.3	63	1.3
4	Structured		455	9.1	60	2.5

circuit voltage (V_{oc}) is slightly higher in the case of flat cells independent of the barrier layer used (Table 3.3). This result could be explained by a higher recombination in the structured cells. Additionally, the thicknesses of blocking and buffer layers could be different in flat and structured cells. Figure 3.22 presents both the EBIC and SEM images of flat and nanostructured cells. According to the EBIC and SEM images, the p–n junction is continuous and follows the shape of ZnO crystals in the case of a structured cell. It can be seen that the p–n junction area of a structured cell is larger than that of a flat cell, and the current collection region is almost expanded into the $CuInS_2$ absorber. Nanostructured solar cells based on ZnO nanorod layer show higher conversion efficiencies due to increased current density caused by increased p-n junction area.

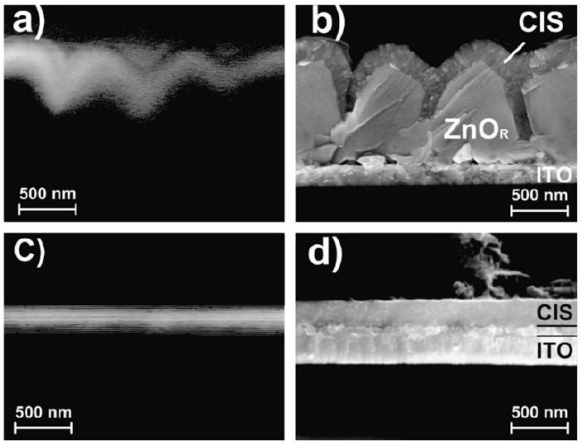

Fig. 3.22. *a) Electron beam induced current (EBIC) and b) SEM cross-sectional views of the structured cell ITO/ZnO_{rod}/TiO_2/In_2S_3/$CuInS_2$. c) EBIC and d) SEM images of the flat cell prepared in the same batch are presented for comparison.*

With our cells were proved the concept of an advantage of a nanostructured solar cell with larger active area compared to a flat thin film cell.

Nanostructured solar cells based on sprayed ZnO nanorod array and using CSP-$CuInS_2$ as an absorber layer showed conversion efficiencies of 2.5 % in the first stage of studies [**IV, V**, 121]. By further development of a nanostructured solar cell, recently the light-to-electricity conversion efficiency of 4.17 % [122] was reached with an optimized structure using extremely thin absorber layer, as well as buffer and blocking layers with optimized thicknesses [121, 122]. According to our best knowledge it is the highest value reported to date for the ZnO nanorod based solar cells with an inorganic absorber layer. For comparison, efficiency less 1 % is reported for a nanostructured solar cell based ZnO nanorods with sprayed $CuInS_2$ absorber [127] and of 2.3 % with CBD-CdSe absorber [124].

Summary

The results from solar cell preparation and characterization could be summarized as follows:

- It has been shown that the sprayed CIS-1.0 film could be used as an absorber layer in a nanostructured solar cell based on ZnO nanorod array with structure: ITO/ZnO_{rod}/('In-S' or TiO_2)/In_2S_3/$CuInS_2$.
- According to the EBIC and SEM images, the p–n junction of the nanostructured solar cell (glass/ITO/ZnO_{rod}/TiO_2/In_2S_3/$CuInS_2$) is continuous

and follows the shape of ZnO crystals. The current density in a nanostructured cell was at least two times higher than that obtained with a flat cell (glass/ITO/TiO_2/In_2S_3/$CuInS_2$). Higher current density, leading to higher conversion efficiency, was mainly due to the increased p-n junction area.

- The nanostructured solar cell with the structure of glass/TCO/ZnO_{rod}/'In-S' /In_2S_3/$CuInS_2$ was prepared by the in-line chemical spray pyrolysis technique with the conversion efficiency of 2.5 %. Recent development by our group results in the conversion efficiency of 4.17 %. According to our best knowledge it is the highest value reported to date for the ZnO nanorod based solar cells with an inorganic absorber layer.

4. CONCLUSIONS

Results of the thesis could be summarized as follows:

1. Copper indium disulfide films grown by the chemical spray pyrolysis (CSP) method at temperatures around 350 °C, using aqueous solutions of $CuCl_2$, $InCl_3$ and $SC(NH_2)_2$ with [Cu]/[In] molar ratio of 1.1 or 1.0, are composed of polycrystalline $CuInS_2$ according to XRD, but contain oxygen bonded to a metal, probably in the form of In_2O_3 phase on the film surface and in bulk, as confirmed by XPS studies. Deposition at temperatures close to 250 °C results in films with low oxygen content (≤1 at.%), the films deposited from solutions with the [Cu]/[In] molar ratio of 1.0 consist of $CuInS_2$ with low crystallinity, and could contain an additional phase according to XRD.

2. According to the surface analysis studies, $CuInS_2$ films deposited by CSP at temperatures close to 350 °C contain additional copper (Cu^{2+}) and sulfur containing phases such as copper sulfide and sulfate on the surface of as-sprayed films independent of the [Cu]/[In] molar ratio in solution. The Cu_xS phase is present in bulk of the film deposited from Cu-rich solution. KCN-treatment removes the Cu_xS phase from the film surface. The Cu^{2+} containing phases were not detected in the film deposited at 250 °C using the [Cu]/[In] molar ratio of 1.0 in spray solution.

3. According to the XPS quantitative elemental analysis from Ar ion etched surfaces, sprayed $CuInS_2$ films grown at temperatures close to 350 °C show graded distribution of the elements (Cu, In, S, O) in the film thickness independent of the precursor molar ratio ([Cu]/[In]) in the spray solution. This observation explains differences in the Cu/In atomic ratio in the films determined by polarographic and EDS analyses. Deposition at lower temperatures, close to 250 °C, results in a uniform distribution of the elements (Cu, In, S) in the film thickness.

4. Post-deposition thermal treatment of sprayed $CuInS_2$ films at 530 °C in the H_2S atmosphere significantly improves the film quality, increasing the crystallite size and optical bandgap, chemical analysis shows removal of chlorine and oxygen, and an increase in sulfur content. According to EDS, the films with elemental composition close to that of $CuInS_2$ have been formed. XPS study confirms that metal oxide is converted into metal sulfide, while non-uniform distribution of the elements in the film thickness of as-sprayed film is preserved upon the H_2S treatment. Diffusion of Na from the substrate into the film occurs during the thermal treatment if soda-

lime glass is used as a substrate.

5. Results of the chemical composition studies of sprayed $CuInS_2$ films showed that deposition of an absorber layer for solar cells by CSP in air should be made at possibly low growth temperatures, at about 250 °C, to keep the formation of oxide phases possibly low and elemental composition in the film thickness uniform. This condition is valid in spite of the fact that the films grown at low temperature from solutions with the [Cu]/[In] molar ratio of 1.0 have small crystallite size, and could contain a high amount of chlorine residues originated from starting chemicals. The crystallite size could be increased and chlorine content decreased by post-deposition thermal treatment. Further studies on the composition of $CuInS_2$ films deposited at low temperature using Cu-rich solutions (Cu/In=1.1) and the effect of post-deposition treatment on the properties of the films deposited at low temperature are needed to clarify the preference of the [Cu]/[In] molar ratio in the spray solution.

6. $CuInS_2$ absorber layer prepared by the CSP method at temperatures below 300°C, using aqueous solutions of $CuCl_2$, $InCl_3$ and $SC(NH_2)_2$ with the [Cu]/[In] molar ratio of 1.0, proved its working ability in a nanostructured solar cell based on a ZnO nanorod array. The light-to-electricity conversion efficiency of 2.5 % was achieved with a structure of ITO/ZnO_{rod}/blocking layer/In_2S_3/$CuInS_2$, entirely prepared by CSP. Further development of a nanostructured solar cell, using an as-sprayed extremely thin $CuInS_2$ absorber layer, resulted in the conversion efficiency of 4.17 %.

ACKNOWLEDGEMENTS

This thesis is based on the experimental work carried out at the Department of Material Science, Tallinn University of Technologies.

I want to thank my supervisor, Leading research scientist Dr. Malle Krunks, Head of the Laboratory of Thin Film Technologies, for her excellent guidance, continuous support and fruitful discussions during these years.

I want to thank Professor Enn Mellikov, Head of the Department of Materials Science, for giving me the possibility to carry out this doctoral thesis, and for useful remarks and discussion.

I want to thank Professor Andres Öpik, Dean of the Faculty of Chemical and Materials Technology, for continuous support and valuable advice.

I would like to thank members of the research group, Dr. Tatjana Dedova, Dr. Ilona Oja Acik for their collaboration and help, special thanks are due to Dr. Arvo Mere for continuous useful remarks and discussions.

It was a pleasure for me to work with Mr. Mati Danilson, Dr. Vida Kazlauskiene, and Dr. Leonard Matisen. I also want to thank them for their help in XPS measurements and for useful discussions.

I wish to express my gratitude to Mrs. Reet Nisumaa for AFM study and Dr. Olga Volobujeva for SEM and EBIC measurements, and for useful remarks and discussion. I am thankful to Dr. Valdek Mikli for the EDS analysis.

I would like to acknowledge the financial support by the Estonian Ministry of Education and Research (SF0142515s03, SF0140092s08), Estonian Science Foundation (grants ETF6954, ETF5612), Estonian Doctoral School of Materials Science and Materials Technology and funding from Estonian Graduate School of ”Functional Materials and Processes“ received from the European Social Fund under project 1.2.0401.09-0079.

My warmest thanks belong to my family.

Atanas Katerski

REFERENCES

1. M.A. Green, *Energy Policy* 28 (2000) 989.
2. K. Ramanathan, M.A. Contreras, C.L. Perkins, S. Asher, F.S. Hasoon, J. Keane, D. Young, M. Romeo, W. Metzger, R. Noufi, J. Ward, A. Duda, *Prog. Photovolt.: Res. Appl.* 11 (2003) 225.
3. X. Wu, J. Keane, R. Dhere, C. DeHart, A. Duda, T.Gessert, D. Levi and P. Sheldon, *Proc. 17th European Photovoltaic Solar Energy Conference* (Munich, Germany, Oct. 2001), 995-1000, WIP, Munich (2002).
4. J. Klaer, R. Klenk, H. W. Schock, *Thin Solid Films* 515 (2007) 5929.
5. R. Klenk, J. Klaer, R. Scheer, M.Ch. Lux-Steiner, I. Luck, N. Meyer, U. Rühle, *Thin Solid Films* 480-481 (2005) 509.
6. B. O'Regan, M. Grätzel, *Nature* 353 (1991) 737.
7. J.L. Shay, J.H. Wernick, *Ternary Chalcopyrite Semiconductors: Growth, Electronic Properties, and Applications,* Pergamon Press, New York, Oxford, 1975.
8. A.N. Tiwari, D.K. Pandya, K.L. Chopra, *Thin Solid Films* 130 (1985) 217.
9. A.N. Tiwari, D.K. Pandya, K.L. Chopra, *Solar Cells* 22 (1987) 263.
10. M.C. Zouaghi, T. Ben Nasrallah, S. Marsillac, J.C. Bernède, S. Belgacem, *Thin Solid Films* 382 (2001) 39.
11. S. Marsillac, M.C. Zouaghi, J.C. Bernède, T. Ben Nasrallah, S. Belgacem, *Sol. Energy Mater. Sol. Cells* 76 (2003) 125.
12. K.S. Ramaiah, V.S. Raja, *Scripta Mater.* 44 (2001) 771.
13. J. Alvarez-Garcia, PhD Thesis, University of Barcelona, Barcelona, Spain, 2002.
14. M. Krunks, J. Madarász, L. Hiltunen, R. Mannonen, E. Mellikov, L. Niinistö *Acta Chem. Scand.* 51 (1997) 294.
15. R. Scheer, K. Diesner, H.J. Lewerenz, *Thin Solid Films* 268 (1995) 130.
16. R. Scheer, M. Alt, I. Luck, H.J. Lewerenz, *Sol. Energy Mater. Sol. Cells* 49 (1997) 423.
17. A.K. Siemer, J. Klaer, I. Luck, J. Bruns, R. Klenk, D. Bräunig, *Sol. Energy Mater. Sol. Cells* 67 (2001) 159.
18. J. Álvarez-García, A. Pérez-Rodríguez, A. Romano-Rodríguez, L. Calvo-Barrio, B. Barcones, J.R. Morante, K. Siemer, I. Luck, R. Klenk, *Thin Solid Films* 387 (2001) 219.
19. A. Antony, A.S. Asha, R. Yoosuf, R. Manoj, M.K. Jayaraj, *Sol. Energy Mater. Sol. Cells* 81 (2004) 407.
20. J. Klaer, J. Bruns, R. Henninger, K. Siemer, R. Klenk, K. Ellmer, D. Braunig, *Semicond. Sci. Technol.* 13 (1998) 1456.

21. K.S. Ramajah, V.S. Raja, *Scripta Mater.* 44 (2001) 771.
22. T.T. John, K.C. Wilson, P.M. Ratheesh Kumar, C. Sudha Kartha, K.P. Vijayakumar, Y. Kashiwaba, T. Abe, Y. Yasuhiro, *Phys. Stat. Sol. (a)* 202 (2005) 79.
23. S. Zweigart, S.M. Sun, G. Bilger, H.W. Schock, *Sol. Energy Mater. Sol. Cells* 41-42 (1996) 219.
24. F. Lenzmann, M. Nanu, O. Kijatkina, A. Belaidi, *Thin Solid Films* 451 – 452 (2004) 639.
25. O. Kijatkina, M. Krunks, A. Mere, B. Mahrov, L. Dloczik, *Thin Solid Films* 431 – 432 (2003) 105.
26. D. Braunger, D. Hariskos, T. Walter, H. W. Schock, *Sol. Energy Mater. Sol. Cells* 40 (1996) 97.
27. H.J. Lewerenz, *Sol. Energy Mater. Sol. Cells* 83 (2004) 395.
28. P. Villiams, M. A. Prince, H. Okamoto, *Handbook of Ternary Alloy Phase Diagrams,* vol. 7, ASM International, 1995.
29. J. J. M. Binsma, L.J. Gilling and J. Bloem, *J. Cryst. Growth* 50 (1980) 429.
30. L. Makhova, R. Szargan, I. Konovalov, *Thin Solid Films* 472 (2005) 157.
31. International Centre for diffraction Data (ICDD), PDF-2 Release 2008.
32. J. Álvarez-García, J. Marcos-Ruzafa, A. Pérez-Rodríguez, A. Romano-Rodríguez, J. R. Morante, R. Scheer, *Thin Solid Films* 361-362 (2000) 208.
33. T. Riedle, PhD Thesis, Technical University of Berlin, Berlin, Germany, 2002.
34. I. Oja, M. Nanu, A. Katerski, M. Krunks, A. Mere, J. Raudoja, A. Goossens, *Thin Solid Films* 480-481 (2005) 82.
35. A. Mere, Ph.D. Thesis, Tallinn University of Technology, Estonia, 2006.
36. J. Álvarez-García, PhD Thesis, University of Barcelona, Barcelona, Spain, 2002.
37. R. Scheer, R. Klenk, J. Klaer, I. Luck, *Sol. Energy* 77 (2004) 777.
38. B.R. Pamplin, *Prog. Cryst. Growth Ch.* 1 (1979) 395.
39. P. Raja Ram, R. Thangaraj, A. K. Sharma, O. P. Agnihotri, *Sol. Cells* 14 (1985) 123.
40. R.P.V. Lakshmi, R. Venugopal, D.R. Reddy, B.K. Reddy, *Solid State Commun.* 82 (1992) 997.
41. C. Messaoudi, H. Bihri, D. Sayah, M. Cedene, M. Abd-Lefdil, *J. Mater. Sci. Lett.* 11 (1992) 1234.
42. M. Ortega-López, A. Moralez-Acevedo, *25th IEEE PVSC*, Washington, May 13-17, 1996, p. 13.
43. M. Krunks, V. Mikli, O. Bijakina, E. Mellikov, *Appl. Surf. Sci.* 142 (1999) 356.
44. M. Krunks, O. Bijakina, T. Varema, V. Mikli, E. Mellikov, *Thin Solid Films* 338 (1999) 125.

45. K. Subba Ramaiah, V. Sundara Raja, *J. Mater. Sci. Mater. Electron.* 10 (1999) 145.
46. G. Hodes, T. Engelhard, J.A. Turner, D. Cahen, *Sol. Energy Mater.* 12 (1985) 211.
47. S. Nakamura, A. Yamamoto, *Sol. Energy Mater. Sol. Cells* 49 (1997) 415.
48. S. Bini, K. Bindu, M. Lakshmi, C. Sudha Kartha, K.P. Vijayakumar, Y. Kashiwaba, T. Abe, *Renew. Energ.* 20 (2000) 405.
49. S. Mahmoud, A.-H. Eid, *Fizika A* 6 (1997) 171.
50. Y. Jiang, Y. Wu, X. Mo, W. Yu, Y. Xie, Yitai Qian, *Inorg. Chem. 39 (*2000) 2964.
51. M. Bär, Ch.-H. Fischer, H.-J. Muffler, S. Zweigart, F. Karg, M.C. Lux-Steiner, *Sol. Energy Mater. Sol. Cells* 75 (2003) 101.
52. C. Camus, N.A. Allsop, S.E. Gledhill, W. Bohne, J. Röhrich, I. Lauermann, M.C. Lux-Steiner, Ch.-H. Fischer, *Thin Solid Films* 516 (2008) 7026.
53. M. Winkler, O. Tober, J. Penndorf, K. Szulzewsky, D. Röser, G. Lippold, K. Otte, *Thin Solid Films* 361-362 (2000) 273.
54. J. Serhan, Z. Djebbour, A. Darga, D. Mencaraglia, N. Naghavi, G. Renou, D. Lincot, J.-F. Guillemoles, *Sol. Energy Mater. Sol. Cells* 49 (1997) 415.
55. R.R. Chamberlin, J.S. Skarman, *J. Electrochem. Soc.* 113 (1966) 86.
56. J.B. Mooney and S.B. Radding, *Ann. Rev. Mater. Sci.* 12 (1982) 81.
57. T. Dedova, Ph.D. Thesis, Tallinn University of Technology, Estonia, 2008.
58. K. Ernits, Ph.D. Thesis, Tallinn University of Technology, Estonia, 2009.
59. S.C.G. Leeuwenburgh, J.G.C. Wolke, J. Schoonman, J.A. Jansen, *Biomaterials* 25 (2004) 641.
60. G. Cao, *Nanostructures and nanomaterials: synthesis, properties and applications,* London, Imperial College Publishers, 2000, p. 451.
61. N. Golego, PhD. Thesis, University of Guelph, Canada, 1998.
62. M. Krunks, T. Dedova, I. Oja Açik, *Thin Solid Films* 515 (2006) 1157.
63. M. Krunks, E. Mellikov, E. Sork, *Thin Solid Films* 145 (1986) 105.
64. A.K. Raturi, R. Thangaraj, P.Raja Ram, B.B. Tripathi, O.P. Agnihotri, *Thin Solid Films* 106 (1983) 257.
65. M. Krunks, V. Mikli, O. Bijakina, H. Rebane, A. Mere, T. Varema, E. Mellikov, *Thin Solid Films* 361-362 (2000) 61.
66. K. Murakami, K. Nakajima, S. Kaneco, *Thin Solid films* 515 (2007) 8632.
67. I. Oja Acik, A. Junolainen, V. Mikli, M. Danilson, M. Krunks, *Appl. Surf. Sci.* 256 (2009) 1391.
68. http://www.spdlab.com
69. P. Bombicz, I. Mutikainen, M. Krunks, T. Leskelä, J. Madarász, L. Niinistö, *Inorg. Chim. Acta* 357 (2004) 513.
70. P. Bombicz, J. Madarász, M. Krunks, L. Niinistö, G. Pokol, *J. Coord. Chem.* 60 (2007) 457.

71. M. Krunks, T. Leskelä, R. Mannonen, L. Niinistö, *J. Therm. Anal. Cal.* 53 (1998) 355.
72. M. Krunks, T. Leskelä, R. Mannonen, L. Niinistö, *J. Therm. Anal. Cal.* 56 (1999) 479.
73. O. Kijatkina, Ph.D. Thesis, Tallinn University of Technology, Estonia, 2004.
74. M. Krunks, T. Leskelä, L. Niinistö, *Jpn. J. Appl. Phys.* 39 (2000) 181.
75. I. Oja Acik, K. Otto, K. Tõnsuaadu, A. Katerski, L. Niinisto, M. Krunks, In: *Proceedings 10th European Symposium on Thermal Analysis and Calorimetry*, Aug. 22-27, 2010, Rotterdam, The Netherlands.
76. R. Scheer, *Res. Trends Vac. Sci. Technol.* 2 (1997) 77.
77. U. Störkel, M. Aggour, C.P. Murrell, H.J. Lewerenz, *Thin Solid Films* 387 (2001) 182.
78. W. Hirpo, S. Dhingra, A.C. Sutorik, M.G. Kanatzidis, *J. Am. Chem. Soc.* 115 (1993) 1597.
79. J.A. Hollingsworth, W.F. Buhro, A.F. Hepp, P.P. Jenkins, M.A. Stan, *Mat. Res. Soc. Symp. Proc.* 495 (1998) 171.
80. J.A. Hollingsworth, A.F. Hepp, W.E. Buhro, *Chem. Vap. Depos.* 5 (1999) 105.
81. J. D. Harris, K. K. Banger, D. A. Scheiman, M. A. Smith, M. H.-C. Jin, A. F. Hepp, *Mat. Sci. Eng. B*98 (2003) 150.
82. M. Krunks, O. Kijatkina, H. Rebane, I. Oja, V. Mikli, A. Mere, *Thin Solid Films* 403-404 (2002) 71.
83. M. Krunks, O. Bijakina , V. Mikli , H. Rebane, T. Varema , M. Altosaar , E. Mellikov, *Sol. Energy Mater. Sol. Cells* 69 (2001) 93.
84. M. Ortega-López, A. Morales-Acevedo, *Thin Solid Films* 330 (1998) 96.
85. M. Krunks, O. Kijatkina, A. Mere, T. Varema, I. Oja, V. Mikli, *Sol. Energy Mater. Sol. Cells* 87 (2005) 207.
86. X. Hou, K.-L. Choy, *Thin Solid Films* 480–481 (2005) 13.
87. A. Mere, A. Katerski, O. Kijatkina, M. Krunks, 2004, *Proceedings 19-th PVSEC*, June 7-11, 2004, Paris, 1973-1976.
88. J. Wienke, M. Krunks, F. Lenzmann, *Semicond. Sci. Technol.* 18 (2003) 876.
89. C.V. Kelly, M.H.-C. Jin, K.K. Banger, J.S. McNatt, J.E. Dickman, A.F. Hepp, *Mat. Sci. Eng. B* 116 (2005) 403.
90. T.T. John, C.S. Kartha, K.P. Vijayakumar, T. Abe, Y. Kashiwaba, *Appl. Phys. A* 82 (2006) 703.
91. A. Goossens, J. Hofhuis, *Nanotechnology* 19 (2008) 424018.
92. S. Siebentritt, *Thin Solid Films* 403-404 (2002) 1.
93. Eds: M.D. Archer, A.J. Nozik, *Nanostructured and Photoelectrochemical Systems for Solar Photon Conversion*, Series on Photoconversion of Solar

Energy, Vol. 3, World Scientific, 2008, p. 780.
94. R. Könenkamp, P. Hoyer, A. Wahi, *J. Appl. Phys.* 79 (1996) 7029.
95. I. Kaiser, K. Ernst, Ch.-H. Fischer, R. Könenkamp, C. Rost, I. Sieber, M. Ch. Lux-Steiner, *Sol. Energy Mater. Sol. Cells* 67 (2001) 89.
96. K. Taretto, U. Rau, *Prog. Photovoltaics: Res. Appl.* 12 (2004) 573.
97. Y. Itzhaik, O. Niitsoo, M. Page, G. Hodes, *J. Phys. Chem. Letters*, 113 (2009) 4254.
98. C. Levy-Clement, A. Katty, S. Bastide, F. Zenia, I. Mora, V. Munoz-Sanjose, *Physica E* 14 (2002) 229.
99. C. Levy-Clement, R. Tena-Zaera, M.A. Ryan, A. Katty, G. Hodes, *Adv. Mater*. 17 (2005) 1512.
100. D. Kievan, T. Dittrich, A. Belaidi, J. Tornow, K. Schwarzburg, N. Allsop, M. Lux-Steiner, *Appl. Phys. Lett*. 92 (2008) 153107.
101. A. Belaidi, T. Dittrich, D. Kieven, J. Tornow, K. Schwarzburg, M. Lux-Steiner, *Phys. Stat. Sol. (RRL)* 2 (2008) 172.
102. J. Goldstein, D. Newbury, D. Joy, C. Lyman, P. Echlin, E. Lifshin, L. Sawyer, J. Michael, *Scanning Electron Microscopy and X-ray Microanalysis*, 3rd Ed., Kluwer Academic, Plenum Publishers, New York (2002) 689 p.
103. V. Mikli, Ph.D. Thesis, Tallinn University of Technology, Estonia, 2003.
104. O. Volobujeva, Ph.D. Thesis, Tallinn University of Technology, Estonia, 2008.
105. D. Briggs, J. T. Grant, *Surface Analysis by Auger and X-Ray Photoelectron Spectroscopy*, Published in association with IM Publications 2003, ISBN 1-901019-04-7.
106. D. Briggs, M. P. Seah, eds., *Practical Surface Analysis by Auger and X-ray Photoelectron Spectroscopy,* Published by Wiley & Sons, 1983, Chichester, UK ISBN 0-471-26279-X.
107. E.A. Davis, N.F. Mott, *Philipp. Mag.* 22 (1970) 903.
108. T.T. John, T. Sebastian, C.S. Kartha, K.P.Vijayakumar, T. Abe, Y. Kashiwaba, *Physica B* 388 (2007) 1.
109. C.D. Wagner, A.V. Naumkin, A. Kraut-Vass, J.W. Allison, C.J. Powell, J.R. Rumble Jr., NIST Standard Reference Database 20, Ver. 3.4, 2006 (Web Version at http://srdata.nist.gov/xps/index.htm).
110. C.C. Chusuei, M.A. Brookshier, D.W. Goodman, *Langmuir* 15 (1999) 2806.
111. T. Yano, M. Ebizuka, S. Shibata, M. Yamane, *J. Electron. Spectrosc. Relat. Phenom.* 131-132 (2003) 133.
112. B. Barcones, A. Pérez-Rodríguez, L. Calvo-Barrio, A. Romano-Rodríguez, J.R. Morante, E. Rudigier, I. Luck, J. Djordjevic, R. Scheer, *Thin Solid Films* 480–481 (2005) 362.

113. Y. He, Ph.D. Thesis, Justus-Liebig University, Giessen, Germany, 2003.
114. B. Asenjo, A.M. Chaparro, M.T. Gutierez, J. Herrero, *Thin Solid Films* 511-512 (2006) 117.
115. P.A. Block, R.A. Brown, D. Robinson, in: *Proceedings of the Fourth International Conference on the Remediation of Chlorinated and Recalcitrant Compounds*, 24-27 May 2004, Monterey, California, USA, Paper 2A-05, Battelle Press, Columbus, Ohio, USA.
116. M. Nanu, L. Reijnen, B. Meester, A. Goossens, J Schoonman, *Thin Solid Films* 431-432 (2003) 492.
117. D. Ferro, V. Piacente, P. Scardala, *J. Mat. Sci. Lett.* 7 (1988) 1301.
118. M. Abaab, M. Kanzari, B. Rezig, M. Brunel, *Sol. Energy Mater. Sol. Cells* 59 (1999) 299.
119. M. Krunks, A. Katerski, T. Dedova, A. Mere, I. Oja Acik, Photovoltaic Cell based on ZnO nanorods, US Provisional Patent application, Priority No. US60/948508, priority date 09.07.2007.
120. https://www.etis.ee/portaal/patentInfo.aspx?ipVID=2463.
121. I. Oja Acik, A. Katerski, A. Mere, J. Aarik, A. Aidla, T. Dedova, M. Krunks, *Thin Solid Films* 517 (2009) 2443.
122. M. Krunks, E. Karber, A. Katerski, K. Otto, I. Oja Acik, T. Dedova, A. Mere, *Sol. Energy Mater. Sol. Cells* 94 (2010) 1191.
123. O. Niitsoo, S. K. Sarkar, C. Pejoux, S. Rühle, D. Cahen, G. Hodes, *J. Photochem. Photobiol. A: Chem.*, 181 (2006) 306.
124. G. Hodes, A. Zaban, In : G. Wilde (Ed), *Frontiers of Nanoscience*, *Nanostructured Materials*, Vol. 1, Chapter 5, Elsevier, Amsterdam, 2009, 232.
125. I. Oja, A. Belaidi, L. Dloczik, M.-Ch. Lux-Steiner, T. Dittrich, *Semicond. Sci. Technol.* 21 (2006) 520.
126. R. Tena-Zaera, M. A. Ryan, A. Katty, G. Hodes, S. Bastide, C. Lévy-Clément, C. R. Chimie 9 (2006) 717.
127. M.H. Valdés, M. Berruet, A. Goossens, M. Vázquez, *Surf. Coat. Technol.* 204 (2010) 3995.

ABSTRACT

The present doctoral thesis is a continuation of the studies on the deposition of $CuInS_2$ films by the chemical spray pyrolysis (CSP) method carried out at the Department of Materials Science. The aim of the doctoral thesis was to study the effect of the deposition process variables such as the film growth temperature and the precursor molar ratio in the spray solution, and post-deposition treatments on the chemical composition of sprayed $CuInS_2$ films to develop an absorber material for solar cells.

$CuInS_2$ is a promising absorber material for thin film solar cells due to its direct bandgap of about 1.5 eV, high absorption coefficient and p-type of conductivity. The CSP method is a simple, low cost, non-vacuum thin film deposition technique where a thin film is obtained by spraying of a solution, containing salts of constituent elements in required proportion, in the form of micron-dimension droplets onto the preheated substrate where the film of thermally more stable material forms.

In this study, $CuInS_2$ films were deposited by the CSP method using aqueous solutions of $CuCl_2$, $InCl_3$ and $SC(NH_2)_2$ with the [Cu]/[In] molar ratio of 1.1 or 1.0 at growth temperatures of 250 °C and around 350 °C. Post-deposition treatments such as chemical etching in the KCN solution and thermal treatment in the H_2S atmosphere we applied to improve the film properties. X-ray Photoelectron Spectroscopy (XPS) was used as the main characterization method to study the chemical composition of thin films. The methods of XRD, EDS, Raman and optical spectroscopy together with electrical resistivity measurements were applied as supporting characterization tools.

The doctoral thesis is based on four papers published in international pre-reviewed journals and an international patent application on the preparation of a nanostructured solar cell where CSP-$CuInS_2$ is used as an absorber layer.

Results of the study showed that independent of the precursor molar ratio in the spray solution, $CuInS_2$ films grown by CSP at ca 350 °C have graded distribution of the elements (Cu, In, S, O) in the film thickness. Films contain oxygen bonded to a metal (in the form of In_2O_3) on the film surface and in the film bulk, and Cu^{2+} containing pieces (copper sulfide and sulfate) on the film surface. The KCN-treatment removes a Cu_xS phase from the film surface. However, Cu_xS phase is present in the film bulk when deposited from the Cu-rich solution. Deposition at 250 °C results in low-crystalline films with a uniform distribution of the elements (Cu, In, S) in the film thickness, where oxygen is present in a trace amount.

Post-deposition thermal treatment of sprayed $CuInS_2$ films at 530 °C in the H_2S atmosphere significantly improves the film quality increasing the crystallite size and optical bandgap, chemical analysis shows removal of chlorine and

oxygen, and an increase in sulfur content. Non-uniform distribution of the elements in the film thickness, if present in as-sprayed film, is preserved upon the H_2S treatment. Diffusion of Na from the substrate into the film occurs during the thermal treatment if soda-lime glass is used as a substrate.

$CuInS_2$ prepared by the CSP method proved its working ability as an absorber layer in a nanostructured solar cell based on the ZnO nanorod window layer. The light-to-electricity conversion efficiency of 2.5 % was achieved with a structure ITO/ZnO_{rod}/blocking layer/In_2S_3/$CuInS_2$, entirely prepared by CSP. By further development of a nanostructured solar cell, the conversion efficiency of 4.17 % was obtained using an as-sprayed extremely thin $CuInS_2$ layer.

KOKKUVÕTE

Käesolev doktoritöö on üks osa TTÜ materjaliteaduse instituudis tehtavast uurimistööst keemilise pihustamise meetodil valmistatavate õhukeste kilede valdkonnas.

Doktoritöö ülesanne oli uurida kilede kasvatamise temperatuuri, lähteainete molaarsuhte ning järeltöötluste mõju pihustuspürolüüsi meetodil kasvatatud $CuInS_2$ kilede keemilisele koostisele. $CuInS_2$ on sobiv materjal kasutamiseks absorberkihina õhukesekilelistes päikesepatareides tänu keelutsooni laiusele 1.5 eV, kõrgele valguse neeldumise tegurile ja p-tüüpi juhtivusele. Keemilise pihustamise meetod on lihtne ja odav õhukeste kilede valmistamise tehnoloogia. Kiled saadakse sobivaid lähteaineid sisaldava lahuse pulveriseerimisel ülipeenikeste piiskadena eelkuumutatud alusplaadile. Kuumal alusplaadil toimub termiselt stabiilsema tahkise kile kasv.

Antud töös kasvatati $CuInS_2$ kiled 250 ja ca 350 °C juures pihustuspürolüüsi meetodil. $CuInS_2$ kilede saamiseks kasutati lähteainetena $CuCl_2$, $InCl_3$ ja $SC(NH_2)_2$ ning pihustati vesilahust, milles [Cu]/[In] molaarsuhe oli 1.1 või 1.0. Järeltöötlustena rakendati söövitamist KCN vesilahuses ja termilist töötlust 530 °C juures H_2S keskkonnas. Kilede keemilise koostise uurimiseks kasutati peamiselt röntgenkiire fotoelektronspektroskoopia (XPS) meetodit. Kilede iseloomustamiseks kasutati täiendavalt XRD, EDS, Raman ja optilise spektroskoopia meetodeid ning elektritakistuse mõõtmisi.

Doktoritöö baseeub neljal teadusartiklil, mis on publitseeritud eelretsenseeritavates teadusajakirjades, ja ühel patenditaotlusel, mis on esitatud nanostruktuurse päikesepatarei, kus absorberkihina kasutatakse pihustuspürolüüsi meetodil valmistatud $CuInS_2$ absorberkihti, tehnoloogia ja disaini kohta.

Uurimistöö tulemused näitasid, et 350 °C juures sadestatud $CuInS_2$ kiled sisaldavad metalli iooniga seotud hapnikku In_2O_3 kujul nii kile pinnal kui kile sisemuses, kusjuures elementide (Cu, In, S, O) kontsentratsioon kile ristlõikes

on ebaühtlane. Kilede pinnal on Cu^{2+} ioone sisaldavad faasid nagu vasksulfiid ja vasksulfaat. Söövitus KCN lahuses eemaldab Cu_xS faasi kile pinnalt. Vaserikaste lahuste ([Cu]/[In] =1.1) pihustamisel saadud kiled sisaldavad Cu_xS faasi kile mahus. Kilede sadestamisel 250 °C juures saadakse kiled, milles hapniku kontsentratsioon on suhteliselt madal ning elementide (Cu, In, S) jaotus kile sisemuses ühtlane. Kiled, mis on valmistatud 250 °C juures pihustades lahust, milles [Cu]/[In] =1.0, on madala kristallilisusega ning sisaldavad lisafaasi.

Termiline järeltöötlus 530 ° juures H_2S atmosfääris parandab oluliselt kilede omadusi suurendades kilede kristallilisust ja keelutsooni väärtust, keemilise analüüsi järgi suureneb kilede puhtus, saadakse kiled, millede elementkoostis on lähedane $CuInS_2$ stöhhiomeetriale. Samas tuleb arvestada asjaoluga, et elementide ebaühtlane jaotus pihustatud kile mahus säilib ka pärast H_2S töötlust ning juhul kui kiled on sadestatud klaasile, toimub Na difusioon klaasalusest kilesse.

Keemiliselt pihustatud $CuInS_2$ kilet saab kasutada absorberhihina nanostruktuursetes päikesepatareides. ZnO nanovarrastel baseeruvas patareis ITO/ZnO_{rod}/blocking-layer/In_2S_3/$CuInS_2$, mille kõik komponendid valmistati pihustuspürolüüsi meetodil, saadi antud uurimistöö raames efektiivsuseks 2.5%. Edasise arenduse tulemusena saavutati üliõhukese $CuInS_2$ absorberiga parateri efektiivsuseks 4.17 %.

PAPER I

M. Krunks, A. Mere, **A. Katerski**, V. Mikli, J. Krustok, Characterization of sprayed $CuInS_2$ films annealed in hydrogen sulphide atmosphere, *Thin Solid Films*, 511-512 (2006) 434-438.

Available online at www.sciencedirect.com
SCIENCE DIRECT®
Thin Solid Films 511–512 (2006) 434–438
thin solid films
www.elsevier.com/locate/tsf

Characterization of sprayed $CuInS_2$ films annealed in hydrogen sulfide atmosphere

M. Krunks [a,*], A. Mere [a], A. Katerski [a], V. Mikli [b], J. Krustok [a]

[a] Department of Materials Science, Tallinn University of Technology, Ehitajate 5, Tallinn 19086, Estonia
[b] Centre for Materials Research, Tallinn University of Technology, Ehitajate 5, Tallinn 19086, Estonia

Available online 19 January 2006

Abstract

The effect of post-deposition annealing in flowing H_2S atmosphere at 530 °C on the properties of sprayed $CuInS_2$ (CIS) thin films was studied. The structure and composition were characterized by XRD, SEM and EDX. The density of carriers was obtained from $C-V$ measurements of CIS/Al Schottky barriers at room temperature (RT), the resistivity was measured at RT and as a function of temperature. H_2S annealing eliminates the deficiency of sulfur and results in closely stoichiometric, well-crystallized films of $CuInS_2$. Annealed films are consisting of grains with a size up to 300 nm. By treatment, the optical band gap increases from 1.44 to 1.49 eV as determined from absorbance spectra. The electrical properties are depending on the cooling rates. The specific resistivity of 10^7 and 10^5 Ω cm and carrier concentrations in the order of 10^{14} and 10^{17} cm^{-3} are characteristics of rapidly and slowly cooled films, respectively. Pronounced parabolic behaviour of the $\ln\sigma$ vs. $1/T$ plot of rapidly cooled samples shows that grain boundaries effect should be considered in the conductivity mechanism. Slow cooling favours the removal of a resistive phase from the grain boundaries and the film conductivity increases. The different predominating defects are assumed to be present in the rapidly and slowly cooled films. The conductivity thermal activation energies of 80 and 160 meV are characteristic of slowly cooled samples deposited from "stoichiometric" or "Cu-rich" solutions, respectively. It shows that not only the treatment conditions but also the film deposition parameters are highly important in the development of the material properties.

Keywords: $CuInS_2$; Spray pyrolysis; Post-deposition treatment; Electrical properties; Structure

1. Introduction

Large-scale introduction of solar energy requires a drastic price reduction. This is why the efforts in the field of thin films cost-effective deposition techniques and new design of solar cells are continuously in progress.

Spray pyrolysis is an inexpensive technique which proved its convenience to deposit homogeneous films over a large area [1]. In the present study the method has been used to prepare thin films of $CuInS_2$. Copper indium disulfide is a potential absorber material for high efficiency solar cells due to its direct band gap of 1.5 eV, although actually the output parameters are low compared to selenide based devices [2].

It has been shown that well-adherent (112) orientated $CuInS_2$ films could be deposited by spray technique [3,4]. As-deposited films grown at temperatures below 400 °C in air contain residues originating from both the precursors and the ambient [5,6]. Post-deposition treatments in reducing and sulfur containing atmospheres were found to be effective to remove undesired residues and improve the structural properties [6,7]. Still, very little attention is paid to the carriers transport properties in the films prepared by chemical methods. The electrical properties of the sprayed $CuInS_2$ films have been studied in few works only [7–9].

In our recent study we showed by Raman spectroscopy that treatment at temperatures around 500 °C in flowing H_2S atmosphere is effective to improve the crystal quality of sprayed $CuInS_2$ films [10]. In the present work we introduce the effect of annealing in H_2S atmosphere at different cooling rates on the crystallinity, stoichiometry, optical and electrical properties of sprayed $CuInS_2$ films.

2. Experimental

$CuInS_2$ (CIS) thin films were obtained by spraying the solution containing $CuCl_2$, $InCl_3$ and $SC(NH_2)_2$ onto pre-

* Corresponding author. Tel.: +372 6203363; fax: +372 6203367.
E-mail address: malle@staff.ttu.ee (M. Krunks).

0040-6090/$ - see front matter © 2005 Elsevier B.V. All rights reserved.
doi:10.1016/j.tsf.2005.11.072

heated ITO covered glass substrates at 370 °C. The exact description of the deposition procedure is published elsewhere [9,10]. In the present work, molar ratios of precursors Cu/In/S of 1:1:3 and 1.1:1:3.15 were used and the spray solutions were called "stoichiometric" and "Cu-rich", respectively. As-deposited films were etched in KCN solution for 5 min (called as-deposited films) in order to remove the Cu_xS phase at the film surface. Post-deposition heat treatments were performed in flowing H_2S atmosphere at 530 °C for 1 and 2 h, followed by rapid or slow cooling with cooling rates about 25 °C/min and 2 °C/min, respectively.

The crystal structure of the films was characterized by the XRD patterns recorded by a Bruker AXS D5005 diffractometer. The average crystallite size was calculated from the FWHM of the (112) diffraction peak of $CuInS_2$ (PDF 27-0159) using the Scherrer formula. The elemental composition of the films was studied by the X-ray microanalysis (EDX) on a Link Analytical AN 10000 spectrometer using an accelerating voltage of 7 kV and a beam current of 3 nA. EDX measurements were made from the surface area of 2×2 μm^2 at four different characteristic points. The film cross-section micrographs were made on Leo Supra 35. The optical band gap was determined from the absorbance measurements using a Varian Techtron model 635 UV–VIS spectrometer.

To perform the conductivity measurements, the Pt–Au contacts with area of 1.83 mm^2 were made by sputtering on the top of the film. The ITO was used as a back contact. A Keithley-616 electrometer was used to measure the film's resistance. The temperature dependent conductivity was measured in the temperature interval 200–400 K using a vacuum cryostat to set the temperature. The concentration of carriers was determined from the capacitance–voltage (C–V) measurements of CIS–Al Schottky barriers prepared by evaporation of Al contacts with area of the 1.83 mm^2 on the top of the CIS layer. C–V measurements were performed at room temperature (RT) using an Autolab PGSTAT 30 set-up.

3. Results and discussion

3.1. Structural and compositional properties

The crystallinity of sprayed CIS films could be significantly improved by post-deposition treatments [6,7,10]. The effect of annealing in flowing H_2S atmosphere at 525 °C with rapid cooling on the structure of sprayed CIS films is reported elsewhere [10]. It has been shown that the annealing for 2 h significantly increases the film crystallinity and relative importance of the chalcopyrite ordered $CuInS_2$. Furthermore, it was established that the treatment was effective to remove the second ternary compound $CuIn_5S_8$, which was present in as-deposited films prepared from Cu-poor solutions.

The use of an annealing time of 60 min and a slow cooling results in well-crystallized $CuInS_2$ films independent of the spray solution composition according to XRD (Fig. 1). XRD patterns of slowly cooled samples are similar to those presented

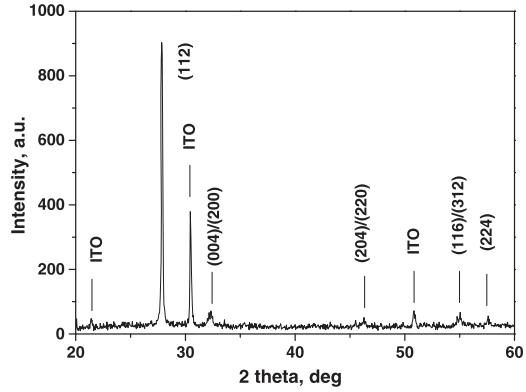

Fig. 1. XRD pattern of the film deposited from the "stoichiometric" (Cu/In = 1.0) solution and annealed for 60 min at 530 °C in flowing H_2S atmosphere and subjected to slow cooling.

for rapidly cooled ones in [10]. The average crystallite size is 98 nm as calculated from the FWHM of the (112) replica of $CuInS_2$ (Fig. 1). For comparison, the treatment for 120 min at 525 °C with rapid cooling results in mean crystallite size of about 90 nm [10].

The development of grains by H_2S annealing is characterized by the SEM cross-sectional micrographs (Fig. 2). It could be seen that as-deposited film, consisting of grains with size less than 20 nm (Fig. 2a), is turned into a film which comprises grains with sizes up to 300 nm on preserved ITO electrode (Fig. 2b). By annealing, significant changes could be observed in the film elemental composition. The deficiency in sulfur (Table 1) and contamination with chlorine with an amount of about 1.5 mass% are characteristic of as-deposited films. The results are in accordance with the literature data [6,7,11]. Upon H_2S treatment, the content of sulfur is significantly increased and the chlorine is not detectable by EDX. The films on glass substrate exhibit nearly stoichiometric composition whereas on ITO covered glass a slightly In-rich composition has been observed (Table 1). In the latter case the impact of indium from ITO electrode is not excluded. The elemental composition of the films from "Cu-rich" solutions is not affected by the treatment time and cooling rates. The case of the films deposited from "stoichiometric" solutions will be discussed in Section 3.3.

3.2. Optical properties

The optical band gap of as-sprayed and H_2S annealed films was deduced from the absorption spectra measured at RT. The absorption coefficient α was calculated using the expression $I=I_0e^{-\alpha t}$, where t is the thickness of the film. Following the conventional analysis, the energy dependent absorption coefficient can be expressed by the relation for the allowed direct transition as $\alpha h\nu = A(h\nu - E_G)^{1/2}$, where A is a parameter depending on the transition probability and E_G is the direct band gap. Thus, E_G is found from the plot $(\alpha h\nu)^2$ vs. the photon energy $h\nu$ by extrapolating the linear portion of the plot up to $\alpha = 0$.

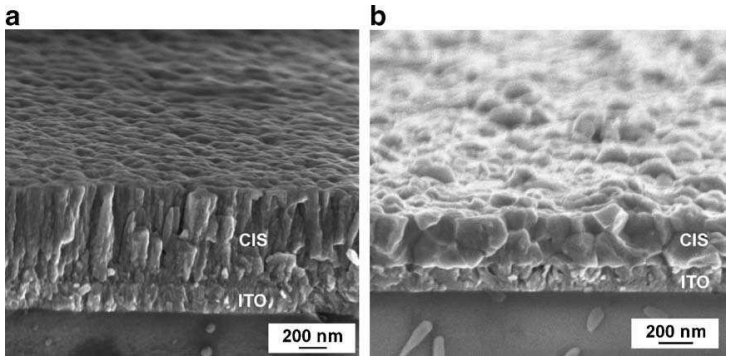

Fig. 2. SEM cross-sectional micrographs of CIS films deposited from "stoichiometric" (Cu/In = 1.0) solutions: (a) as-deposited; (b) annealed for 60 min at 530 °C in flowing H_2S atmosphere and subjected to slow cooling.

As-sprayed films show the optical energy gap of 1.44 eV, corresponding to the literature data for spray-deposited $CuInS_2$ films [4,5], as well as for those prepared by reactive annealing [12] or sulfurization of Cu–In alloys [13]. The treatment was found to increase the band gap energy (Fig. 3). It appears that H_2S treatment followed by rapid cooling results in E_G approximately 1.46 and 1.48 eV using the treatment duration of 1 or 2 h, respectively. Using the treatment time of 1 h followed by slow cooling, the band gap reaches a value close to 1.49 eV. The increase in energy gap is reported for $CuInS_2$ films subjected to annealing in sulfur atmosphere [14]. Observed widening of optical band gap could be explained by the improved crystallinity, nearly stoichiometric composition and higher purity of annealed films as shown above and in [10].

3.3. Electrical properties

The films were characterized by specific resistivity, carrier type, concentration, and temperature dependent conductivity measurements. Hot probe measurements confirm the p-type conductivity of all our films. Mott-Schottky model has been used to determine the concentration of carriers. The results are presented in Table 2.

As-deposited samples show a resistivity of about 10^4 Ω cm. Similar resistivity values are reported for $CuInS_2$ films prepared by spray [8] and reactive sputtering [12]. H_2S treatment, which was found to improve the film's structural and optical properties, significantly decreases the conductivity and concentration of carriers (Table 2). The influence of different cooling rates is distinctly expressed whereas the deposition parameter (Cu/In in the solution) has minor effect (Table 2). Specific resistivity of 10^7 Ω cm and concentration of carriers in the order of 10^{14} cm^{-3} is characteristic of rapidly cooled films (Table 2). Such low carrier concentration is reported for $CuInS_2$ films prepared by sulfurization of stacked Cu–In layers [15] and reactive sputtering in H_2S [12] as well for as-grown single crystals [16]. It is believed that such low carrier density is a sign of heavy compensation since the concentration of intrinsic defects in this material is reported to be much higher [16]. Applying slow cooling after the treatment for 1 h, an increase in conductivity and carriers' density has been observed (Table 2). This observed behaviour is similar to that described for polycrystalline $CuInS_2$ films grown by coevaporation and subjected to annealing in sulfur atmosphere [17], where the higher conductivity of slowly cooled films was explained by the saturation of sulfur vacancies during the cool-down period.

The results of temperature dependent conductivity measurements are presented as a plot of $\ln\sigma$ vs. $1000/T$ in Fig. 4. We have assumed that the mobility of holes does not significantly vary within the temperature region used. It could be seen that as-sprayed samples follow the thermally activated electrical conductivity according to the Arrhenius

Table 1
Elemental composition by EDX of CIS films as-sprayed and annealed at 530 °C in H_2S atmosphere, as a function of the treatment time and cooling conditions

Substrate	Cu/In/S in solution	Annealing time (min)	Cooling rate	Cu (at.%)	In (at.%)	S (at.%)	Cu/In	S/(Cu+In)
Glass	1.1:1:3.15	–	–	26.40	26.64	44.36	0.99	0.83
	1:1:3	120	Rapid	25.79	24.51	49.70	1.05	0.99
			Rapid*	0.45	35.25	64.48	0.01	1.83
	1.1:1:3.15	120	Rapid	24.67	25.28	50.05	0.98	1.00
ITO	1.1:1:3.15	120	Slow	24.30	26.40	49.20	0.92	0.97
	1.1:1:3.15	60	Rapid	24.76	26.04	49.07	0.95	0.97
	1.1:1:3.15	60	Slow	24.34	26.08	49.48	0.93	0.98
	1:1:3	60	Slow	24.14	25.72	48.41	0.94	0.97

*From the flake-like crystallites on the surface.

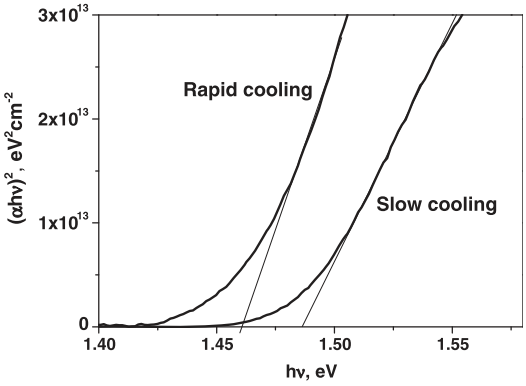

Fig. 3. The plot of $(\alpha h\nu)^2$ vs. energy for $CuInS_2$ films deposited from "Cu-rich" solution (Cu/In=1.1) and treated for 60 min at 530 °C in flowing H_2S atmosphere and subjected to rapid or slow cooling.

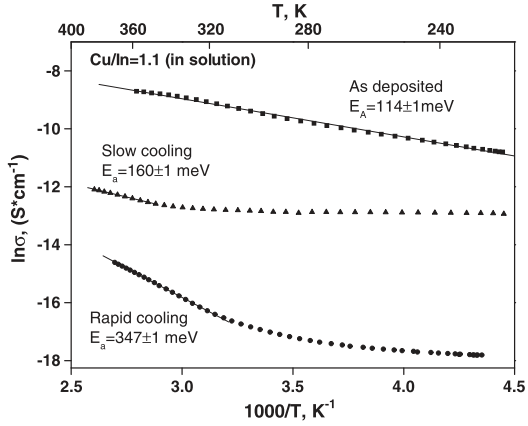

Fig. 4. The plot of $\ln\sigma$ vs. $1000/T$ for as-deposited from "Cu-rich" solution (Cu/In=1.1) and annealed for 60 min at 530 °C in flowing H_2S atmosphere $CuInS_2$ films subjected to rapid or slow cooling.

relation $\sigma=\sigma_0\exp(-E_a/kT)$, where σ_0 is a pre-exponential factor, E_a is the activation energy and k is the Boltzmann's constant. The thermal activation energies of 114 meV and 170 meV were obtained for as-sprayed films deposited from "Cu-rich" and "stoichiometric" solutions, respectively.

The plots of $\ln\sigma$ vs. $1000/T$ of H_2S treated films show parabolic behaviour (Fig. 4) and thus the mixed conductivity activation mechanisms due to the defect levels and grain boundary effects could be proposed [7,18,19]. Parabolic behaviour is highly pronounced for the films subjected to rapid cooling. By allowing the samples to cool down slowly, an increase in conductivity with less pronounced curvature of $\ln\sigma$ vs. $1000/T$ plot could be observed.

In high temperature region ($T>320$ K) the plot of $\ln\sigma$ vs. $1000/T$ of H_2S treated films follows the Arrhenius dependence for both rapidly and slowly cooled samples. Infinitely high activation energies of 340 and 520 meV were found for rapidly cooled samples prepared from "Cu-rich" and "stoichiometric" solutions, respectively (Table 2). We believe that these activation energies indicate that there are residues of some unknown phase between the grains in rapidly cooled samples and are not caused by some very deep acceptor level in $CuInS_2$. An indium and sulfur containing phase was detected on the surface of the film from "stoichiometric" solution after rapid cooling (Table 1, marked by asterisk). Similar phase could be present at grain boundaries as well. The existence of an indium sulfide phase has been observed at grain boundaries of sprayed CIS films annealed in sulfur atmosphere [7].

Table 2
Specific resistivity (ρ), carrier concentration (N_p) at room temperature and conductivity thermal activation energy (E_a) for CIS films as-deposited and annealed at 530 °C in H_2S atmosphere

Cu/In/S in solution	Treatment time (min)	Cooling	ρ (Ω cm)	N_p (cm^{-3})	E_a (meV)
1:1:3	–	–	$4.6\cdot10^4$	$4.0\cdot10^{16}$	170
	120	Rapid	$1.0\cdot10^7$	$2.2\cdot10^{14}$	520
	60	Slow	$6.9\cdot10^5$	$1.5\cdot10^{17}$	83
1.1:1:3.15	–	–	$2.5\cdot10^4$	$1.9\cdot10^{17}$	114
	120	Rapid	$4.0\cdot10^7$	$3.2\cdot10^{14}$	347
	60	Slow	$2.5\cdot10^5$	$2.3\cdot10^{17}$	160

By slow cooling, this highly resistive phase disappears and the conductivity of samples increases. Thus, the slow cooling results in the conductivity thermal activation energies of 80 and 160 meV (for the samples grown from "stoichiometric" and "Cu-rich" solutions, respectively), which could be assigned to the acceptor levels in $CuInS_2$.

4. Conclusions

The post-deposition annealing of sprayed CIS films in flowing H_2S atmosphere significantly improves the film's crystallinity and stoichiometry by increasing the sulfur content. The mean crystallite size in H_2S annealed films is close to 100 nm as determined from the XRD pattern. Annealed films are consisting of grains with size up to 300 nm according to SEM. The optical band gap could be increased up to 1.49 eV, which is the highest value reported for the $CuInS_2$ films initially prepared by spray technique.

H_2S treatment, which was a right action to improve the films structural and optical properties has an adverse effect on the electrical properties, particularly when cooled rapidly. The specific resistivity of 10^7 Ω cm and carrier concentrations in order of 10^{14} cm^{-3} are characteristic of rapidly cooled films. Such low carrier density indicates that the material could be highly compensated. The temperature dependent conductivity measurements show that the grain boundaries effect should be considered in the conductivity mechanism. We believe that there are residues of some unknown phase between the grains in these samples.

The film conductivity could be increased using slow cooling which favours the removal of highly resistive phase from the grain boundaries. The increased carrier density refers to the changes in the predominating defects compared to the rapidly cooled films. The conductivity thermal activation energies of 80 and 160 meV, which could be assigned to acceptor levels in

$CuInS_2$, are dependent on the Cu/In molar ratio in the spray solution. Thus, not only the treatment conditions but also the film deposition parameters are highly important in the development of the material properties.

Acknowledgements

This work was supported by the European Commission Project ENK6-CT-2002-80664 and the Estonian Science Foundation Grant Nos. 5612 and 5149.

References

[1] P.S. Patil, Mater. Chem. Phys. 59 (1999) 185.
[2] H.J. Lewerenz, Sol. Energy Mater. Sol. Cells 83 (2004) 395.
[3] J.D. Harris, K.K. Banger, D.A. Scheiman, M.A. Smith, M.H.-C. Jin, A.F. Hepp, Mater. Sci. Eng., B 98 (2003) 150.
[4] M. Krunks, O. Bijakina, T. Varema, V. Mikli, E. Mellikov, Thin Solid Films 338 (1999) 125.
[5] M.C. Zouaghi, T.B. Nasrallah, S. Marsillac, J.C. Bernede, S. Belgacem, Thin Solid Films 382 (2001) 39.
[6] M. Krunks, O. Kijatkina, H. Rebane, I. Oja, V. Mikli, A. Mere, Thin Solid Films 403–404 (2002) 71.
[7] S. Marsillac, M.C. Zouagi, J.C. Bernede, T.B. Nasrallah, S. Belgacem, Sol. Energy Mater. Sol. Cells 76 (2003) 125.
[8] M. Ortega-Lopez, A. Morales-Acevedo, Thin Solid Films 330 (1998) 96.
[9] A. Mere, O. Kijatkina, H. Rebane, J. Krustok, M. Krunks, J. Phys. Chem. Solids 64 (2003) 2025.
[10] I. Oja, M. Nanu, A. Katerski, M. Krunks, A. Mere, J. Raudoja, A. Goossens, Thin Solid Films 480–481 (2005) 82.
[11] M. Krunks, O. Kijatkina, A. Mere, T. Varema, I. Oja, V. Mikli, Sol. Energy Mater. Sol. Cells 87 (2005) 207.
[12] Y.B. He, T. Krämer, A. Polity, R. Gregor, W. Kriegseis, I. Österreicher, D. Hasselkamp, B.K. Meyer, Thin Solid Films 431–432 (2003) 231.
[13] A. Antony, A.S. Asha, R. Yoosuf, R. Manoj, M.K. Jayaraj, Sol. Energy Mater. Sol. Cells 81 (2004) 407.
[14] M. Abaab, M. Kanzari, B. Rezig, M. Brunel, Sol. Energy Mater. Sol. Cells 59 (1999) 299.
[15] S. Bandyopadhyaya, S. Chaudhuri, A.K. Pal, Sol. Energy Mater. Sol. Cells 60 (2000) 323.
[16] J.H. Schön, E. Bucher, Phys. Status Solidi, A 171 (1999) 511.
[17] R. Scheer, M. Alt, I. Luck, H.J. Lewerenz, Sol. Energy Mater. Sol. Cells 49 (1997) 423.
[18] R.R. Philip, B. Pradeep, G.S. Okram, V. Ganesan, Semicond. Sci. Technol. 19 (2004) 798.
[19] S. Siebentritt, S. Schuler, J. Phys. Chem. Solids 64 (2003) 1621.

PAPER II

A. Katerski, A. Mere, V. Kazlauskiene, J. Miskinis, A. Saar, L. Matisen, A. Kikas, M. Krunks, Surface analysis of spray deposited copper indium disulfide films, *Thin Solid Films* 516 (2008) 7110-7115.

Available online at www.sciencedirect.com
ScienceDirect
Thin Solid Films 516 (2008) 7110–7115
www.elsevier.com/locate/tsf

Surface analysis of spray deposited copper indium disulfide films

Atanas Katerski [a], Arvo Mere [a], Vida Kazlauskiene [b], Juozas Miskinis [b], Agu Saar [c], Leonard Matisen [c], Arvo Kikas [c], Malle Krunks [a,*]

[a] Department of Materials Science, Tallinn University of Technology, Ehitajate tee 5, EE-19086 Tallinn, Estonia
[b] Institute of Materials Science and Applied Research, Vilnius University, Naugarduko Str. 24, LT-2006 Vilnius, Lithuania
[c] Institute of Physics, University of Tartu, Riia 142, Tartu EE-51014, Estonia

Available online 21 February 2008

Abstract

$CuInS_2$ films were deposited by spray pyrolysis method at 350 °C. Films were characterized by XPS, AFM and electrical resistivity. The effect of chemical etchings in KCN and $(NH_4)_2S_2O_8$ solutions and thermal treatment at 530 °C in flowing hydrogen sulphide on the film surface composition has been studied. Indium oxide as main secondary phase in surface region of KCN-etched films is probably responsible of high surface conductivity and failure to prepare substrate configuration solar cell. Oxygen bounded to metal is present in the film bulk revealed by O1s BE of 530.0 eV of Ar^+ sputtered profile. Hydrogen sulfide treatment transforms indium oxide into indium sulfide. Etching in ammonium persulfate solution has found to be effective to remove conductive upper layer resulting in surface with composition Cu:In:S = 28.3:22.5:49.3. According to XPS, sprayed films show phase composition grading from the film surface to depth.

Keywords: $CuInS_2$; Spray pyrolysis; XPS; Electrical properties

1. Introduction

$CuInS_2$ (CIS) has great potential for photovoltaic applications due to its high absorption coefficient more than 10^4 cm^{-1} and optimum band gap of 1.5 eV. In comparison with analogous Se-based compound $CuInSe_2$, $CuInS_2$ offers some advantages as no addition of gallium for bandgap widening is required and more simple deposition process could be used to obtain high quality films. Recently the two-stage process consisting in sulfurization of metallic precursor layers has been scaled up for the industrial production of CIS solar modules [1]. In addition, various techniques as co-evaporation [2], atomic layer deposition (ALD) [3], ion layer gas reaction (ILGAR) [4,5], chemical bath deposition (CBD) [6] and chemical spray pyrolysis [7,8] have been used prepare $CuInS_2$ films. Spray pyrolysis is an attractive method for deposition of large-area films due to its simplicity and low cost, and has been used to prepare the photovoltaic structures [9–12]. There are difficulties to obtain single phase CIS films without additional phases by chemical spray method as it has been reported earlier [12–15]. Studies on formation and thermal decomposition of $CuInS_2$ precursors refer to complexity of thin films formation in spray pyrolysis process [16–18]. Therefore, the control of the film bulk and particularly of surface composition is vital to optimize the films manufacturing parameters for efficient photovoltaic structures. X-ray photoelectron spectroscopy (XPS) is a powerful tool to obtain such kind information. XPS studies of sprayed $CuInS_2$ films have briefly been introduced in few works only [15,19]. $CuInS_2$ films by spray showed highly In-rich surface [15]. Secondary phase of In_2O_3 in the sprayed film and its segregation at the grain boundaries is reported by Marsillac et al. [19].

The aim of the present study is to characterise the elemental composition of sprayed CIS films by XPS. Polarographic chemical analysis, atomic force microscopy (AFM) and electrical measurements (resistivity) of the films and I–V curves of solar cells have been used as supporting tools. The effect of chemical treatments and annealing in hydrogen sulfide atmosphere on properties of $CuInS_2$ films is discussed.

* Corresponding author. Tel.: +372 6203363.
E-mail address: malle@staff.ttu.ee (M. Krunks).

0040-6090/$ - see front matter © 2007 Elsevier B.V. All rights reserved.
doi:10.1016/j.tsf.2007.12.027

2. Experimental

$CuInS_2$ (CIS) films were deposited by spray of an aqueous solution containing chlorides of copper and indium at molar ratio Cu/In = 1.1, and thiourea ($SC(NH_2)_2$) onto the preheated ITO-glass substrates. The parameters of the spray procedure such as growth temperature of 350 °C, spray solution volume of 100 ml, solution concentration and feeding rate were kept constant for all samples. As-deposited films were etched 5 min in 5% KCN solution at room temperature. Post-deposition thermal treatment of KCN-etched films has been performed for 60 min at 530 °C in flowing H_2S atmosphere.

The samples were characterized by XPS, AFM and electrical resistivity measurements. XPS measurements were performed in the UHV chamber of the electron spectrometer LAS-3000 ISA-Riber and SCIENTA SES 100 using the Mg Kα radiation ($h\nu = 1253.6$ eV; FWHM of 0.7 eV). Energy calibration was performed, taking the C1s line at 284.6 eV as a reference. An error of measured absolute energies is equal to or less than 0.1 eV. For some samples the atomic concentrations of the elements were calculated using Scofield's ionization cross-sections with no corrections for λ (the mean free path of photoelectrons) and analyzer transmission function (only for LAS-3000 ISA-Riber). The most intense core levels, i.e. Cu2p, In3d, O1s and S2p, Na1s were used in the analysis. To obtain information of the film bulk composition, Ar^+ sputtering has been used for the depth profiling. In addition, chemical etching in the 0.01 M $(NH_4)_2S_2O_8$ solution has been used to remove upper layers of the film.

The electrical resistivity of the films was calculated using the following conventional equation:

$$\rho = \frac{R \cdot A}{l},$$

where ρ is the resistivity, R is the resistance of the film (resistance was calculated from the I–V curve, measured by the AUTOLAB PGSTAT 30 set-up), l is the length of the current path between the contacts, A is the cross-sectional area of the current channel. To characterise the sprayed film inhomogeneity, the electrical resistance of sprayed CIS films was measured by two routes — across the film ("perpendicular" resistance) and along the surface ("longitudinal" resistance) using the films sprayed onto the ITO/glass substrate and glass substrate, respectively, in the same deposition process.

AFM images were obtained using NT-MDT scanning head Smena, Scanning Probe Image Processor SPIP V3.2.4.0 and MicroMasch cantilevers CSC 21 with silicon probe tip in contact mode.

3. Results and discussion

3.1. Phase composition of as-sprayed and KCN-etched CIS films

Fig. 1 shows the XPS spectra of $Cu2p_{3/2}$, $In3d_{5/2}$, O1s and S2p core levels of as-sprayed and 5 min-KCN-etched CIS films. Both films are consisting of crystalline $CuInS_2$ confirmed by XRD (not presented, see for example Ref. [14]). According to

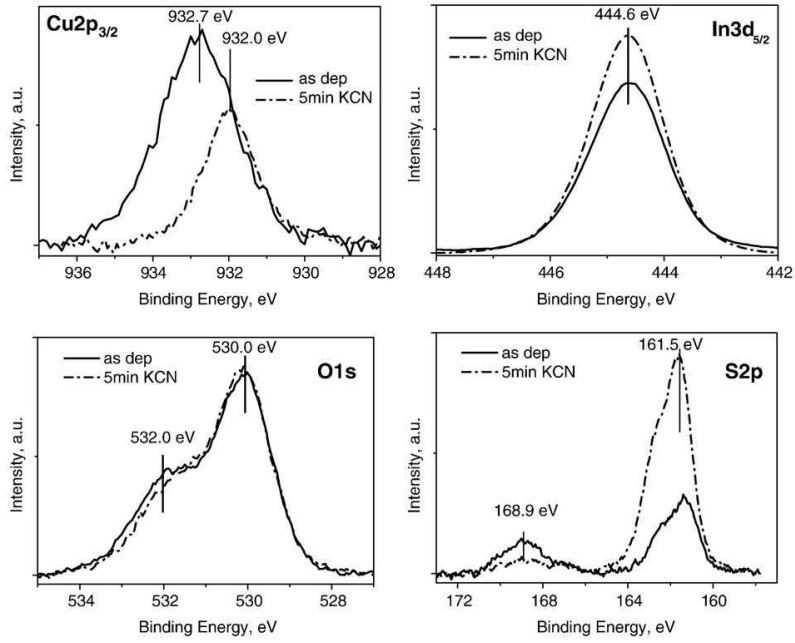

Fig. 1. $Cu2p_{3/2}$, $In3d_{5/2}$, O1s and S2p core levels spectra of as-sprayed (solid line) and 5 min-KCN-etched (dashed line) CIS films.

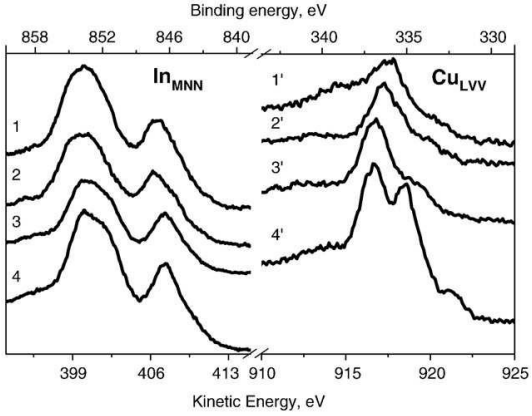

Fig. 2. In $M_{45}N_{45}N_{45}$ and Cu $L_{23}VV$ Auger spectra of as-deposited (1, 1′), KCN-etched (2, 2′), as-deposited film after 15 min of Ar-sputtering (3, 3′) and KCN-etched film after 15 min of Ar-sputtering (4, 4′).

the XPS spectra of as-sprayed films, the binding energies (BE) of $Cu2p_{3/2}$, $In3d_{5/2}$ and S2p are 932.7, 444.6 and 161.5 eV, respectively. The binding energies recorded are close to that of copper, indium and sulfur in spray deposited CIS films [15,20]. The O1s spectrum shows two peaks at 532.0 and 530.0 eV corresponding to the oxygen in adsorbed $(OH)^-$ groups and bonded to the metal (Me–O), respectively [21]. Strong signals of indium and oxygen refer that In-oxide could be the main metal oxide phase. Our XPS spectra do not show the peaks at binding energies around 198–200 eV, characteristic of chlorine, observed in spectra of sprayed CIS films by Zouaghi et al. [15].

The $Cu2p_{3/2}$ core level peak of as-deposited film at 932.7 eV has FWHM of 2.1 eV. Binding energies characteristic of Cu^{1+} and Cu^{2+} states are in the interval of 932.0 – 932.8 eV and 932.7 – 934.1 eV, thus both states of Cu are possible. Weak copper shake-up peaks at around 940 and 944 eV were observed in the wide-scan XPS spectrum of as-deposited CIS film indicating the existence of phases containing copper in the Cu^{2+} state (for example, see Ref. [22]). In addition to the sulfur BE of 161.5 eV characteristic of sulfides also the BE signal at 169 eV, characteristic of sulfates [21], can be clearly seen on the S2p core level spectrum (Fig. 1).

After KCN etching, BE of the $Cu2p_{3/2}$ is 932.0 eV and FWHM of the peak is decreased to 1.65 eV (Fig. 1). KCN etching decreases the intensity of the S2p peak characteristic of sulfate (168.9 eV) and increases the intensity of sulfide peak, whereas no significant changes were observed in the binding energies and intensities of $In3d_{5/2}$ and O1s peaks.

Changes in the film surface composition by KCN etching could be characterized using the $Cu2p_{3/2}$, $In3d_{5/2}$, S2p and O1s (BE = 530.0 eV) integrated area ratios. By KCN etching, the Cu/In ratio is decreased from 0.45 to 0.18, Cu/S from 3.8 to 0.9, whereas no significant changes have been observed in the In/O ratios. Observed changes in the composition support the EDX results on removal of Cu–S phases by KCN etching [23].

Comparison of the Auger spectra of as-deposited, KCN-etched and Ar-bombarded samples is presented in Fig. 2. In $M_{45}N_{45}N_{45}$ Auger maxima of as-deposited and KCN-etched

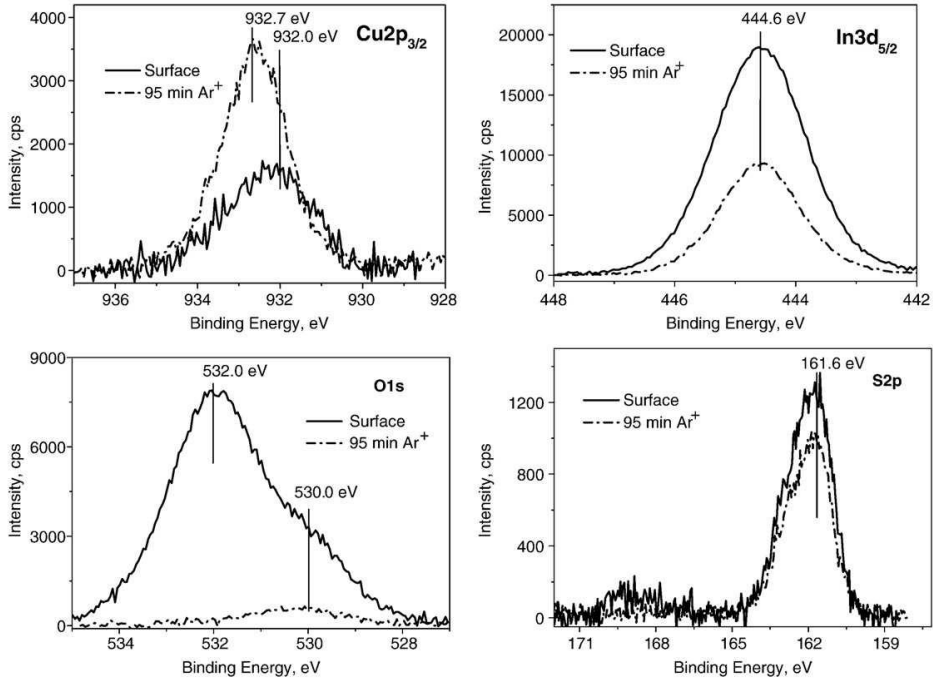

Fig. 3. $Cu2p_{3/2}$, $In3d_{5/2}$, O1s and S2p core levels spectra of as-deposited and KCN-etched (solid line) and of 95 min Ar^+-sputtered (dashed line) CIS films.

Table 1
Composition of CIS films according to the XPS analysis

		In	Cu	S	O (MeO)	Na	In/Cu	Cu/S	In/S	In/O
		at%	at%	at%	at%	at%				
As-dep. (KCN-etched)	Surface	32.1	3.2	31.7	30.5	2.5	10.0	0.1	1.0	1.1
	95 min Ar^+ sputtered (~170 nm)	28.3	11.2	44.0	16.5	0	2.5	0.3	0.6	1.7
	Chemically etched (~150 nm)	28.3	22.5	49.3	0	0	1.3	0.5	0.6	–
+H_2S treated	Surface	17.8	3.7	59.9	0	19	4.8	0.1	0.3	–
	35 min Ar^+ sputtered	29.6	19.4	45.1	0	5.9	1.5	0.4	0.7	–

samples have similar energies (Fig. 2, curves 1 and 2). Ar+ bombardment of both as-deposited and KCN-etched films causes In Auger maxima shift of ~ 0.7 eV to lower binding energies (Fig. 2, curves 3 and 4) indicating lower impact of In-oxides in the film compared to that on top [24].

Concerning the Cu $L_{23}VV$ Auger peak, the KCN etching causes some shift towards higher binding energies. Ar-sputtering results in the shift of ~0.7 eV towards higher BE indicating the presence of the Cu^{1+} containing phases on Ar-cleaned surfaces (Fig. 2, curve 3′). Surprisingly, there appears an additional peak at KE around 918 eV (BE~335 eV) in Cu-LVV-Auger spectra of KCN-etched sample after Ar-bombardment (Fig. 2, curve 4′), which could be of the Cu^{2+} based pieces [25,26] or due to Cu^{1+} in octahedral coordination [22]. According to XPS study, the phases of $CuInS_2$, In_2O_3, Cu–S and a metal sulfate are present on the surface of as-deposited film. Cu–S and metal sulfate are removed by etching in KCN aqueous solution.

3.2. Quantitative elemental composition of as-deposited CIS films

XPS spectra of $Cu2p_{3/2}$, $In3d_{5/2}$, O1s and S2p core levels of KCN-etched CIS films after "strong" Ar^+ sputtering (etching depth~170 nm) are presented in Fig. 3 (XPS spectrum of KCN-etched film before Ar^+ sputtering is given for comparison). Increased intensity of copper signal could be clearly seen. The signal from oxygen in metal oxide (BE=530 eV) is still present but significantly decreased in comparison with that on the film surface. The atomic concentrations of the elements on the film surface and at the depth of ~170 nm were calculated from integrated areas of $Cu2p_{3/2}$, $In3d_{5/2}$, O1s and S2p core levels spectra using Schofield's cross-sections. Content of oxygen has been calculated from the O1s core level (BE=530.0 eV) spectrum. The atomic concentrations are presented in Table 1.

General trends observed are that surface of KCN-etched CIS film is highly indium and oxygen rich, and their content is decreasing while copper concentration is increasing from the surface to the film depth. The concentrations of the elements on the surface of KCN-etched film are similar to that reported by Zouaghi et al. [15]. Surprisingly, the atomic concentrations in spray deposited CIS film are very similar to that reported for electrodeposited $CuInS_2$ [25].

Polarographic chemical analysis was applied as a supporting tool to determine the film composition. According to the polarographic analysis, the Cu/In=1.06 in as-deposited films (no KCN etching) is close to the precursors molar ratio in the spray solution (Cu/In=1.1). KCN etching makes the film slightly In-rich (Cu/In=0.9). Results of polarographic analysis are in accordance with EDX results published earlier [13,23].

Taking into account both polarographic and XPS results, it could be concluded that sprayed CIS films have different elemental as well as phase composition in the film surface and bulk areas.

3.3. Effect of chemical etching on composition and electrical properties of sprayed CIS films

Chemical etching in ammonium persulfate solution has been used to dissolve the upper In-oxide rich part of CIS film. Fig. 4 presents the AFM picture of the film after 6 minute etching. For this sample part of the film was covered with a tape and only

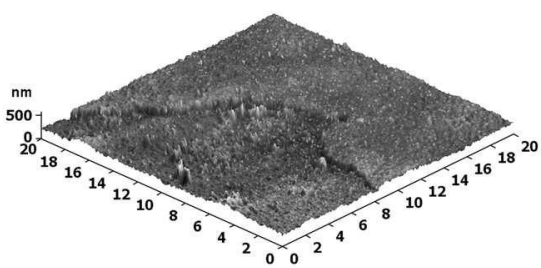

Fig. 4. AFM picture of as-deposited CIS film after etching in 0.01 M $(NH_4)_2S_2O_8$ solution. Etching time 6 min.

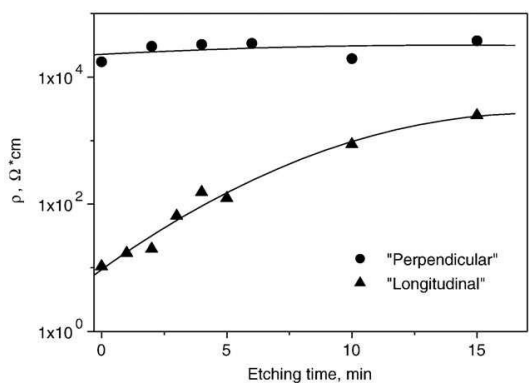

Fig. 5. Specific electrical resistivities of chemically etched CIS films depending of etching time. The film resistance was measured across the film ("perpendicular" resistivity) or along the film surface ("longitudinal" resistivity).

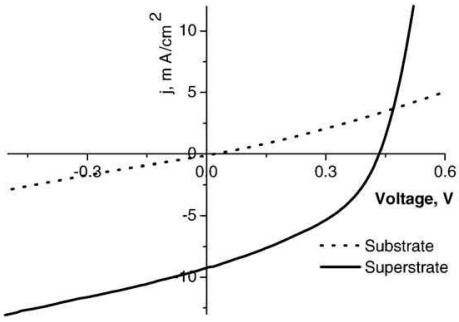

Fig. 6. Current–voltage characteristics of a superstrate (ITO/ZnO/CdS/CIS, solid line) and substrate (ITO/CIS/CdS/ZnO, dashed line) configuration solar cells based on sprayed CIS absorber layer under the halogen lamp illumination of 100 mW/cm^2.

uncovered area has been etched. The etching depth was ~150 nm as evaluated from the step in AFM image. The elemental composition of the etched surface as calculated from the XPS data is presented in Table 1. There is no oxygen on the etched surface and the Cu:In:S=28.3:22.5:49.3. Thus, the surface of chemically etched film is only slightly In-rich compared to the stoichiometric $CuInS_2$. This result is close to that reported for KCN treated CIS films prepared by sputtering of elements followed by annealing in sulfur containing atmosphere [27].

We observed that electrical resistivities of the films calculated from the film resistances measured in "longitudinal" and "perpendicular" modes (see Experimental) are different [28]. Specific electrical resistivities of step-by-step chemically etched CIS film are presented in Fig. 5. It could be seen that specific resistivities of un-etched sample measured in two modes differ more than three orders of magnitude. As "perpendicular" resistivity is much higher than "longitudinal" one it could be speculated that the film surface is more conductive than bulk. By increasing the etching time, "longitudinal" specific resistivity increases obviously due to the removal of more conductive upper layer and comes closer to that measured in perpendicular mode. "Perpendicular" resistivity is nearly constant and does not depend on etching. The electrical measurements also refer to the film graded composition.

I–V curves of solar cell structures based on sprayed CIS using substrate and superstrate configurations are presented in Fig. 6. Sprayed CIS absorber based solar cell can be prepared using superstrate configuration of the cell (ITO/ZnO/buffer/CIS). In this case the CIS absorber layer is sprayed onto the previously deposited window and buffer layers [9,28]. It could be speculated that more conductive upper layer is also responsible for the failed heterojunction preparation using substrate configuration (buffer and window layers are deposited onto the absorber layer) of the cell.

3.4. Effect of annealing in hydrogen sulfide atmosphere on composition of sprayed CIS films

Post-deposition annealing in H_2S atmosphere at temperatures above 500 °C has been found to increase sprayed CIS films crystallinity, energy gap and chalcopyrite ordering [14,29]. Simultaneously, the electrical resistivity of the films increases [29]. XPS spectra recorded from the surface and after Ar^+

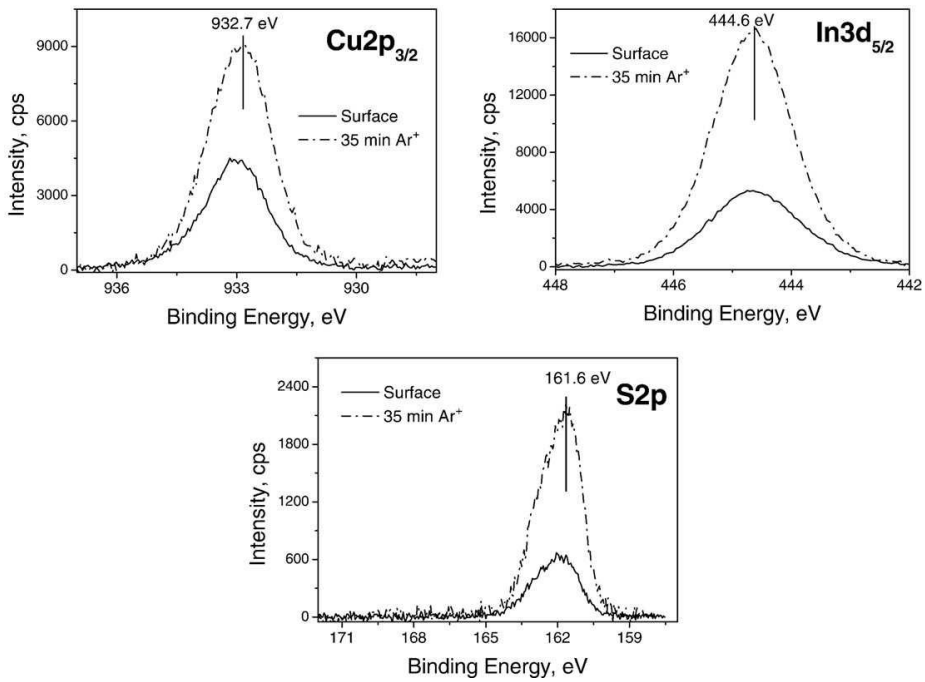

Fig. 7. Cu2p$_{3/2}$, In3d$_{5/2}$ and S2p core levels spectra of H_2S treated CIS films.

sputtering are presented in Fig. 7. Increase of the Cu, In and S peak intensities after Ar-sputtering is obviously due to removal of a highly Na contaminated surface layer (Table 1). The position of $Cu2p_{3/2}$ core level peak (BE = 932.7 eV) of H_2S treated films is independent on the depth profiling. Copper binding energy in H_2S treated sample is similar to that recorded in the depth of as-deposited sample (See Fig. 3). There is no shift in In and S core level binding energies in comparison with the samples without H_2S treatment. Me–O bond is not observed after H_2S treatment. Atomic composition of the sample is given in Table 1. Film surface is highly In- and S-rich, but In/Cu is lower than that in KCN-etched sample before hydrogen sulfide treatment. It could be supposed that In-oxide phase is transformed into In-sulfide upon annealing and some part of In-sulfide is left into the vapor phase. In-sulfide phase in the film could be responsible for high resistivity of H_2S treated films [29]. Marsillac et al. believed that In-sulfide phase in sulfur atmosphere annealed CIS films is located on grain boundaries [19]. Based on $Cu2p_{3/2}$ core level binding energy of 932.7 eV it can be supposed that H_2S treated film is contaminated with some Cu^{2+} containing pieces. Nevertheless we have no straight evidence, it could be speculated that CuS is present in trace amounts as the H_2S treated film detached from the substrate by prolonged KCN etching.

4. Conclusions

X-ray photoelectron spectroscopic study reveals the presence of indium oxide, copper sulfide and a sulfate as main secondary phases in the uppermost surface layer of $CuInS_2$ film deposited by spray at 350 °C in air. KCN etching removes copper sulfide as expected leaving behind highly indium oxide rich film surface. Using Ar^+ sputter depth profiling it appears that film remains In-rich in bulk region although oxygen concentration decreases from film top to down. Results of the film electrical characterization show that film surface is more conductive than bulk. This observation helps to explain failure of preparation of substrate configuration sprayed copper indium disulfide based solar cell. Etching in ammonium persulfate solution has been found to be effective to remove conductive upper layer resulting in the film composition of Cu:In:S = 28.3:22.5:49.3. Nevertheless the thermal treatment in hydrogen sulfide atmosphere significantly improves the sprayed films crystallinity and chalcopyrite ordering, indium oxide originally present in the sprayed film, is converted into the sulfide. Thus spray conditions should be optimized leading to as low as possible oxygen content in as-deposited films.

Acknowledgements

Support by the Estonian Science Foundation grants ETF6954 and 6536 are gratefully acknowledged. A. Katerski wishes to thank the Estonian Doctoral School of Materials Science and Materials Technology (MMTDK) for financial support. K. Kerm is thanked for polarographic measurements and R. Nisumaa for AFM study.

References

[1] R. Klenk, J. Klaer, R. Scheer, M.Ch. Lux-Steiner, I. Luck, N. Meyer, U. Rühle, Thin Solid Films 480–481 (2005) 509.
[2] D. Braunger, Th. Dürr, D. Hariskos, C. Köble, Th. Walter, N. Wieser, H.W. Schock, Proc. 25th IEEE Photovoltaic Specialists Conf., Washington, U.S.A., May 13–17, 1996, IEEE, New York, 1996, p. 1001.
[3] M. Nanu, L. Reijnen, B. Meester, A. Goossens, J. Schoonman, Thin Solid Films 431–432 (2003) 492.
[4] J. Möller, Ch.-H. Fischer, H.-J. Muffler, R. Könenkamp, I. Kaiser, C. Kelch, M.C. Lux-Steiner, Thin Solid Films 361–362 (2000) 113.
[5] J. Qiu, Z. Jin, J. Qian, Y. Shi, W. Wu, Mater. Lett. 59 (2005) 2735.
[6] S. Bini, K. Bindu, M. Lakshmi, C. Sudha Kartha, K.P. Vijayakumar, Y. Kashiwaba, T. Abe, Ren Energi 20 (2000) 405.
[7] M. Krunks, V. Mikli, O. Bijakina, H. Rebane, A. Mere, T. Varema, E. Mellikov, Thin Solid Films 361–362 (2000) 61.
[8] M. Krunks, V. Mikli, O. Bijakina, E. Mellikov, Appl. Surf. Sci. 142 (1999) 356.
[9] A. Mere, A. Katerski, O. Kijatkina, M. Krunks, Paris, France, June 7–11, 2004, Proc. 19th Europ. Photovolt. Sol. En. Conf., 2004, p. 1973.
[10] J. Wienke, M. Krunks, F. Lenzmann, Semicond. Sci. Technol. 18 (2003) 876.
[11] T.T. John, M. Mathew, C.S. Kartha, K.P. Vijayakumar, T. Abe, Y. Kashiwaba, Sol. Energy Mater. Sol. Cells 89 (2005) 27.
[12] B. Zanden, C. Joanta, H. Donker, M. Nanu, B. Meester, Dresden, Germany, September 4–8, 2006, Proc. 21st Europ. Photovolt. Sol. En. Conf., 2006, p. 267.
[13] M. Krunks, O. Kijatkina, H. Rebane, I. Oja, V. Mikli, A. Mere, Thin Solid Films 403–404 (2002) 71.
[14] I. Oja, M. Nanu, A. Katerski, M. Krunks, A. Mere, J. Raudoja, A. Goossens, Thin Solid Films 480–481 (2005) 82.
[15] M.C. Zouaghi, T.B. Nasrallah, S. Marsillac, J.C. Bernède, S. Belgacem, Thin Solid Films 382 (2001) 39.
[16] M. Krunks, T. Leskelä, R. Mannonen, L. Niinistö, J. Therm. Anal. 53 (1998) 355.
[17] M. Krunks, T. Leskelä, L. Niinistö, Jpn. J. Appl. Phys. 39 (2000) 181.
[18] D.G. Hehemann, J.E. Lau, J.D. Harris, M.D. Hoops, N.V. Duffy, P.E. Fanwick, O. Khan, M.H.-C. Jin, A.F. Hepp, Mat. Sci. Eng. B 116 (2005) 381.
[19] S. Marsillac, M.C. Zouaghi, J.C. Bernede, T. Ben Nasrallah, S. Belgacem, Sol. Energy Mater. Sol. Cells 76 (2003) 125.
[20] T.T. John, T. Sebastian, C.S. Kartha, K.P. Vijayakumar, T. Abe, Y. Kashiwaba, Physica, B 388 (2007) 1.
[21] C.D. Wagner, A.V. Naumkin, A. Kraut-Vass, J.W. Allison, C.J. Powell, J.R. Rumble Jr., NIST Standard Reference Database 20, Ver. 3.4, , 2006 (Web Version at http://srdata.nist.gov/xps/index.htm).
[22] T. Yano, M. Ebizuka, S. Shibata, M. Yamane, J. Electron. Spectrosc. Relat. Phenom. 131–132 (2003) 133.
[23] M. Krunks, O. Kijatkina, A. Mere, T. Varema, I. Oja, V. Mikli, Sol. Energy Mater. Sol. Cells 87 (2005) 207.
[24] Y. He, Ph.D. Thesis, Justus-Liebig University, Giessen, Germany, 2003.
[25] B. Asenjo, A.M. Chaparro, M.T. Gutierrez, J. Herrero, Thin Solid Films 511–512 (2006) 117.
[26] B. Timmermans, F. Reniers, A. Hubin, C. Buess-Herman, Appl. Surf. Sci. 144–145 (1999) 54.
[27] K. Müller, R. Scheer, Y. Burkov, D. Schmeißer, Thin Solid Films 451–452 (2004) 120.
[28] A. Mere, Ph.D. Thesis, Tallinn University of Technology, Estonia, 2006.
[29] M. Krunks, A. Mere, A. Katerski, V. Mikli, J. Krustok, Thin Solid Films 511–512 (2006) 434.

PAPER III

A. Katerski, M. Danilson, A. Mere, M. Krunks, Effect of the growth temperature on chemical composition of spray-deposited $CuInS_2$ films, *Energy Procedia*, 2 (2010) 103-107.

Available online at www.sciencedirect.com
ScienceDirect
Energy Procedia 2 (2010) 103–107
Energy Procedia
www.elsevier.com/locate/procedia

E-MRS Spring meeting 2009, Symposium B

Effect of the growth temperature on chemical composition of spray-deposited $CuInS_2$ thin films

A. Katerski, M. Danilson, A. Mere, M. Krunks*

Department of Materials Science, Tallinn University of Technology, Ehitajate tee 5, EE-19086 Tallinn, Estonia
Received 1 June 2009; received in revised form 1 December 2009; accepted 20 December 2009

Abstract

$CuInS_2$ films were deposited by spray pyrolysis method at 250 ºC and 350 ºC using aqueous solutions of $CuCl_2$, $InCl_3$ and $SC(NH_2)_2$ at molar ratio of precursors Cu:In:S=1:1:3 in spray solution. Films were characterized by X-ray diffraction (XRD), Raman and X-ray photoelectron spectroscopy (XPS) techniques. According to XPS, the films grown at 350 ºC have Cu^{2+} containing pieces on the surface, the film composition in bulk region is not homogeneous and contains metal bonded oxygen in amount of 5-8 at.%. Deposition at 250 °C reduces the content of oxygen down to ~ 1 at. %, the films are low-crystalline with uniform distribution of the elements throughout the film and contain some excess of sulfur compared to stoichiometric $CuInS_2$.

Keywords: $CuInS_2$; Spray Pyrolysis; Thin Films; X-ray photoelectron spectroscopy; X-ray diffraction

Introduction

$CuInS_2$ (CIS) with chalcopyrite structure has been successfully used as a light absorber material in different types of solar cells. Optimum band gap of 1.5 eV, high absorption coefficient (more than 10^4 cm^{-1}) and chemical stability make this material important for photovoltaic applications. Thin film solar cells with CIS absorber made by rapid thermal processing and reactive magnetron sputtering techniques exhibit conversion efficiencies of 11.4 % [1, 2]. For economical reasons, it will be useful to prepare thin films using a low-cost deposition technique. One of such methods is spray pyrolysis technique, which allows obtain large-area films at extremely low cost [3, 4]. Extremely thin absorber layer (ETA) cells with sprayed CIS absorber show conversion efficiencies ~ 7 % [5] and ~ 4 % [6], made on TiO_2 or ZnO nanostructures, respectively. The control of the film surface and bulk composition is extremely important to optimize the film preparation conditions to obtain the absorber material with properties suitable for efficient photovoltaic structures. X-ray photoelectron spectroscopy (XPS) employing argon ion sputtering is a technique to obtain this information. In the literature, there are few investigations on chemical composition of sprayed CIS films by XPS [7-9]. CIS films obtained by spray of Cu-rich solution resulted in the films with In-rich surface [7, 9] and contain In_2O_3 as a secondary phase [8, 9] which one is segregated at the grain boundaries [8]. The aim of the present study is to show the effect of the CIS deposition temperature on the properties of the thin films when spraying aqueous solutions with equimolar concentrations of indium and copper

* Corresponding author. Tel.: +372 620-33-63; fax: +372 620-20-20.
E-mail address: malle@staff.ttu.ee.

1876-6102
doi:10.1016/j.egypro.2010.07.016

chlorides. The films are characterized by XRD, Raman and XPS techniques. The effect of deposition temperature on the structure and elemental composition of spray-deposited CIS films is discussed.

Experimental

$CuInS_2$ films were deposited by spray of an aqueous solution containing $CuCl_2$, $InCl_3$ and $SC(NH_2)_2$ at precursors molar ratio of Cu:In:S=1:1:3 onto the preheated glass substrates. The films were deposited at growth temperatures of 250 or 350 °C whereat other deposition parameters such as spray solution volume of 50 ml, solution concentration ($[Cu^{2+}]$ = 2 mmol/l) and feeding rate were kept constant for all samples.

The crystal structure of the sprayed films was characterized by XRD patterns recorded on a Rigaku Ultima IV diffractometer. Micro-Raman scattering measurements were performed at room temperature with the excitation wavelength of 532 nm and output power of 2 mW on Horiba Jobin Yvon Model HR 800 spectrometer. X-ray photoelectron spectroscopic (XPS) measurements were performed using a Kratos AXIS Ultra DLD X-ray Photoelectron Spectrometer in conjunction with a 165 mm hemispherical electron energy analyser and delay-line detector. Analysis was carried out with monochromatic Al Kα X-rays (1486.6 eV) operating at 15 kV and 225 W. All XPS spectra were recorded using an aperture slot of 300 x 700 microns and pass energy of 20 eV. Binding energy values for $CuInS_2$ were calculated on the basis of the C1s peak at 285.0 eV. The atomic concentrations were determined from $Cu2p_{3/2}$, $In3d_{5/2}$, O1s, S2p, Cl2p and Si2p core level peak areas and sensitivity factors provided by the Vision 2.2.6 analysis software. To obtain information of the film bulk composition, minibeam I ion (Ar^+) source (4 kV, 20 mA, $5 \cdot 10^{-8}$ Torr, 60 s per cycle) has been used for the depth profiling.

Results and discussion

Figure 1 presents the XRD and Raman spectra of the films deposited at 250 and 350 °C. According to XRD (Fig. 1a), the film grown at 250 °C has poor crystallinity, the main diffraction peaks are belonging to the $CuInS_2$ phase (PDF card No. 00-027-0159). An additional diffraction peak at 2θ=26.4° (marked by 'x' in Fig. 1.a) is recorded and could belong to In_xS_y or $CuIn_5S_8$ phases [11]. Deposition at 350 °C leads to narrowing of the diffraction peaks indicating an increase in crystallite size. The crystallite size of 8 and 20 nm have been calculated from the XRD patterns of sprayed films deposited at 250 and 350 °C, respectively. The film grown at 350 °C show an additional diffraction peak at 2θ=30.5° belonging to the (222) diffraction peak of In_2O_3 phase (PDF card No. 00-006-0416). These results are in good correspondence with the earlier results on spray-deposited CIS films [3, 10, 11]. Fig. 1 b shows the Raman spectra of as-deposited CIS films grown at 250 and 350 ºC. It can be seen that the most intensive Raman band consists of two bands, A_1 band of chalcopyrite (CH) ordered compound at 294 cm^{-1} and A_1* band of Cu–Au (CA) ordered phase at 305 cm^{-1} [11]. Although the crystallinity of the films was strongly affected by the deposition temperature (Fig.1a), the short-range ordering of sprayed $CuInS_2$ films is similar and almost independent of the deposition temperature in the temperature region of 250-350 °C (Fig 1.b).

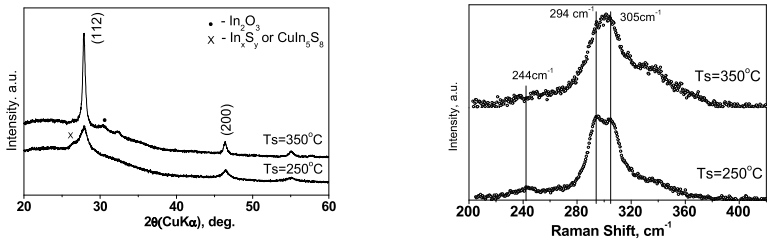

a)

Fig. 1. XRD patterns a) and Raman spectra b) of as-sprayed $CuInS_2$ films deposited at 250 and 350 ºC.

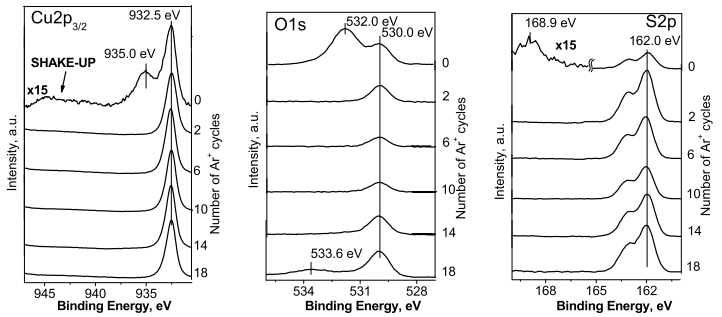

Fig. 2. Cu2p, O1s and S2p core levels spectra of spray deposited $CuInS_2$ films taken from the film surface and after different Ar^+ sputtering cycles. The film was grown at 350 ºC.

According to XPS spectra of CIS films prepared by spray of aqueous solutions with molar ratio of precursors Cu:In:S=1:1:3 at 250 and 350 °C, the binding energies (BE) of $Cu2p_{3/2}$, $In3d_{5/2}$ and S2p core levels are placed at 932.5 eV, 445.0 eV and 162.0 eV, respectively. The binding energies recorded correspond to that of copper, indium and sulfur in spray deposited CIS films [7, 9]. The O1s core level peaks at BE of 532.0 and 530.0 eV, characteristic of oxygen in adsorbed $(OH)^-$ groups and oxygen bonded to metal (Me-O) [12], respectively, were present in the XPS spectra recorded from the film surface. Also weak response from Cl2p at BE=198.7 eV has been detected in XPS spectra due to contamination originated from the metal chloride precursors. Content of chlorine impurity was about 1.0-1.5 at. % in the film deposited at 250 °C, its content drops below 1 at. % when the film was prepared at higher temperature.

Figure 2 presents XPS spectra of $Cu2p_{3/2}$, O1s and S2p core levels of CIS film deposited at 350 °C after different Ar^+ ion etching cycles. Number of the Ar^+ sputtering cycles is given in the graphs: the upper spectrum is recorded from the non-cleaned surface, by increasing the number of etching cycles the signal is recorded from the film bulk region down to the substrate. Due to similarity of In3d binding energies in $CuInS_2$ and in possible secondary phases such as In_2O_3, In_2S_3 etc., the chemical shift of In3d core level peak was not observed. Independent of the deposition temperature and profiling depth, the BE of $In3d_{5/2}$ is located at 445.0 eV. This is a reason do not present In3d spectra in Figure 2. The second $Cu2p_{3/2}$ core level peak at 935.0 eV and shake-up satellites in the BE region of 940-944 eV, both characteristic of Cu^{2+} state [13], are recorded from the non-cleaned surface (Fig.2). Also the second peak of S2p core level at BE=168.9 eV, corresponding to sulfur in sulfates, was detected on the surface (Fig. 2). These extra peaks were not detected after Ar^+ sputtering. The intensity of O1s core level peak at BE= 530.0 eV (Me-O) is decreasing from the film surface to bulk. It can be observed that the Me-O peak intensity increases before the signal at BE=533.6 eV, characteristic of oxygen in silicates (in glass) [12], becomes apparent.

In the case of CIS films deposited at 250 ºC, the secondary peaks of $Cu2p_{3/2}$ and S2p core levels with BE of 935.0 eV and 168.9 eV, respectively, were not detected on the film surface (XPS spectra of the films deposited at 250 °C are not presented). The O1s peak at BE=532.0 eV was present in the spectrum recorded from non-cleaned surface and refers to the surface contamination from ambient. The intensity of O1s line at BE=530.0 eV was low on the surface and in the film bulk. The positions as well as the intensities of $Cu2p_{3/2}$, $In3d_{5/2}$ and S2p core level peaks were constant throughout the film.

The atomic concentrations of the elements *vs.* the number of Ar^+ ion sputtering cycles of the films deposited at different temperatures are presented in Figure 3. Figure 3a shows the results of the depth profiling analysis of CIS film deposited at 350 ºC. It can be seen that the distribution of the elements in the film is not constant and the film thickness could be divided into three regions. Non-uniform distribution of In and Cu is characteristic for the first (surface) region, whereat Cu/In is much lower than 1. In the second region, the composition is still In-rich, but concentrations of In, Cu and O are almost constant and concentration of sulfur starts to decrease. In the third

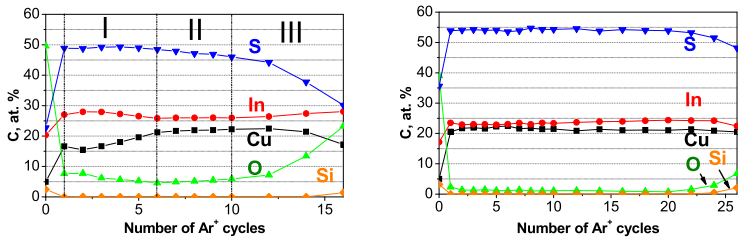

Fig. 3. The elements concentration depth profiling in CIS films deposited at 350°C (a) and 250 °C (b) onto glass substrates

region, the concentration of sulfur is decreasing from about of 44 to 30 at. % and is accompanied by an increase in amount of oxygen (Me-O). The presence of In_2O_3 phase was confirmed by XRD (Fig. 1a). The XPS depth profiling shows that In_2O_3 phase is present throughout the film thickness. Even more, the amount of oxygen (Me-O) is increasing (and sulfur concentration is decreasing) before the signal from glass substrate (Si) becomes apparent at about 15 Ar^+ sputtering cycles (Fig. 3a). It refers that In_2O_3 phase is easily formed in an initial stage of the film growth at this deposition temperature.

Concentration depth profiling of CIS film deposited at 250 ºC (Fig. 3b) shows homogeneous distribution of elements such as Cu, In and S throughout the film. Content of oxygen (Me-O) in the film is about 1 at. %. Concentration of sulfur is above 50 at. % and refers to a sulfur-rich film compared to the stoichiometric $CuInS_2$. Obviously, secondary phases such as In_xS_y or $CuIn_5S_8$ could be present in the film deposited at 250 °C. This assumption is supported by the XRD pattern of the film (Fig.1) and is correspondence with literature data on CIS films deposited at low temperatures [8].

Conclusions

Spray pyrolysis deposition of aqueous solutions containing $CuCl_2$ and $InCl_3$ in equimolar concentrations and thiourea (Cu:In:S=1:1:3) at temperatures close to 350 °C results in polycrystalline $CuInS_2$ films with the crystallite size of 20 nm. The films grown at 250 °C have the crystallite size in the order of 8 nm. According to Raman spectroscopy studies both the chalcopyrite and Cu-Au ordered $CuInS_2$ phases are present, and the short-range ordering is almost independent of the growth temperature. According to XPS of the film deposited at 350 °C, the Cu^{2+} containing pieces are present on the surface of the film, the film elemental composition in the bulk region is not homogeneous, content of oxygen (oxygen bonded to metal) is 5-8 at.%. Oxygen is present in the form of In_2O_3 as also confirmed by XRD.

In this study we showed that $CuInS_2$ films with low amount of oxygen (1 at.% or less) and uniform distribution of the copper, indium and sulfur throughout the film can be produced by chemical spray pyrolysis technique in open air using the deposition temperature close to 250 °C. These films are slightly sulfur-rich which refers that a sulfur-containing secondary phase could be present as well.

Acknowledgements

The study is financially supported by the Estonian Ministry of Education and Research (target financing project SF0140092s08) and the Estonian Science Foundation (grant ETF6954). M. Danilson likes to thank World Federation of Scientists for support.

References

[1] K. Siemer, J. Klaer, I. Luck, J. Bruns, R. Klenk, D. Braunig; 2001; ”Efficient $CuInS_2$ solar cells from a rapid thermal process (RTP)”; *Sol. Energ. Mater. Solar Cells*, 67, 159-166.

[2] S. Seeger, K. Ellmer; 2009; “Reactive magnetron sputtering of $CuInS_2$ absorbers for thin film solar cells: Problems and prospects”; *Thin Solid Films*, 517, 3143-3147.

[3] M. Krunks, V. Mikli, O. Bijakina, H. Rebane, A. Mere, T. Varema, E. Mellikov; 2000; „Composition and structure of $CuInS_2$ films prepared by spray pyrolysis”; *Thin Solid Films*, 361–362, 61-64.

[4] M. Krunks, V. Mikli, O. Bijakina, E. Mellikov; 1999; „Growth and recrystallization of $CuInS_2$ films in spray pyrolytic process”; *Appl. Surf. Sci.*, 142, 356-361.

[5] A. Goossens, J. Hofhuis; 2008; ”Spray-deposited solar cells”; *Nanotechnology*, 19, 424018.

[6] A. Mere, A. Katerski, T. Dedova, I. Oja Acik, M. Krunks; 2008; „ Extremely thin absorber layer nanostructured solar cell by chemical spray pyrolysis”; Proc. 23rd Eur. Photovolt. Sol. En. Conf., 1-5 Sept. 2008, Valencia, Spain.

[7] M.C. Zouaghi, T.B. Nasrallah, S. Marsillac, J.C. Bernède, S. Belgacem; 2001; „Physico-chemical characterization of spray-deposited $CuInS_2$ thin films”; *Thin Solid Films*, 382, 39-46.

[8] S. Marsillac, M.C. Zouaghi, J.C. Bernede, T. Ben Nasrallah, S. Belgacem; 2003; „Evolution of the properties of spray-deposited $CuInS_2$ thin films with post-annealing treatment”; *Sol. Energy Mater. Sol. Cells*, 76, 125-134.

[9] A. Katerski, A. Mere, V. Kazlauskiene, J. Miskinis, A. Saar, L. Matisen, A. Kikas, M. Krunks; 2008; „Surface analysis of spray deposited copper indium disulfide films”; *Thin Solid Films*; 516, 7110-7115.

[10] M. Krunks, O. Kijatkina, H. Rebane, I. Oja, V. Mikli, A. Mere; 2002; „Composition of $CuInS_2$ thin films prepared by spray pyrolysis”; *Thin Solid Films*, 403–404, 71-75.

[11] I. Oja, M. Nanu, A. Katerski, M. Krunks, A. Mere, J. Raudoja, A. Goossens; 2005; „Crystal quality studies of $CuInS_2$ films prepared by spray pyrolysis”; *Thin Solid Films*, 480–481, 82-86.

[12] C. D. Wagner, A.V. Naumkin, A. Kraut-Vass, J.W. Allison, C.J. Powell, and J.R. Rumble Jr., NIST Standard Reference Database 20, Ver. 3.4 (2006) (Web Version at http://srdata.nist.gov/xps/index.htm).

[13] T. Yano, M. Ebizuka, S. Shibata, M. Yamane; 2003; „Anomalous chemical shifts of Cu 2p and Cu LMM Auger spectra of silicate glasses”; *Thin Solid Films*, 131-132, 133-144.

PAPER IV

M. Krunks, **A. Katerski**, T. Dedova, I. Oja Acik, A. Mere, Nanostructured solar cell based on spray pyrolysis deposited ZnO nanorod array, *Sol. Energy Mater. Sol. Cells* 92 (2008) 1016-1019.

Solar Energy Materials & Solar Cells 92 (2008) 1016–1019

Contents lists available at ScienceDirect

Solar Energy Materials & Solar Cells

journal homepage: www.elsevier.com/locate/solmat

Nanostructured solar cell based on spray pyrolysis deposited ZnO nanorod array

M. Krunks *, A. Katerski, T. Dedova, I. Oja Acik, A. Mere

Department of Materials Science, Tallinn University of Technology, Ehitajate tee 5, Tallinn 19086, Estonia

ARTICLE INFO

Article history:
Received 11 December 2007
Accepted 2 March 2008
Available online 11 April 2008

Keywords:
ZnO nanorod
Solar cell
Extremely thin absorber layer
Chemical spray pyrolysis

ABSTRACT

In this paper we present a realization of an extremely thin absorber (ETA) layer solar cell by the chemical spray pyrolysis method. $CuInS_2$ absorber was deposited onto a blocking layer coated ZnO nanorods grown on a transparent conductive oxide. Layers and cells were characterized by optical and Raman spectroscopy, and scanning electron microscopy. Current–voltage, spectral response and electron beam induced current measurements were applied to solar cells. ZnO nanorod cell showed twice higher short circuit current density than the flat reference. ETA cells with efficiency of 2.2% ($j = 12\ mA/cm^2$, $V_{oc} = 425\ mV$, FF = 43%) and of 2.5% were prepared using TiO_2-anatase and an indium sulfide blocking layer, respectively.

1. Introduction

Low-cost deposition techniques and new designs are of continuous interest to reduce production costs of photovoltaic devices. In recent years, nanostructure use in photovoltaic devices has attracted major interest. Dye sensitized photoelectrochemical solar cell (DSSC) based on nanoporous titanium dioxide is the best-known representative of the family of nanostructured PV devices [1]. Stability problems of DSSC, including its solid-state modifications, promote development of the concept of extremely thin absorber (ETA) cell which uses an extra thin absorber sandwiched between two strongly interpenetrating transparent wide bandgap semiconductors [2]. TiO_2 is the most frequently used n-type nanostructured window material in the ETA cell. As an alternative, nanostructured columnar zinc oxide has been used to prepare ZnO/CdTe ETA cell [3]. Inorganic absorber materials like CdTe [3,4] and CdSe [5–7] have been used in nanostructured ZnO based cells. The conversion efficiency of 2.3% has been achieved in ZnO nanowire based ETA cells [5,6]. ZnO nanowire layers for photovoltaic application have been fabricated by electrodeposition [3–7], metal organic vapour deposition [8] and hydrothermal growth [9].

Recently a low-cost deposition route to grow ZnO nanorod arrays on conductive transparent electrodes by chemical spray was developed by our group [10–12]. In this study, we describe the preparation and properties of solar cells based on nanostructured layers comprising ZnO nanorods and copper–indium disulfide absorber layer. Both ZnO nanorods and the absorber layer were deposited by the chemical spray pyrolysis method.

2. Experimental

ZnO nanorods were deposited by spray of zinc chloride aqueous solutions onto the indium tin oxide (ITO) covered glass substrates at deposition temperatures slightly above 500 °C. ZnO nanorod layer (ZnO_R) deposition by the spray technique is reported in detail in our previous studies [10–12]. To prepare a ZnO structured layer based solar cell, the following layers were deposited by keeping the sequence: ZnO_R, TiO_2 or 'InS' blocking layer, In_2S_3 and finally, $CuInS_2$ (CIS). A thin film of TiO_2 as a blocking layer was prepared by the sol–gel dip coating method using the titanium tetra-isopropoxide based titania sol [13]. As an alternative, a dense layer of indium sulfide was used instead of a TiO_2 blocking layer. This layer (named 'InS') was deposited by spray using the solution containing $InCl_3$ and thiocarbamide ($SC(NH_2)_2$) in a molar ratio of In:S = 1:3 at pH~5. Indium sulfide (In_2S_3) buffer layer was deposited by spray using the spray solution of $InCl_3$ and $SC(NH_2)_2$ with the molar ratio of In:S = 1:3 at $InCl_3$ concentration of 2×10^{-3} mol/l and pH~3. $CuInS_2$ (CIS) absorber layer was deposited by spray using the solution containing $InCl_3$, $CuCl_2$ and $SC(NH_2)_2$ at the molar ratios of Cu:In:S = 1:1:3, following the preparation route described elsewhere [14]. Indium sulfide layers and CIS absorber layer were grown at a similar temperature close to 300 °C. Flat solar cells (no ZnO rods) as reference samples were prepared simultaneously with the structured cells. Component layers were identified by their bandgap (E_g) or Raman spectra. The optical transmittance

* Corresponding author.
E-mail address: malle@staff.ttu.ee (M. Krunks).

0927-0248/$ - see front matter © 2008 Elsevier B.V. All rights reserved.
doi:10.1016/j.solmat.2008.03.002

and reflectance spectra of the component layers and the structures were measured in the wavelength range of 200–2500 nm at room temperature on a Jasco V-670 UV–VIS–NIR spectrophotometer fitted with an integrating sphere. Raman spectra of the layers were recorded in the backscattering nonpolarized mode at room temperature using a confocal laser micro-Raman spectrometer HORIBA Jobin Yvon Model HR 800. The excitation radiation wavelength was 532.0 nm and the intensity was 10^7 W/m^2.

Surface morphology and cross-section views of the structures were examined by high-resolution scanning electron microscopy (SEM) on Zeiss HR FESEM Ultra 55. The image of p–n junction was investigated with the help of electron beam induced current (EBIC) detector. Photoconversion of the solar cells was characterized by *I–V* curves in the dark and under the halogen lamp illumination (intensity 100 mW/cm^2). External quantum efficiency (EQE) spectrum of the solar cells was measured in the wavelength range of 400–1200 nm using 100 W halogen tungsten quartz (HTQ) lamp and SPM-2 monochromator ($f = 40$ cm). Graphite was used to make electrical contacts.

3. Results and discussion

3.1. Choice and characterization of solar cell component layers

In this study we prepared solar cell onto the spray deposited nanostructured ZnO layers comprising elongated crystals. SEM cross-sectional micrograph of the ZnO nanorod layer on ITO electrode is presented in Fig. 1a. TiO_2 blocking layer was deposited onto the structured zinc oxide to protect ZnO from dissolution during the deposition of acidic solution to form In_2S_3 buffer and copper indium disulfide absorber layers. Another role of TiO_2 blocking layer was to avoid electrical short-circuiting of the solar cell structure. In previous studies, a continuous ZnO or TiO_2 layer has been deposited first on the conducting transparent electrode to avoid any contact and consequent short-circuiting between the front and back contact [4,5,7,15] and ZnO rods were grown on those metal oxide layers.

Fig. 2 shows Raman spectrum of the flat TiO_2 film as a reference sample prepared in parallel to depositing TiO_2 onto the structured ZnO layer. Raman peaks at 144, 196, 398, 518 and 638 cm^{-1} confirm the formation of TiO_2–anatase film [16].

An alternative blocking layer, 'InS', was deposited by spray in order to reduce the preparation time, to keep spray process continuous and thus to simplify the solar cell fabrication process. According to the SEM study (SEM microphoto is not presented), thin, dense and pinhole-free 'InS' film was formed. Both indium sulfide films, 'InS' blocking layer and In_2S_3 buffer layer, show a similar band gap value of 2.0 eV (Fig. 3). The bandgap of indium sulfide films was calculated from the optical transmittance and reflectance spectra, assuming the indirect transition type and linearity of $(\alpha h\nu)^{1/2}$ vs. $h\nu$ plot.

The sequence of component layers in the solar cells based on nanostructured ZnO and their flat references together with cell numbering is as follows:

1. ITO/TiO_2/In_2S_3/CIS (flat);
2. ITO/ZnO_R/TiO_2/In_2S_3/CIS (structured);
3. ITO/'InS'/In_2S_3/CIS (flat);
4. ITO/ZnO_R/'InS'/In_2S_3/CIS (structured).

SEM cross-sectional microphoto of ITO/ZnO_R/TiO_2/In_2S_3/CIS structure (cell 2) is presented in Fig. 1b. As can be seen, ZnO crystals in the solar cell structure are covered with a CIS layer with

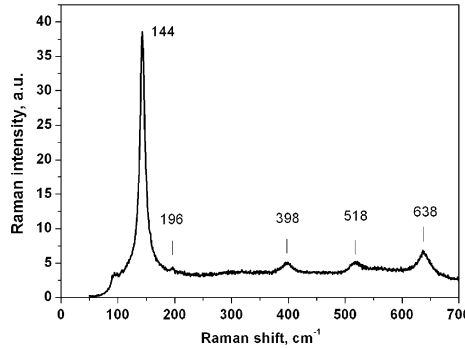

Fig. 2. Raman spectrum of the TiO_2 film made by sol–gel dip coating on a glass substrate and annealed for 30 min at 450 °C in air.

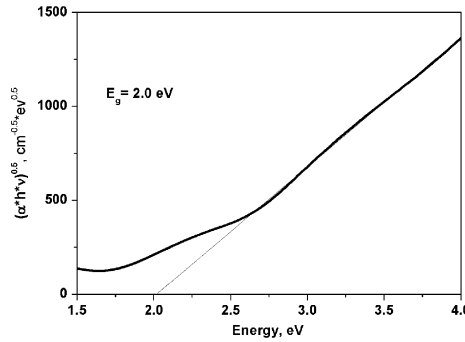

Fig. 3. Determination of the optical bandgap of the spray deposited indium sulfide buffer layer.

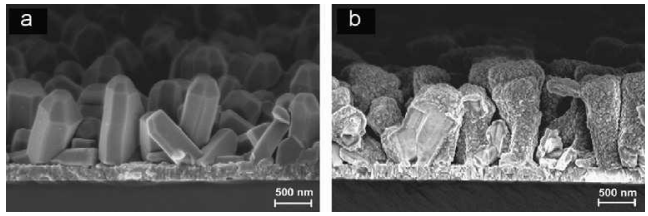

Fig. 1. SEM cross-sections of spray deposited ZnO nanostructured layer on indium tin oxide (ITO) covered glass substrate (a), and the solar cell structure (ITO/ZnO_R/TiO_2/In_2S_3/CIS) before conducting (b).

a thickness lower than 50 nm. Thus, the solar cell formed could be classified as an ETA layer solar cell. CIS layer thickness is almost uniform on top and side planes of the ZnO crystals, as shown by the cross-section of one broken crystal (Fig. 1b). The blocking layer of TiO_2 and the buffer layer of In_2S_3 cannot be clearly distinguished from the SEM microphoto, due to their low thickness.

3.2. Optical properties of solar cells

Fig. 4 presents the transmittance spectra of the substrate (glass/ITO), substrate with ZnO rods (glass/ITO/ZnO_R) and the completed cell (glass/ITO/ZnO_R/TiO_2/In_2S_3/CIS). In the case of glass/ITO/ZnO_R sample interference fringes disappear (curve 2 in Fig. 4), which indicates the loss of the flat morphology. The energy gap close to 3.2 eV for ZnO and 1.4 eV for CIS was estimated from these spectra, using the relation for the direct transition.

The effective reflectance (R_E, determined as the ratio of integrated reflectance to the integrated photon flux) and the effective absorbance (A_E, determined as the ratio of integrated absorbance to the integrated photon flux) are solar cell relevant parameters characterizing the light trapping ability of the photovoltaic device [4,6]. R_E and A_E were calculated for the flat (cell 1) and structured cell (cell 2) using total reflectance and transmittance spectra recorded in the wavelength range of 400–800 nm. The results are summarized in Table 1. A_E of the structured cell (~56%) is 14% higher than that of the flat cell (~42%) mainly due to the higher reflectivity of the latter. Structured cell 2 has A_E~56% and R_E~35% vs. A_E~89% and R_E~8% of the glass/SnO_2/ZnO/ZnO_R/CdSe cell [6]. Consequently, the ZnO_R/CdSe cell, where CdSe absorber with a layer thickness of 30–40 nm was deposited onto the ZnO rods with a length of ~2 μm, indicates a much better light trapping ability than the structure composed of sprayed rods with a length of ~1 μm (Fig. 1). To achieve a higher light trapping in the structures based on sprayed ZnO rods, longer and thinner rods should be used.

3.3. Solar cell output characteristics

I–V curves of flat (cell 1) and structured (cell 2) cells are presented in Fig. 5. Solar cell output parameters of flat and structured cells with different blocking layers are summarized in Table 2. Solar cell output parameters show that current density (j) of the cell built on ZnO nanorods is at least two times higher than that of the flat cell prepared simultaneously with the structured one. Current density of 12 mA/cm^2 achieved for structured cell 2 is three times higher than that obtained on ZnO_R/CdSe structure

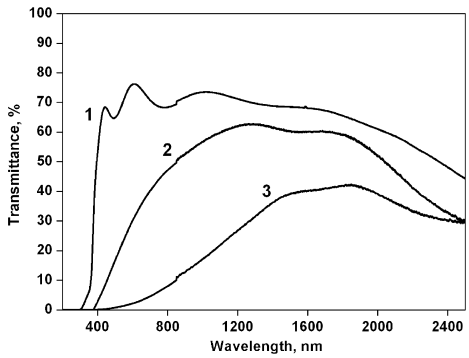

Fig. 4. Optical transmittance spectra of glass/ITO substrate (1), glass/ITO/ZnO_R (2) and completed solar cell structure glass/ITO/ZnO_R/TiO_2/In_2S_3/CIS (3).

Table 1
Effective reflectance (R_E) and effective absorbance (A_E) of the flat and structured cell in the spectral region of 400–800 nm

Structure type	R_E (%)	A_E (%)
Flat	43	42
Structured	35	56

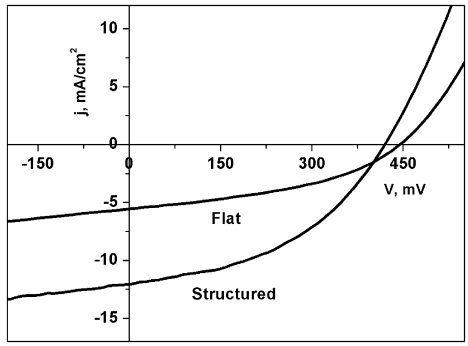

Fig. 5. Current–voltage characteristics of flat (cell 1: ITO/TiO_2/In_2S_3/CIS) and structured (cell 2: ITO/ZnO_R/TiO_2/In_2S_3/CIS) solar cells under halogen lamp illumination of 100 mW/cm^2.

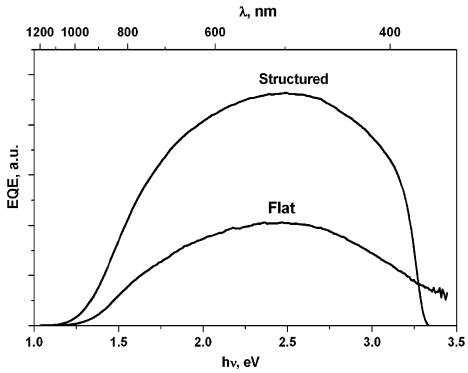

Fig. 6. External quantum efficiency (EQE) spectra of the flat and structured solar cells. Flat cell—cell 1, ITO/TiO_2/In_2S_3/CIS; structured cell—cell 2, ITO/ZnO_R/TiO_2/In_2S_3/CIS.

Table 2
Output characteristics of the flat and structured solar cells under the halogen lamp illumination intensity of 100 mW/cm^2

Cell no.	Cell structure	Blocking layer	V_{oc} (mV)	j (mA/cm^2)	FF (%)	Eff. (%)
1	Flat	TiO_2	445	5.5	41	1.0
2	Structured		425	12.0	43	2.2
3	Flat	'InS'	485	4.3	63	1.3
4	Structured		455	9.1	60	2.5

Cell numbering is given in Section 3.1.

(4 mA/cm^2) made by electrochemical deposition in spite of the fact that much better light trapping was observed in the ZnO_R/CdSe cell [5,6]. Open circuit voltage (V_{oc}) is slightly higher in the case of flat samples independent of the barrier layer used. This behaviour could be explained by a higher recombination in the

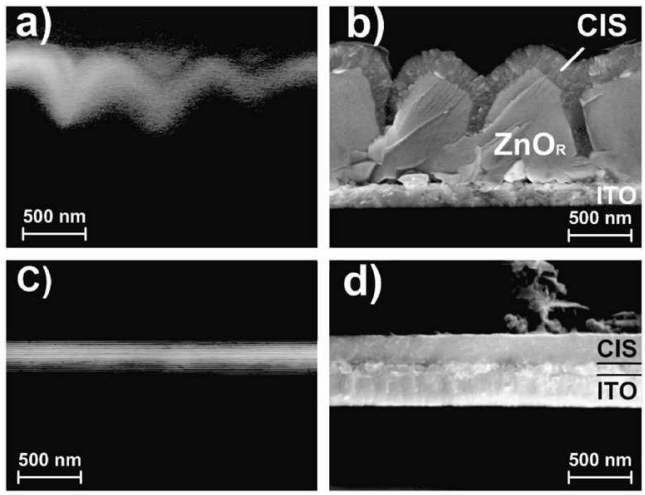

Fig. 7. Electron beam induced current (EBIC) (a) and SEM (b) cross-sectional views of the structured cell ITO/ZnO$_R$/TiO$_2$/In$_2$S$_3$/CIS. EBIC (c) and SEM (d) images of the flat cell prepared in the same batch are presented for comparison.

structured cells. Additionally, the thicknesses of blocking and buffer layers could be different in flat and structured cells. Thicknesses of component layers have been found to control the output parameters of ETA cells prepared by SILAR technique [17]. No marked differences were found in the fill factors (FF) of the structured and flat cells. Interestingly, the FF of the cells based on sprayed 'InS' blocking layer were always higher (~60%) than those of TiO_2 layer samples (~40%) (Table 2). In the current stage of studies, we cannot make any conclusions yet of which blocking layers should be preferred.

EQE spectra of structured and flat cells are presented in Fig. 6. As expected, the EQE graphs of the flat and structured cells show a similar shape. At the same time, the cell based on ZnO rods shows higher EQE (Fig. 6), and about twice higher current density than the flat cell (Fig. 5). Fig. 7 presents the EBIC image (a) and the SEM image (b), both recorded from the same cross-section area of the structured sample. According to the EBIC and SEM images, the p–n junction is continuous and follows the shape of ZnO crystals. EBIC and SEM images of the flat cell are presented for comparison (Fig. 7c and d). It can be seen that the p–n junction area of the structured cell is larger than that of the flat cell. The current collective region is almost expanded into the CIS absorber, as seen from the junction EBIC views (Fig. 7a and c). Thus, the increased current density of structured cell is mainly due to increased p–n junction area.

4. Conclusions

It has been shown experimentally that ZnO nanorod arrays grown by the spray pyrolysis method could be successfully used to fabricate a nanostructured solar cell. The conversion efficiency of 2.5% was obtained using the spray pyrolysis technique for both ZnO nanorod and copper indium disulfide absorber layers. To our knowledge, it is the highest value reported to date for the ZnO nanorod based solar cells, based on an inorganic absorber layer.

The increase in the short-circuit current density due to the increased p–n junction area is mainly responsible for the higher efficiency of the structured cell compared to the flat analogue. As the preparation technology is simple and fast, operates at low or moderate temperatures and there is no need for expensive and sophisticated apparatus, thus it could be prospective for fabrication of efficient solar cells with large area at low cost. A detailed study of physical properties of the cell and further development of the deposition process are in progress.

Acknowledgment

Financial support by the Estonian Science Foundation Grant 6954 is gratefully acknowledged.

Mrs. O. Volobujeva is thanked for the SEM study.

References

[1] B. O'Regan, M. Grätzel, Nature 353 (1991) 737.
[2] K. Ernst, A. Belaidi, R. Könenkamp, Semicond. Sci. Technol. 18 (2003) 475.
[3] C. Lévy-Clément, A. Katty, S. Bastide, F. Zenia, I. Mora, V. Munoz-Sanjose, Physica E 14 (2002) 229.
[4] R. Tena-Zaera, A. Katty, S. Bastide, C. Lévy-Clément, B. O'Regan, V. Muñoz-Sanjosé, Thin Solid Films 483 (2005) 372.
[5] C. Lévy-Clément, R. Tena-Zaera, M.A. Ryan, A. Katty, G. Hodes, Adv. Mater. 17 (2005) 1512.
[6] R. Tena-Zaera, M.A. Ryan, A. Katty, G. Hodes, S. Bastide, C. Lévy-Clément, C. R. Chim. 9 (2006) 717.
[7] R. Tena-Zaera, J. Elias, A. Katty, S. Bastide, C. Lévy-Clément, Proceedings of the Twenty first European PV Solar Energy Conference, 4–8 September 2006, Dresden, Germany, 2006, p. 238.
[8] J.B. Baxter, E.S. Aydil, Sol. Energy Mater. Sol. Cells 90 (2006) 607.
[9] M. Guo, P. Diao, X. Wang, S. Cai, J. Solid State Chem. 178 (2005) 3210.
[10] M. Krunks, T. Dedova, I. Oja Açik, Thin Solid Films 515 (2006) 1157.
[11] T. Dedova, M. Krunks, A. Mere, J. Klauson, O. Volobujeva, in: J. Christen, et al. (Eds.), Zinc Oxide and Related Materials, vol. 957, Materials Research Society, Warrendale, PA, 2007, 0957-K10-26.
[12] T. Dedova, M. Krunks, M. Grossberg, O. Volobujeva, I. Oja Acik, Superlatt. Microstruct. 42 (2007) 444.
[13] I. Oja, A. Mere, M. Krunks, R. Nisumaa, C.H. Solterbeck, M. Es-Souni, Thin Solid Films 515 (2006) 674.
[14] M. Krunks, O. Kijatkina, A. Mere, T. Varema, I. Oja, V. Mikli, Sol. Energy Mater. Sol. Cells 87 (2005) 207.
[15] M. Biancardo, F.C. Krebs, Sol. Energy Mater. Sol. Cells 91 (2007) 1755.
[16] T. Ohsaka, F. Izumi, Y. Fujiki, J. Raman Spectrosc. 7 (2005) 321.
[17] I. Oja, A. Belaidi, L. Dloczik, M.-Ch. Lux-Steiner, T. Dittrich, Semicond. Sci. Technol. 21 (2006) 520.

PATENT APPLICATION V

M. Krunks, **A. Katerski**, T. Dedova, A. Mere, I. Oja Acik, Photovoltaic cell based on zinc oxide nanorods and the method for making the same, International patent application WO2009/006910A2 (Priority No. US60/948508, priority date 09.07.2007).

(12) INTERNATIONAL APPLICATION PUBLISHED UNDER THE PATENT COOPERATION TREATY (PCT)

(19) World Intellectual Property Organization
International Bureau

(43) International Publication Date
15 January 2009 (15.01.2009)

PCT

(10) International Publication Number
WO 2009/006910 A2

(51) International Patent Classification:
H01L 31/0352 (2006.01)

(21) International Application Number:
PCT/EE2008/000019

(22) International Filing Date: 9 July 2008 (09.07.2008)

(25) Filing Language: English

(26) Publication Language: English

(30) Priority Data:
60/948,508 9 July 2007 (09.07.2007) US

(71) Applicant *(for all designated States except US)*: **TALLINN UNIVERSITY OF TECHNOLOGY** [EE/EE]; Pr Kersti Peekma, TAO, Ehitajate 5, EE19086 Tallinn (EE).

(72) Inventors; and

(75) Inventors/Applicants *(for US only)*: **KRUNKS, Malle** [EE/EE]; Saha 6, EE10920 Tallinn (EE). **KATERSKI, Atanas** [BG/EE]; Rõika 24, EE10617 Tallinn (EE). **DEDOVA, Tatjana** [EE/EE]; Kalevipoja põik 5-63, EE13614 Tallinn (EE). **MERE, Arvo** [EE/EE]; Rävala pst 15-5, EE10143 Tallinn (EE). **OJA ACIK, Ilona** [EE/EE]; Akadeemia tee 5-404A, EE12611 Tallinn (EE).

(74) Agent: **KOPPEL, Mart Enn**; Ehitajate tee 5, EE19086 Tallinn (EE).

(81) Designated States *(unless otherwise indicated, for every kind of national protection available)*: AE, AG, AL, AM, AO, AT, AU, AZ, BA, BB, BG, BH, BR, BW, BY, BZ, CA, CH, CN, CO, CR, CU, CZ, DE, DK, DM, DO, DZ, EC, EE, EG, ES, FI, GB, GD, GE, GH, GM, GT, HN, HR, HU, ID, IL, IN, IS, JP, KE, KG, KM, KN, KP, KR, KZ, LA, LC, LK, LR, LS, LT, LU, LY, MA, MD, ME, MG, MK, MN, MW, MX, MY, MZ, NA, NG, NI, NO, NZ, OM, PG, PH, PL, PT, RO, RS, RU, SC, SD, SE, SG, SK, SL, SM, ST, SV, SY, TJ, TM, TN, TR, TT, TZ, UA, UG, US, UZ, VC, VN, ZA, ZM, ZW.

(84) Designated States *(unless otherwise indicated, for every kind of regional protection available)*: ARIPO (BW, GH, GM, KE, LS, MW, MZ, NA, SD, SL, SZ, TZ, UG, ZM, ZW), Eurasian (AM, AZ, BY, KG, KZ, MD, RU, TJ, TM), European (AT, BE, BG, CH, CY, CZ, DE, DK, EE, ES, FI, FR, GB, GR, HR, HU, IE, IS, IT, LT, LU, LV, MC, MT, NL, NO, PL, PT, RO, SE, SI, SK, TR), OAPI (BF, BJ, CF, CG, CI, CM, GA, GN, GQ, GW, ML, MR, NE, SN, TD, TG).

Published:
— *without international search report and to be republished upon receipt of that report*

(54) **Title:** PHOTOVOLTAIC CELL BASED ON ZINC OXIDE NANORODS AND METHOD FOR MAKING THE SAME

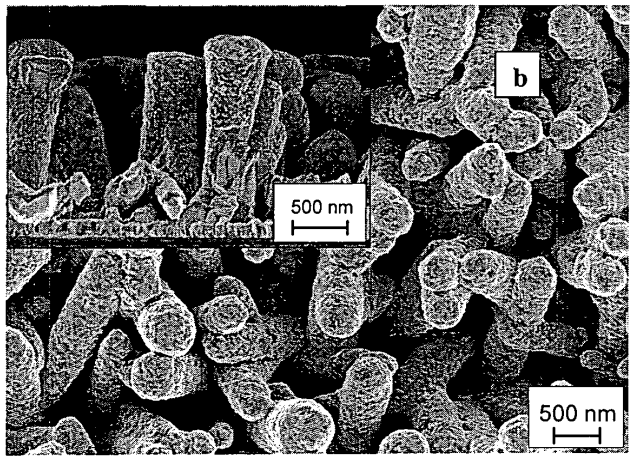

FIG 2B

(57) **Abstract:** A new photovoltaic (PV) cell structure, prepared on transparent substrate with transparent conductive oxide (TCO) layer and having nanorod zinc oxide layer. The cell has a thin conductive layer of doped zinc oxide deposited on the nanorod zinc oxide layer, an extremely thin blocking layer of titanium oxide or indium sulfide on the thin conductive layer, a buffer layer of indium sulfide on the extremely thin blocking layer, an absorber layer, comprising copper indium disulfide on said buffer layer and one electrode attached to the transparent conductive oxide layer and a second electrode attached to the absorber layer. Also, a method of preparing a zinc oxide nanorod PV cell entirely by chemical spray pyrolysis is disclosed. Efficiency up to 3,9% is achieved by simple continuous non-vacuum process.

WO 2009/006910 A2

PHOTOVOLTAIC CELL BASED ON ZINC OXIDE NANORODS AND METHOD FOR MAKING THE SAME

Background of the invention

Technical field

The invention relates to photovoltaic cells and methods of making photovoltaic cells, particularly to methods of manufacturing photovoltaic cells on ZnO nanorod structures, whereas all layers of the nanorod structure are preferably prepared by chemical spray pyrolysis.

Background art

Photovoltaic (PV) cell is a device that converts light energy into electrical energy. Harnessing solar energy with inexpensive materials and manufacturing methods is an important challenge. Low cost deposition techniques and new designs of PV devices are needed to reduce the production costs. There has been much interest of using nanostructures in PV devices. Dye sensitized photoelectrochemical solar cell (DSSC) based on nanoporous titanium dioxide is the most known nanostructured PV device (B. O'Regan and M. Grätzel, Nature 353, 737 (1991)). Unsolved problem with DSSC is its instability, also of its solid-state modifications. Another approach is an extremely thin absorber (eta) cell which has an extra thin absorber sandwiched between two strongly interpenetrating transparent wide band gap semiconductors (K. Ernst, et al, Semicond. Sci. Technol. 18, 475 (2003)). Most frequently used n-type nanostructured window material for the eta-solar cell is porous TiO_2. Alternatively, ZnO nanowires or columnar ZnO structures have been used to prepare ZnO eta-cells (C. Lévy-Clément, et al, Physica E 14, 229 (2002)). Inorganic absorber materials like CdTe (C. Lévy-Clément, et al above; R. Tena-Zaera, et al, Thin Solid Films 483, 372 (2005)), CdSe (Lévy-Clément, et al, Advanced Materials 17, 1512 (2005); R. Tena-Zaera, et al, C.R. Chimie 9, 717 (2006); R. Tena-Zaera, et al Proceedings 21st European PV Solar Energy Conf., 4-8 Sept. 2006, Dresden, Germany (2006), p.238) or In_2S_3 (D. Kieven et al, Applied Physics Letters 92, 153107 (2008) have been used in ZnO based cells. The conversion efficiencies of 2.3-2.5% are reached in ZnO nanowire based eta-cells (see C.R.Chimie, above; D. Kieven et al, above).

ZnO nanowire layers for photovoltaic applications have been fabricated by electrodeposition (see C. Lévy-Clément, R. Tena-Zaera above), metalorganic vapour deposition (J. B. Baxter and E.S. Aydil, Sol. Energ. Mater. Solar Cells 90, 607 (2006)), hydrothermal growth (M. Guo, P. Diao, X. Wang and S. Cai, J. Solid State Chem. 178, 3210 (2005) and solution deposition (D. Kieven et al, above).

In US patent application to Yang et al (Publication No. US 2005/0009224A1) is described a method of growing zinc oxide nanowires (aspect ratios between about 10 to about 500) on transparent conductive oxide (TCO) covered substrate, such as glass, and dye sensitized solar cells, organic-inorganic solar cells and solid state sensitized solar cells built on such nanowires. The nanowires in Yang are deposited by solution based processes, e.g., by dip coating process.

Recently we have developed a low-cost deposition method of growing zinc oxide nanorod arrays on conductive transparent electrodes by chemical spray (M. Krunks, et al, US provisional application 60/671232; international patent application PCT/EE2006/000002, published as WO2006108425).

Disclosure of the invention

Embodiments of the invention are directed to novel structures of a photovoltaic (PV) cell, based on nanorod layer, and methods for making the same.

One aspect of the invention is a new PV cell, comprising a transparent substrate covered with transparent conductive oxide (TCO) layer, a nanorod metal oxide layer on said TCO layer, a (chemically) blocking layer on said nanorod metal oxide layer, a buffer layer on said blocking layer, an absorber layer on said buffer layer, and electrical contacts attached to said absorber layer and to said TCO layer.

According to one embodiment, the nanorod metal oxide layer is a ZnO nanorod layer. According to one embodiment, the ZnO nanorod layer is deposited by spray from solution containing $ZnCl_2$.

According to one embodiment, the transparent substrate is glass, and the TCO layer is an indium tin oxide (ITO), doped SnO_2, or doped ZnO layer.

According to one embodiment, the extremely thin blocking layer comprises TiO_2 and has thickness less than 10nm, preferably less than 5nm. According to one embodiment, the extremely thin blocking layer comprises In_xS_y. According to one embodiment, the buffer layer comprises In_2S_3, CdS or ZnS. According to one embodiment, the absorber layer comprises $CuInS_2$, or other Cu-based chalcopyrites such as $CuInS_2$, $CuInSe_2$, $CuInGaS_2$, $CuInGaSe_2$ and their solid solutions, or analogous Ag-based compounds and their solid solutions; or In-free CZTS –type compounds, such as Cu_2ZnSnS_4, $Cu_2ZnSnSe_4$ and/or their solid solutions.

According to one embodiment, the PV cell further comprises a thin conductive layer between said nanorod metal oxide layer and said blocking layer. According to one embodiment, said conductive layer is a doped metal oxide layer, such as indium or aluminium ZnO layer.

One embodiment of the invention is a PV cell, comprising a glass substrate covered with an ITO layer, a nanorod zinc oxide layer, deposited by spray from solution containing $ZnCl_2$; an indium-doped zinc oxide layer, deposited by spray from a solution comprising zinc acetate and indium ions (In^{3+} ions); a blocking layer, prepared by dip coating or by spray from titanium alkoxide sol; a buffer layer comprising In_2S_3 and prepared by spray; and absorber layer, comprising $CuInS_2$, prepared by spray.

Another aspect of the invention is a method for manufacturing PV cells with structures as described above. Such structures are prepared solely by or mostly by chemical spray pyrolysis deposition.

According to one embodiment, the method comprises depositing a metal oxide, such as ZnO nanorod layer by chemical spray deposition on a transparent conductive oxide layer on a transparent substrate; depositing an extra thin blocking layer on said nanorod layer, said extra thin blocking layer comprising TiO_2 or In_xS_y (where x and y are integer numbers); depositing a buffer layer on said thin blocking layer, said buffer layer comprising In_2S_3; and depositing an absorber layer on said buffer layer, said absorber layer comprising $CuInS_2$; and attaching electrical contacts to said transparent oxide layer and to said absorber layer.

According to one embodiment, the metal oxide nanorod layer is deposited by spray from solution containing $ZnCl_2$.

According to one embodiment, the method additionally comprises a step of depositing a conductive doped metal oxide layer on said metal oxide nanorod layer.

Brief description of the drawings

The technical essence of the invention is described in details by following figures.

Fig. 1 shows a simplified schematic view of a photovoltaic cell according to the invention;

Fig. 2 shows SEM images of a ZnO nanocolumnar layer before and after (inset) spraying on that acidic (pH ~2.8) solution (Fig. 2A) and a solar cell structure $ZnO_R/TiO_2/In_2S_3$/CIS (Fig. 2B).

Fig. 3A shows a flowchart illustrating the method of manufacturing the PV cell according to one embodiment of the invention.

Fig. 3B shows a flowchart illustrating the method of manufacturing the PV cell according to another embodiment of the invention.

Fig. 4A is a current –voltage characteristics of a PV cell according to the invention (structured cell) compared to a flat PV cell (respectively, cell 1 and cell 2 shown in Table 1) under halogen lamp illumination of 100 mW/cm2.

Fig. 4B is a current-voltage characteristics (in dark and under the illumination) of all-layers-sprayed PV cell ITO/ZnO_R/TiO2/In2S3/CuInS2 with a cell conversion efficiency of the cell 2.6 % (cell 4 shown in Table 1).

Fig. 4C is a current-voltage characteristics of structured PV cells with different thickness of spray-deposited TiO2 layer. Thickness is controlled by number of the spray pulses shown by Arabic numerals on the graph.

Fig. 4D is a current-voltage characteristics (in dark and under the illumination) of all layers sprayed structured PV cell ITO/$ZnO_R/In_xS_y/In_2S_3/CuInS_2$ with a cell conversion efficiency 3.9 % (cell 6 shown in Table 1).

Fig. 5 shows electron beam induced current (EBIC) (Fig. 5A) and SEM (Fig 5B) images of the cross section of a structured solar cell TCO/ZnO_R/ZnO:In/TiO_2/In_2S_3/CIS.

Fig. 6 is a spectral response of a PV cell according to the invention (structured cell) compared to a flat PV cell (respectively, cell 1 and cell 2 shown in Table 1).

Modes for carrying out the invention

The photovoltaic cell (PV cell, or solar cell) according to one embodiment of the present invention is schematically depicted in FIG. 1. The PV cell is built on suitable transparent substrate 1 that is covered with transparent conductive oxide (TCO) layer 2. Glass is one of the most suitable materials for the substrate. TCO layer is typically tin oxide, e.g., fluorine-doped tin oxide (SnO_2:F, or FTO), or indium tin oxide (ITO) or indium, fluorine or aluminum-doped zinc oxide (ZnO:In, ZnO:F, or ZnO:Al). TCO-covered glass is commercially available from many manufacturers.

A nanorod layer 3, such as zinc oxide nanorod (ZnO_R) layer is deposited on said TCO substrate. The nanorod layer is preferably prepared by chemical spray pyrolysis deposition (hereinafter, spray). ZnO layer comprises elongated crystals. According to selective area electron diffraction (SAED) study the sprayed ZnO nanorods grown at temperatures above 500 °C are single crystals. According to the photoluminescence studies which shows strong near-band-edge (NBE) emission in UV region and very weak green emission, the sprayed ZnO nanorods are of high crystal quality and chemical purity.

Electrical characterization, incl Kelvin probe measurements reveal that ZnO nanorods by spray may be single crystals with low concentration of free carriers. For better carrier collection, a thin conductive metal oxide layer 4, such as indium-doped zinc oxide (ZnO:In) layer is deposited on the nanorod layer 3 and generally follows the shape of the rods. The conductive layer 4 is also preferably prepared by spray. In background art, the ZnO rods, typically prepared by electrodeposition, are heavily doped.

An extra thin blocking layer 5 (with thickness less than 50 nm, preferably less than 10 nm, most preferably less than 5nm) is deposited on said conductive layer. Blocking layer 5 can comprise TiO_2 and can be made by sol-gel spray or spin coating or dip coating using a titanium alkoxide based sol. Other chemically inert oxides such as Al_2O_3, ZrO_2 and Nb_2O_5 can be also used. The blocking layer protects the ZnO from chemical dissolution in acidic medium during next deposition steps of solar cell fabrication, namely during the spray

deposition of acidic (pH~3) solution to make In_2S_3 buffer and copper indium disulfide (CIS) absorber layers. Blocking layer also avoids the electrical short circuiting of the solar cell structure. The thickness of the blocking layer should be optimized to provide tunneling of the carriers.

The blocking layer 5 may comprise indium sulfide or titanium dioxide and may be deposited by spray. This reduces the preparation time and preserves continual spray process and thus, provides simple and straightforward solar cell fabrication process. According to the SEM study, thin, dense and pinhole-free films of InS or TiO_2 can be formed by spray.

The buffer layer 6 is deposited on the blocking layer 5. Buffer layer may comprise In_2S_3 and is preferably deposited by spray. Absorber layer 7 is deposited on buffer layer. Absorber layer is preferably CIS ($CuInS_2$) layer, preferably deposited by spray. However, other chemical vapor deposition and solution based techniques may be also used. Also other absorber materials may be used, such as other Cu-based chalcopyrites such as $CuInSe_2$, $CuInGaS_2$, $CuInGaSe_2$ and their solid solutions, or suitable Ag-based materials and their solid solutions; or In-free multinary compounds, CZTS, such as Cu_2ZnSnS_4, $Cu_2ZnSnSe_4$.

The solar cell has electrodes attached to the p-type absorber layer as a back contact 8 and to transparent conductive oxide layer as a front contact 9. For the back contact any suitable method and material commonly used for electrodes can be used, e.g., metals with high work function Co, Au, Ni, Pd, Pt or graphite or hole conductor layer PEDOT:PSS, CuSCN, CuI, $CuAlO_2$, NiO with a contact formed of suitable metal such as Co, Au, Ni, Pd, Pt.

Figs. 3A and 3B show flowchart, illustrating the methods of manufacturing PV cells according to the embodiments of the invention.

The method shown in Fig. 3A comprises step 100 of depositing a nanorod layer 3 of metal oxide by spray on suitable TCO substrate, such as ITO covered glass. Metal oxide is preferably zinc oxide. Then follows step 300 of depositing an extra thin blocking layer 5 on said nanorod layer, covering the tops and sides of the rods. The blocking layer is preferably also deposited by spray and comprises In_xS_y (where x and y are integer numbers), or TiO_2. Follows step 400 of depositing a buffer layer 6 on the blocking layer 5. The buffer layer may comprise In_2S_3 and is also preferably deposited by spray. Then follows step 500 of depositing

absorber layer 7 on the buffer layer. Absorber layer is preferably CIS ($CuInS_2$) layer, and is preferably deposited by spray. The final step 600 is attaching suitable electrodes to the transparent conductive oxide layer 2 and to the absorber layer 7.

The nanorod layer prepared by spray consists of single crystals while such crystals may be, depending on the deposition parameters, of very high purity. To improve the carrier collection in such PV cell, additional conductive layer may be needed between the nanorod layer and the blocking layer. To manufacture such PV cells, the method is modified as shown in Fig. 3B. The method additionally comprises step 200 after step 100. Step 200 is depositing a thin conductive layer 4 of doped metal oxide, such as indium or aluminium doped zinc oxide onto the nanorod layer 3 by spray, covering the tops and the sides of the rods. Then follows step 300 of depositing an extra thin blocking layer 5 on said thin conductive layer. Other steps 400, 500 and 600 are as described above.

Example 1

Zinc oxide (ZnO) nanorods were deposited by spray of zinc chloride ($ZnCl_2$) aqueous solution onto indium tin oxide (ITO) covered glass substrates placed on the hot plate (laboratory device developed by Tallinn University of Technology) heated up to about 600 °C. The concentration of $ZnCl_2$ in spray solution was about 0.1 mol/l. ZnO nanorod (ZnO_R) layers deposition by spray technique are described in more details in our PCT application PCT/EE2006/000002, published as WO2006108425.

The next layers of the solar cell were deposited in the following order: a thin conductive layer of indium doped zinc oxide (ZnO:In), an extra thin blocking layer TiO_2, a buffer layer In_2S_3 and finally, $CuInS_2$ (CIS) absorber layer.

The conductive layer of indium-doped zinc oxide (ZnO:In) was deposited onto the ZnO nanorods at hot plate temperature of about 500 °C from about 20 ml of about 0.2 mol/l $Zn(CH_3COO)_2$ solution containing $InCl_3$ ([In]/(Zn]= 3 at %).

The extra thin blocking layer of TiO_2 with thickness less than or about 10 nm was prepared by sol-gel dip coating method by immersing the substrate in the titania sol (acetylacetone stabilised titaniumtetraisopropoxide, prepared at TTIP:acacH=1:1 in ethanol (other alcohols, such as isopropanol, 2-metoxyethanol may be used) where TTIP=titaniumtetraisopropoxide,

$C_{12}H_{28}O_4Ti$ and acacH= acetylacetone, $C_5H_8O_2$). Dip coating was made at room temperature followed by drying at about 80°C, and then heated for about 30 minutes at about 450 °C in a laboratory oven.

Indium sulfide (In_2S_3) buffer layer was deposited by spray using an aqueous spray solution of $InCl_3$ and $SC(NH_2)_2$ with molar ratio of In:S =1:3 at concentration of $InCl_3$ of $2x10^{-3}$ mol/l and pH ~ 3.

$CuInS_2$ (CIS) absorber layer was deposited by spray using a solution containing $InCl_3$, $CuCl_2$ and $SC(NH_2)_2$ at molar ratios of Cu:In:S=1:1:3 and following the deposition route described in details in our US patent application published as US20050271827. Indium sulfide layers and CIS absorber layer were deposited at similar temperature of 300 °C.

For comparison, flat PV cells (i.e., with flat ZnO layer instead of ZnO_R layer) were prepared simultaneously with the structured samples. As can be seen from Fig. 4 and from Table 1, examples 1 and 2, the structured PV cell has substantially higher current j and efficiency.

Example 2

Zinc oxide (ZnO) nanorods with length of about 1 micron were deposited as in Example 1.

TiO_2 films were deposited by sol-gel spray pyrolysis method onto the substrate with ZnO rods using a sol composed of a titanium alkoxide (titanium (IV)isopropoxide) with concentration 0.1 mol/l and a stabilizer (acetylacetone) at molar ratio of 1:2 to 1:4 in ethanol (other alcohols may be used). The sol was pulverized onto the substrate heated up to 450° C employing 2 to 20 spray pulses (1 second spray+30 second pause). Sprayed TiO_2 films were amorphous according to Raman spectra. X-ray photoelectron spectroscopic study revealed that four spray pulses had produced a continuous and pinhole free TiO_2 film with the thickness of less than 5 nm on planar surfaces.

Indium sulfide (In_2S_3) buffer layer and $CuInS_2$ (CIS) absorber layer were deposited as in Example 1.

TiO_2 film from 2-4 spray pulses forms a chemical blocking layer on ZnO rods resulting simultaneously in reduction of the electrical short circuits between front and back contacts and sufficient tunneling of the charge carriers through the interface barrier. Applying thicker

TiO_2 films led to S-shaped I-V curves of the solar cells (see Fig. 4C), accompanied by a drastic decrease in the cell fill factor and efficiency due to an additional rectifying interface in the circuit. The best all-layers-sprayed $ZnO_R/TiO_2/In_2S_3$/CIS cell shows conversion efficiency of 2.6 % (Voc=450 mV, j= 11 mA/cm2, FF=54%) versus 1.6 % of the flat PV cell under white light illumination of 100 mW/cm2. I-V curves of the structured solar cell with sprayed TiO_2 layer from 4 spray pulses is presented in Fig. 4B.

Example 3

Zinc oxide (ZnO) nanorod layer was deposited by spray. 50 ml of $ZnCl_2$ aqueous solution with concentration of 0.07 mol/l with pH of 2.0-2.2 was sprayed at the rate of 2.5 ml/min onto pre-heated ITO electrode coated glass substrates kept at constant temperature of about 600-620°C. Acidity of the solution was adjusted via addition of HCl into the aqueous solution of $ZnCl_2$. The substrates were continuously rotated to obtain uniform layers. The air was used as carrier gas with air flow rate 8 l/min.

Using acidic spray solution with pH of around 2 instead of 5 supports the formation of a layer composed of ZnO nanorods, i.e., elongated crystals instead of a compact layer of ZnO. The use of acidic solution reduces the number of ZnO nucleation centers by dissolving the smaller nucleation centers and allowing rods to grow on bigger centers without growing together. Using acidic spray solution makes the process much less dependant on the surface properties of the TCO layer and thus makes easier to find suitable TCO substrates for manufacturing PV cells. Also, ZnO nanorods grown from acidic solution are more conductive than nanorods from non-acidic solution.

Thin, compact and dense layer of In_xS_y was deposited on the ZnO nanorod layer by spray using 25 ml of the spray solution containing $InCl_3$ and thiocarbamide $SC(NH_2)_2$ at molar ratio of In:S =1:3 with $InCl_3$ concentration of $4x10^{-4}$ mol/l and solution pH ~ 5, solution spray rate of about 1 ml/min, the substrate temperature was kept constant at about 300 °C. In_xS_y is composed of In and S atoms and there is no oxygen in the layer according to the X-ray photoelectron spectroscopy. Band gap of In_xS_y is 2.0 eV, assuming indirect transitions, and thus, similar to that of In_2S_3. Layer of In_xS_y on ZnO rods is amorphous according to Raman spectroscopy; extremely thin layer of In_xS_y is compact and without pinholes and covers uniformly ZnO rods according to SEM study.

In_2S_3 buffer layer was deposited as in Examples 1 and 2.

$CuInS_2$ absorber layer was deposited as in Examples 1 and 2.

Conductive carbon paste was used to make a back contact to CuInS2 absorber. Carbon paste contacts with determined area were prepared, solvent was removed by heating the contacts for 60 minutes at 200 °C in air. Our best cell showed the conversion efficiency of 3.9 % (Voc= 457 mV, j= 14.1 mA/cm2, FF= 60.3 %) under the white light illumination 100 mW/cm2. I-V curves of the solar cell in dark and under the illumination are presented in Fig. 4D.

Table 1 shows output characteristics of flat and structured solar cells under the halogen lamp illumination with intensity of 100 mW/cm2, where cell No denotes:

1- TCO / ZnO:In / TiO_2(by dip) / In_2S_3 / CIS (flat);

2- TCO / ZnO_R / ZnO:In/TiO_2 (by dip) / In_2S_3/ CIS (structured);

3- TCO / ZnO:In / TiO_2 (by spray)/ In_2S_3 / CIS (flat);

4- TCO / ZnOR/ ZnO:In / TiO_2 (by spray)/ In_2S_3 / CIS (flat

5- TCO / ZnO / In_xS_y / In_2S_3 / CIS (flat);

6- TCO / ZnO_R / ZnO:In / In_xS_y / In_2S_3 / CIS (structured).

Table 1

Cell No.	Cell structure	Chemically Blocking layer	Voc, mV	j, mA/cm^2	FF, %	Eff., %
1	flat	TiO_2 (dipping)	445	5.5	41	1.0
2	Structured	"	425	12.0	43	2.2
3	Flat	TiO_2 (spray)	440	6.2	58	1.6
4	Structured	"	450	11.0	54	2.6
5	Flat	In_xS_y	485	4.3	63	1.3
6	Structured	In_xS_y, no ann.	420	12.8	53	2.9
		In_xS_y, annealed	457	14.1	60	3.9

Although this invention is described with respect to a set of aspects and embodiments, modifications thereto will be apparent to those skilled in the art. The foregoing description of the embodiments of the invention has been presented for the purposes of illustration and description. It is not intended to be exhaustive or to limit the invention to the precise form disclosed. Many modifications and variations are possible in light of this disclosure. It is intended that the scope of the invention be limited not by this detailed description, but rather by the claims appended hereto.

CLAIMS

1. A photovoltaic cell structure, comprising:
   a transparent substrate covered with a transparent conductive oxide layer;
   a nanorod zinc oxide layer, deposited to said transparent conductive oxide layer;
   an extremely thin blocking layer shelling said nanorods of said zinc oxide layer, said blocking layer comprising TiO_2 or In_xS_y, wherein x, y are integer numbers;
   a buffer layer on said extremely thin blocking layer, said buffer layer comprising a material selected from a group of In_2S_3, CdS and ZnS;
   an absorber layer on said buffer layer, said absorber layer comprising a material selected from the group of $CuInS_2$, $CuInSe_2$, $CuInGaS_2$, $CuInGaSe_2$, Cu_2ZnSnS_4 and $Cu_2ZnSnSe_4$; and
   a pair of electrodes, the first electrode attached to said transparent conductive oxide layer and the second electrode attached to said absorber layer.

2. A photovoltaic cell structure as in claim 1, comprising a thin conductive layer of doped zinc oxide deposited on said nanorod zinc oxide layer.

3. A photovoltaic cell structure as in claim 2, wherein said thin conductive layer is indium doped zinc oxide layer.

4. A photovoltaic cell structure as in claims 1 to 3, wherein said transparent substrate is glass, transparent conductive oxide is selected from the group of indium tin oxide, fluorine-doped tin oxide, and indium-, fluorine- or aluminum-doped zinc oxide.

5. A photovoltaic cell structure as in claim 4, wherein all layers of the photovoltaic cell are prepared by chemical spray deposition.

6. A photovoltaic cell structure as in claims 1 to 5, wherein said extremely thin blocking layer comprising TiO_2 has thickness less than 10nm.

7. A photovoltaic cell structure as in claims 1 to 5, wherein said extremely thin blocking layer comprising TiO_2 has thickness less than 5nm.

8. A method of manufacturing a photovoltaic cell, comprising:
   depositing a zinc oxide nanorod layer by chemical spray deposition onto a transparent

substrate covered with transparent conductive oxide layer;
depositing a conductive layer of doped zinc oxide by chemical spray deposition onto said zinc oxide nanorod layer;
depositing an extremely thin blocking layer by chemical spray deposition onto said doped conductive zinc oxide layer for chemically protecting said zinc oxide nanorod layer during the next steps of manufacturing, said extremely thin blocking layer comprising TiO_2 or In_xS_y, wherein x, y are integer numbers;
depositing a buffer layer by chemical spray deposition onto said extremely thin blocking layer, said buffer layer comprising In_2S_3;
depositing an absorber layer by chemical spray deposition onto said buffer layer, said absorber layer comprising $CuInS_2$; and
attaching electrical contacts to said transparent oxide layer and to said absorber layer, wherein all layers are deposited by chemical spray deposition.

9. A method of manufacturing a photovoltaic cell, comprising:
depositing a zinc oxide nanorod layer by chemical spray deposition onto a transparent substrate covered with transparent conductive oxide layer;
depositing an extremely thin blocking layer on said zinc oxide nanorod layer for chemically protecting said zinc oxide nanorod layer during the next steps of manufacturing, said extremely thin blocking layer comprising TiO_2 or In_xS_y, wherein x, y are integer numbers;
depositing a buffer layer on said thin blocking layer, said buffer layer comprising In_2S_3.
depositing an absorber layer on said buffer layer, said absorber layer comprising $CuInS_2$; and
attaching electrical contacts to said transparent oxide layer and to said absorber layer.

10. A method of manufacturing a photovoltaic cell, comprising:
providing a transparent substrate covered with a transparent conductive oxide layer;
depositing a zinc oxide nanorod layer onto said transparent conductive oxide layer by chemical spray deposition from a solution comprising a Zn precursor and a solvent, onto said transparent conductive oxide layer, wherein said precursor is selected from a group of $ZnCl_2$ and $Zn(CH_3COO)_2$ and said solvent comprises H_2O ;

adjusting the pH level of the solution between 1.5 to 2.5 by adding an acid into said solution;

depositing an extremely thin blocking layer on said zinc oxide nanorod layer, said extremely thin blocking layer comprising TiO_2 or In_xS_y, wherein x, y are integer numbers;

depositing a buffer layer on said extremely thin blocking layer, said buffer layer comprising a material selected from a group of In_2S_3, CdS and ZnS; and

depositing an absorber layer on said buffer layer, said absorber layer comprising a material selected from the group of $CuInS_2$, $CuInSe_2$, $CuInGaS_2$, $CuInGaSe_2$, Cu_2ZnSnS_4 and $Cu_2ZnSnSe_4$.

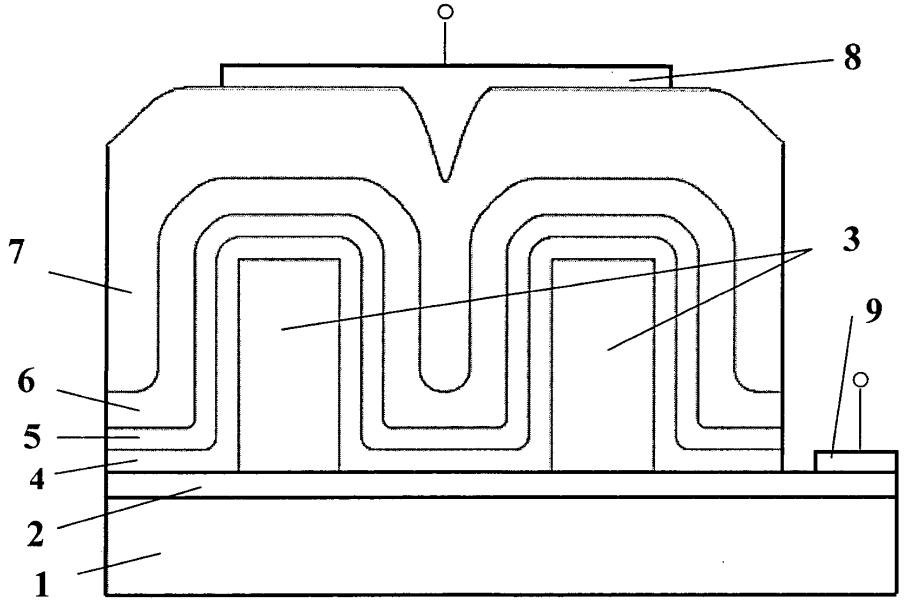

FIG. 1

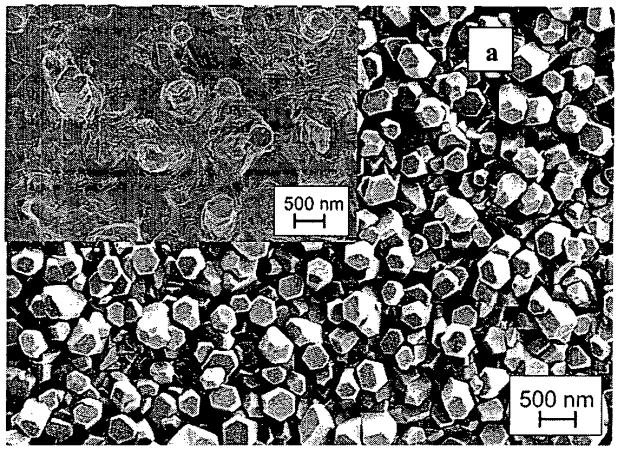

FIG 2A

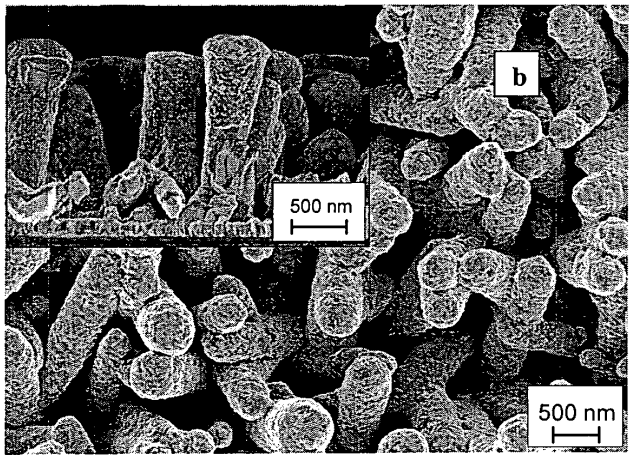

FIG 2B

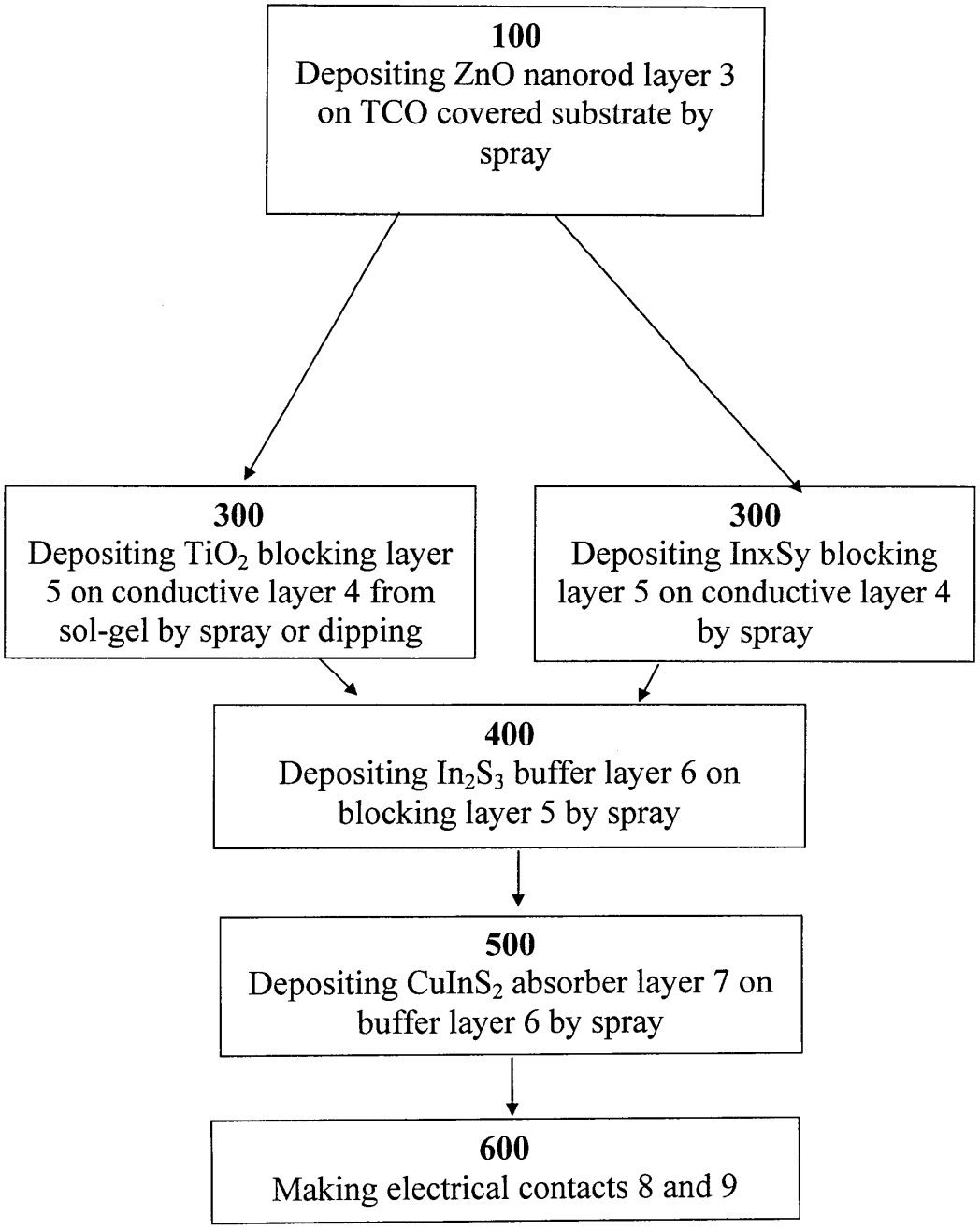
100
Depositing ZnO nanorod layer 3 on TCO covered substrate by spray
300
Depositing TiO_2 blocking layer 5 on conductive layer 4 from sol-gel by spray or dipping
300
Depositing InxSy blocking layer 5 on conductive layer 4 by spray
400
Depositing In_2S_3 buffer layer 6 on blocking layer 5 by spray
500
Depositing $CuInS_2$ absorber layer 7 on buffer layer 6 by spray
600
Making electrical contacts 8 and 9

FIG. 3A

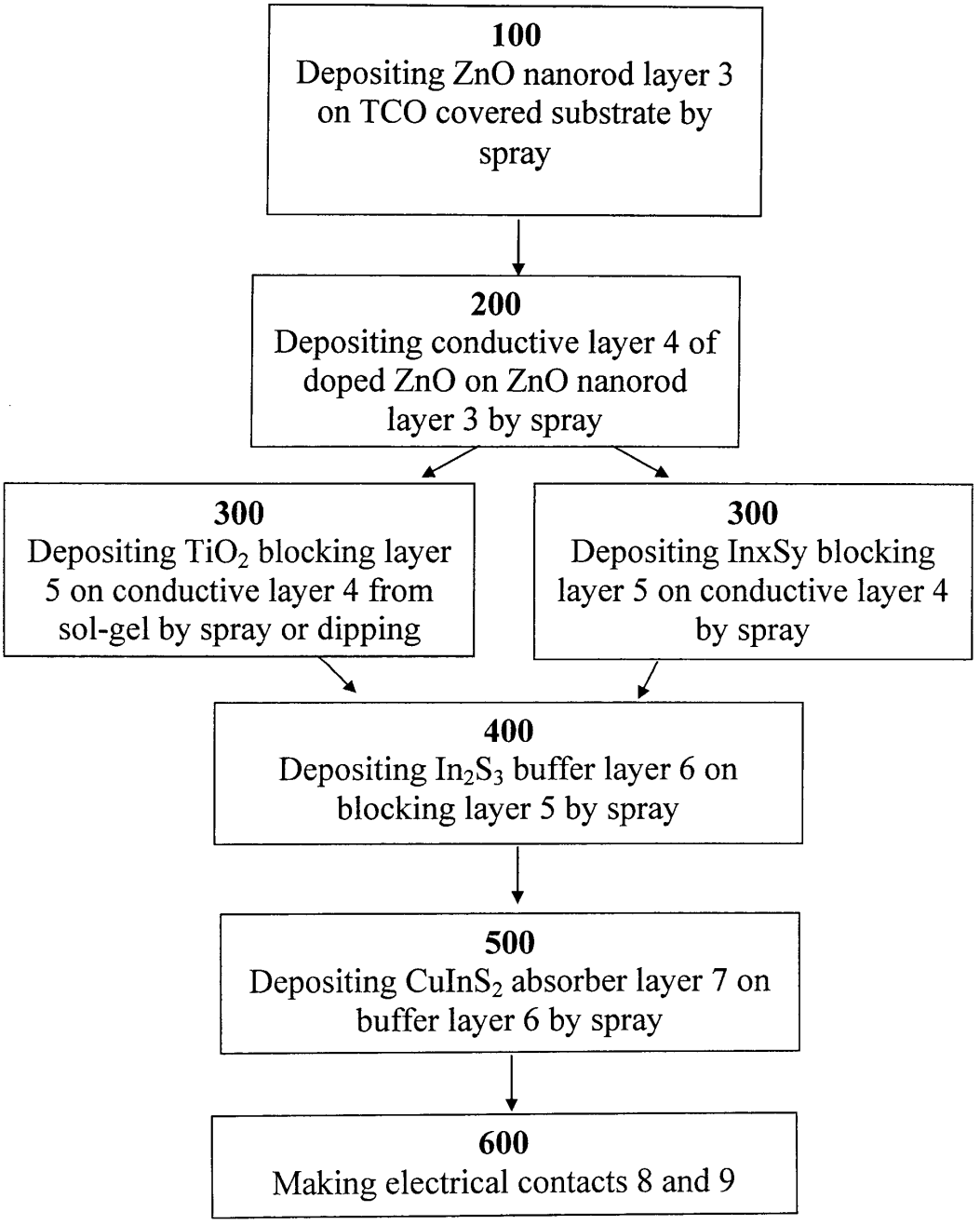
100
Depositing ZnO nanorod layer 3 on TCO covered substrate by spray
200
Depositing conductive layer 4 of doped ZnO on ZnO nanorod layer 3 by spray
300
Depositing TiO_2 blocking layer 5 on conductive layer 4 from sol-gel by spray or dipping
300
Depositing InxSy blocking layer 5 on conductive layer 4 by spray
400
Depositing In_2S_3 buffer layer 6 on blocking layer 5 by spray
500
Depositing $CuInS_2$ absorber layer 7 on buffer layer 6 by spray
600
Making electrical contacts 8 and 9

FIG. 3B

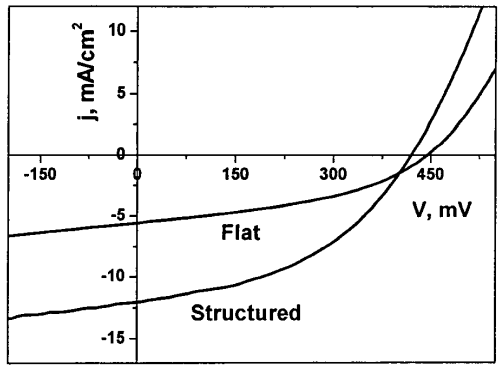

FIG. 4A

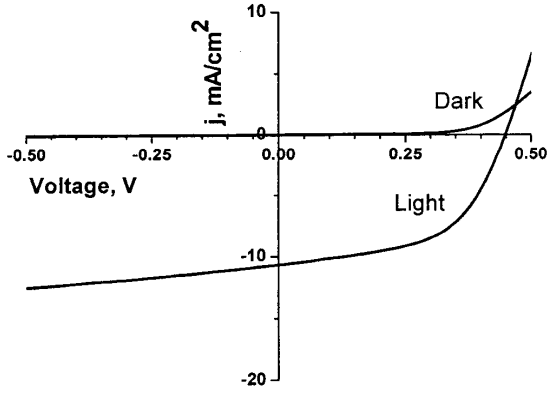

FIG. 4B

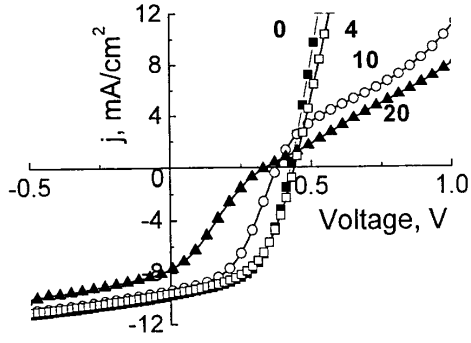

FIG. 4C

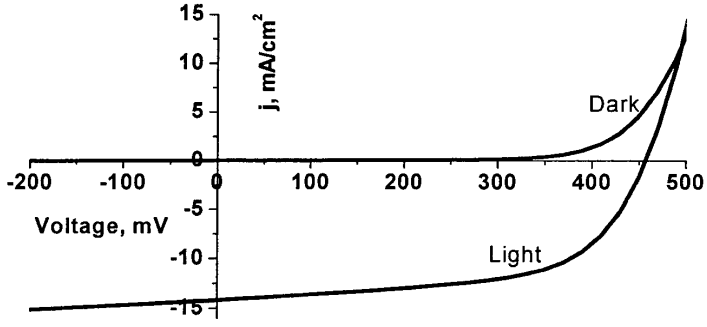

FIG 4D

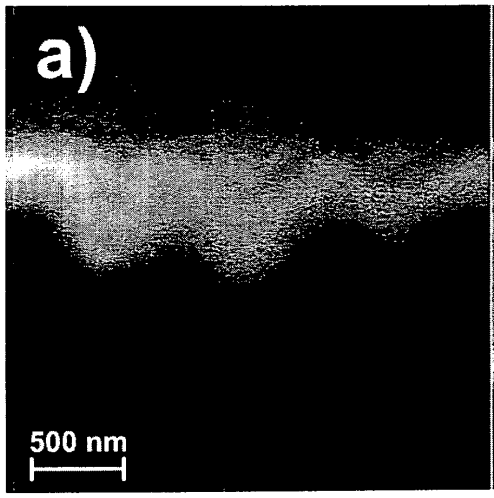

FIG 5A

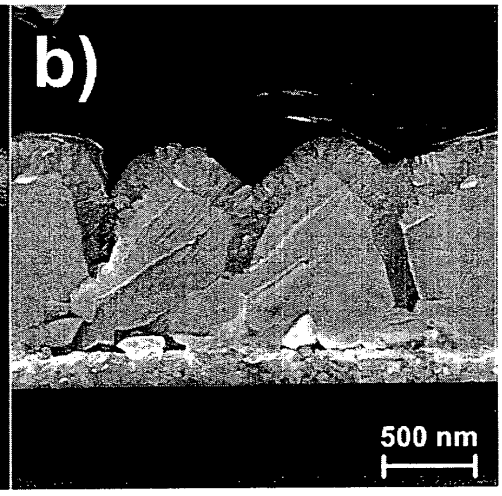

FIG 5B

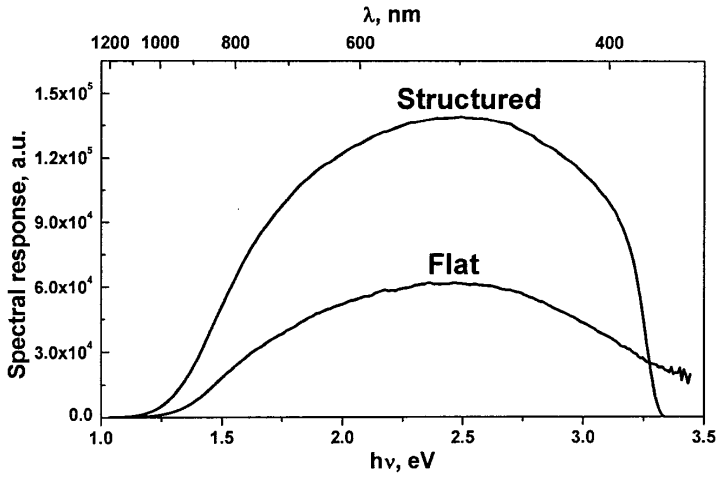
λ, nm
1200 1000 800 600 400
Structured
Flat
Spectral response, a.u.
1.5x10^5
1.2x10^5
9.0x10^4
6.0x10^4
3.0x10^4
0.0
1.0 1.5 2.0 2.5 3.0 3.5
hν, eV

FIG. 6

APPENDIX B

ELULOOKIRJELDUS

Üldine info

Ees- ja perekonnanimi:	**Atanas Katerski**
Sünniaeg ja -koht:	18.02.1969, Sofia, Bulgaaria
Kodakondsus:	Bulgaaria
Telefon:	+372 6203369
E-mail:	akaterski@staff.ttu.ee

Hariduskäik

2005-	Tallinna Tehnikaülikool, keemia- ja materjalitehnoloogia teaduskond, REV doktorant
1989-1994	Keemilise Tehnoloogia ja Metallurgia Ülikool, Sofia, keemiatehnoloogia teaduskond, elektroonika materjalide ja ülipuhaste ainete tehnoloogia eriala, keemiainsener
1976-1987	Sofia 8. Vasil Levski nim. Gümnaasium, keskharidus

Teenistuskäik

2005-	Tallinna Tehnikaülikool, materjaliteaduse instituut, teadur
2003-2005	Tallinna Tehnikaülikool, materjaliteaduse instituut, külalisteadur
1994-2003	Bulgaaria Teaduste Akadeemia, üld- ja anorgaanilise keemia instituut, keemik

Täiendusõpe

1. Tallinna Tehnikaülikool, keemia ja materjali-tehnoloogia teaduskond, doktoriseminarid 2006-2010
2. Tartu Ülikool ja Tallinna Tehnikaülikool doktorikooli „Funktsionaalsed materjalid ja tehnoloogiad“ (FMTDK) teaduskonverents, 25.02-26.02.2010, Dorpati konverentsikeskus, Tartu, Eesti
3. Materjaliteaduse ja materjalide tehnoloogia doktorikooli (MMTDK) talvekool, 19.02.-20.02.2008, Kääriku, Eesti
4. Tartu Ülikool, füüsikainstituut, Tartu, detsember 2007,

XPS-mõõtmised, külalisteadur

5. Materjaliteaduse ja materjalide tehnoloogia doktorikool (MMTDK), suvekool, 27.06-29.06. 2007, Kääriku, Eesti
6. Materjaliteaduse ja materjalide tehnoloogia doktorikooli (MMTDK) teaduskonverents, 28.02-1.03.2007, Hotell London, Tartu, Eesti
7. Materjaliteaduse ja materjalide tehnoloogia doktorikooli (MMTDK) talvekool, 2.02.-3.02.2007, Pühajärve, Eesti
8. Young Scientist Summer School on Photovoltaics, 21.08-25.08. 2006, "Villa Andropoff", Pärnumaa, Eesti.
9. Vilniuse Ülikool, materjaliteaduse ja rakendusuuringute instituut, Vilnius, Leedu, veebruar ja mai 2006, XPS mõõtmised, külalisteadur
10. Materjaliteaduse ja materjalide tehnoloogia doktorikool (MMTDK), talvekool, 2.02.-3.02.2006, Tartu
11. MaxLab, Lundi Ülikool, Rootsi, veebruar 2004, PES mõõtmised sünkrotronil, külalisteadur

Tunnustused

2010	Parim posterettekanne FMTDK teaduskonverentsil 25.02.-26.02.2010, Dorpat, Tartu.
1998	Pronksmedal näituselt "East-West Euro Intellect Exhibition of Invention", Research and Innovation: 1998, Sofia, Bulgaaria

CURRICULUM VITAE

General data

Name and surname:	**Atanas Katerski**
Date and place of birth:	18.02.1969, Sofia, Bulgaria
Citizenship:	Bulgarian
Phone:	+372 6203369
Email:	akaterski@staff.ttu.ee

Education

2005 -	Tallinn University of Technology (TUT), PhD student (REV)
1989 -1994	University of Chemical Technology and Metallurgy, Sofia, Faculty of Chemical Technology, speciality: technology of high purity materials for microelectronics, Dipl. Engineer (chemist)
1976-1987	Vasil Levski Gymnasium (High School No.8) Sofia, secondary education

Professional experience

2005 -	Tallinn University of Technology, Department of Materials Science, researcher
2003 - 2005	Tallinn University of Technology, Department of Materials Science, visiting researcher
1994 – 2003	Bulgarian Academy of Science, Institute of General and Inorganic Chemistry, chemist

Training courses

1. Participation at the Doctoral students' workshops of the Faculty of Chemical and Materials Technology at Tallinn University of Technology, 2006-2010, Tallinn, Estonia
2. Tartu University and Tallinn University of Technology Doctoral School of "Functional Materials and Processes" (FMTDK), Scientific Conference 25.02.-26.02.2010, Dorpat Conference Center, Tartu, Estonia
3. Doctoral School of Material Science and Material

Technology (MMTDK), Winter School, 19.02.-20.02.2008, Kääriku, Estonia
4. Tartu University, Institute of Physics, Tartu, Estonia, Dec. 2007, XPS measurements, guest researcher
5. Doctoral School of Material Science and Material Technology (MMTDK), Summer School, 27.06-29.06.2007, Kääriku, Estonia
6. Doctoral School of Material Science and Material Technology (MMTDK), Scientific Conference 28.02-01.03.2007, Hotel London, Tartu, Estonia
7. Doctoral School of Material Science and Material Technology (MMTDK), Winter School, 2.02-3.02.2007, Pühajärve, Estonia
8. Young Scientist Summer School on Photovoltaics, 21.08-25.08.2006, "Villa Andropoff", Pärnu, Estonia
9. Vilnius University, Institute of Materials Science and Applied Research, Vilnius, Lithuania, February and May 2006, XPS measurements, guest researcher
10. Doctoral School of Material Science and Material technology (MMTDK), Winter School, 2.02-3.02.2006, Tartu, Estonia
11. MaxLab, Lund, Sweden, February 2004, PES measurements on synchrotron source, guest researcher

Awards

2010	Estonian PhD student Scientific Conference on Functional Materials, 25.02-26.02.2010, FMTDK-2010, Dorpat Conference Center, Tartu, Estonia, the best poster presentation
1998	Bronze medal on the "East-West Euro Intellect Exhibition of Invention", Research and Innovation: 1998, Sofia, Bulgaria

List of publications

1. M. Krunks, I. Oja Acik, **A. Katerski**, T. Dedova, A. Mere, Extremely thin absorber layer solar cells on zinc oxide nanostructures by chemical spray, *Sol. Energy Mater. Sol. Cells* 94 (2010) 1191-1195.
2. **A. Katerski**, M. Danilson, A. Mere, M. Krunks, Effect of the growth temperature on chemical composition of spray-deposited $CuInS_2$ films, *Energy Procedia* 2 (2010) 103-107.
3. K. Otto, **A. Katerski**, A. Mere, M. Krunks, Spray Pyrolysis Deposition of Indium Sulfide Thin Films, *Thin Solid Films*, doi:10.1016/j.tsf.2010.12.027.
4. E. Kärber, **A. Katerski,** I. Oja Acik, V. Mikli, A. Mere, M. Krunks, Effect of H_2S treatment on properties of $CuInS_2$ thin films deposited by chemical spray pyrolysis at low temperature, *Thin Solid Films,* doi:10.1016/j.tsf.2010.12.185.
5. I. Oja Acik, **A. Katerski**, A. Mere, J. Aarik, A. Aidla, T. Dedova, M. Krunks, Nanostructured solar cell by spray pyrolysis: Effect of titania barrier layer on the cell performance, *Thin Solid Films* 517 (2009) 2443-2447.
6. **A. Katerski**, A. Mere, V. Kazlauskiene, J. Miskinis, A. Saar, L. Matisen, A. Kikas, M. Krunks, Surface analysis of spray deposited copper indium disulfide films, *Thin Solid Films* 516 (2008) 7110-7115.
7. M. Krunks, A. Mere, **A. Katerski**, Copper indiumdisulfide films by chemical spray pyrolysis for photovoltaics, *Proceedings Intern. Conf. Solar Cells IC SOLACE*, Cochin Univ. of Technology, Kochi, Kerala, India, 2008, p.16-19.
8. M. Krunks, **A. Katerski**, T. Dedova, I. Oja Acik, A.Mere, Nanostructured solar cell based on spray pyrolysis deposited ZnO nanorod array, *Sol. Energy Mater. Sol. Cells* 92 (2008) 1016-1019.
9. A. Mere, **A. Katerski**, T. Dedova, I. Oja Acik, M. Krunks, Extremely thin absorber layer nanostructured solar cell by chemical spray pyrolysis, *Proceedings 23rd European Photovoltaic Solar Energy Conference* on CD-ROM, Article No. 3.DO.5.1, 23rd EUPVSEC 1-5 Sept. 2008, Valencia, Spain
10. M. Krunks, A. Mere**, A. Katerski**, V. Mikli, J. Krustok, Characterization of sprayed $CuInS_2$ films annealed in hydrogen sulphide atmosphere, *Thin Solid Films*, 511-512 (2006) 434-438.
11. I. Oja, M. Nanu, **A. Katerski**, M. Krunks, A. Mere, J.Raudoja, A. Goossens, Crystal quality studies of $CuInS_2$ films prepared by spray pyrolysis, *Thin Solid Films*, 480-481 (2005) 82-86.

12. A. Mere, **A. Katerski,** O. Kijatkina, M. Krunks, (2004). Solar Cell Structures by Non –Vacuum Techniques Based on Sprayed $CuInS_2$ Absorber Layers. In: *Proceedings of 19-th European Photovoltaic Solar Energy Conference*, Paris, 2004: 19-th European Photovoltaic Solar Energy Conference, Paris, 2004, p. 1973 - 1976.

13. **A. Katerski**, M. Stoev, Photochemical deposition of nanosize CdS layers. E. Balabanova, I. Dragieva (Eds.), *Nanoscience & Nanotechnology'02*, Heron Publishing, Sofia, 2002, p.41 - 42.

14. M. Stoev, A. Amova, **A. Katerski,** Criation of PV solar complexes in Bulgaria, *Balkan Physics Letters*, BPU-4, (2000) 639 - 642.

15. M. Stoev, A. Amova, I. Amov, **A. Katerski,** Analysis of PV data during solar eclipse '99, *Balkan Physics Letters*, BPU-4, (2000) 651 - 654.

16. M. Stoev, **A. Katerski,** R. Stefanov, Surface and thin film analysis of CdTe layers for solar cells, *Vacuum*, 47 (1996) 1231 - 1234.

17. M. Stoev, **A. Katerski**, XPS and XRD Study of Photoconductive CdS Films obtained by a Chemical Bath Deposition Process, *J. Mater. Chem.*, 6 (1996) 377 - 380.

Inventions:

M. Krunks, **A. Katerski**, T. Dedova, A. Mere, I. Oja Acik, Photovoltaic cell based on zinc oxide nanorods and the method for making the same, International patent application WO2009/006910A2 (Priority No. US60/948508, priority date 09.07.2007).

DISSERTATIONS DEFENDED AT TALLINN UNIVERSITY OF TECHNOLOGY ON *NATURAL AND EXACT SCIENCES*

1. **Olav Kongas**. Nonlinear dynamics in modeling cardiac arrhytmias. 1998.

2. **Kalju Vanatalu**. Optimization of processes of microbial biosynthesis of isotopically labeled biomolecules and their complexes. 1999.

3. **Ahto Buldas**. An algebraic approach to the structure of graphs. 1999.

4. **Monika Drews**. A metabolic study of insect cells in batch and continuous culture: application of chemostat and turbidostat to the production of recombinant proteins.1999.

5. **Eola Valdre**. Endothelial-specific regulation of vessel formation: role of receptor tyrosine kinases. 2000.

6. **Kalju Lott**. Doping and defect thermodynamic equilibrium in ZnS. 2000.

7. **Reet Koljak**. Novel fatty acid dioxygenases from the corals *Plexaura homomalla* and *Gersemia fruticosa.* 2001.

8. **Anne Paju**. Asymmetric oxidation of prochiral and racemic ketones by using sharpless catalyst. 2001.

9. **Marko Vendelin**. Cardiac mechanoenergetics *in silico*. 2001.

10. **Pearu Peterson**. Multi-soliton interactions and the inverse problem of wave crest. 2001.

11. **Anne Menert**. Microcalorimetry of anaerobic digestion. 2001.

12. **Toomas Tiivel**. The role of the mitochondrial outer membrane in *in vivo* regulation of respiration in normal heart and skeletal muscle cell. 2002.

13. **Olle Hints**. Ordovician scolecodonts of Estonia and neighbouring areas: taxonomy, distribution, palaeoecology, and application. 2002.

14. **Jaak Nõlvak**. Chitinozoan biostratigrapy in the Ordovician of Baltoscandia. 2002.

15. **Liivi Kluge**. On algebraic structure of pre-operad. 2002.

16. **Jaanus Lass**. Biosignal interpretation: Study of cardiac arrhytmias and electromagnetic field effects on human nervous system. 2002.

17. **Janek Peterson**. Synthesis, structural characterization and modification of PAMAM dendrimers. 2002.

18. **Merike Vaher**. Room temperature ionic liquids as background electrolyte additives in capillary electrophoresis. 2002.

19. **Valdek Mikli**. Electron microscopy and image analysis study of powdered hardmetal materials and optoelectronic thin films. 2003.

20. **Mart Viljus**. The microstructure and properties of fine-grained cermets. 2003.

21. **Signe Kask**. Identification and characterization of dairy-related *Lactobacillus.* 2003.

22. **Tiiu-Mai Laht**. Influence of microstructure of the curd on enzymatic and microbiological processes in Swiss-type cheese. 2003.

23. **Anne Kuusksalu**. 2–5A synthetase in the marine sponge *Geodia cydonium*. 2003.

24. **Sergei Bereznev**. Solar cells based on polycristalline copper-indium chalcogenides and conductive polymers. 2003.

25. **Kadri Kriis**. Asymmetric synthesis of C2-symmetric bimorpholines and their application as chiral ligands in the transfer hydrogenation of aromatic ketones. 2004.

26. **Jekaterina Reut**. Polypyrrole coatings on conducting and insulating substracts. 2004.

27. **Sven Nõmm**. Realization and identification of discrete-time nonlinear systems. 2004.

28. **Olga Kijatkina**. Deposition of copper indium disulphide films by chemical spray pyrolysis. 2004.

29. **Gert Tamberg**. On sampling operators defined by Rogosinski, Hann and Blackman windows. 2004.

30. **Monika Übner**. Interaction of humic substances with metal cations. 2004.

31. **Kaarel Adamberg**. Growth characteristics of non-starter lactic acid bacteria from cheese. 2004.

32. **Imre Vallikivi**. Lipase-catalysed reactions of prostaglandins. 2004.

33. **Merike Peld**. Substituted apatites as sorbents for heavy metals. 2005.

34. **Vitali Syritski**. Study of synthesis and redox switching of polypyrrole and poly(3,4-ethylenedioxythiophene) by using *in-situ* techniques. 2004.

35. **Lee Põllumaa**. Evaluation of ecotoxicological effects related to oil shale industry. 2004.

36. **Riina Aav**. Synthesis of 9,11-secosterols intermediates. 2005.

37. **Andres Braunbrück**. Wave interaction in weakly inhomogeneous materials. 2005.

38. **Robert Kitt**. Generalised scale-invariance in financial time series. 2005.

39. **Juss Pavelson**. Mesoscale physical processes and the related impact on the summer nutrient fields and phytoplankton blooms in the western Gulf of Finland. 2005.

40. **Olari Ilison**. Solitons and solitary waves in media with higher order dispersive and nonlinear effects. 2005.

41. **Maksim Säkki**. Intermittency and long-range structurization of heart rate. 2005.

42. **Enli Kiipli**. Modelling seawater chemistry of the East Baltic Basin in the late Ordovician–Early Silurian. 2005.

43. **Igor Golovtsov**. Modification of conductive properties and processability of polyparaphenylene, polypyrrole and polyaniline. 2005.

44. **Katrin Laos**. Interaction between furcellaran and the globular proteins (bovine serum albumin β-lactoglobulin). 2005.

45. **Arvo Mere**. Structural and electrical properties of spray deposited copper indium disulphide films for solar cells. 2006.

46. **Sille Ehala**. Development and application of various on- and off-line analytical methods for the analysis of bioactive compounds. 2006.

47. **Maria Kulp**. Capillary electrophoretic monitoring of biochemical reaction kinetics. 2006.

48. **Anu Aaspõllu.** Proteinases from *Vipera lebetina* snake venom affecting hemostasis. 2006.

49. **Lyudmila Chekulayeva**. Photosensitized inactivation of tumor cells by porphyrins and chlorins. 2006.

50. **Merle Uudsemaa**. Quantum-chemical modeling of solvated first row transition metal ions. 2006.

51. **Tagli Pitsi**. Nutrition situation of pre-school children in Estonia from 1995 to 2004. 2006.

52. **Angela Ivask**. Luminescent recombinant sensor bacteria for the analysis of bioavailable heavy metals. 2006.

53. **Tiina Lõugas**. Study on physico-chemical properties and some bioactive compounds of sea buckthorn (*Hippophae rhamnoides* L.). 2006.

54. **Kaja Kasemets**. Effect of changing environmental conditions on the fermentative growth of Saccharomyces cerevisae S288C: auxo-accelerostat study. 2006.

55. **Ildar Nisamedtinov**. Application of 13C and fluorescence labeling in metabolic studies of Saccharomyces spp. 2006.

56. **Alar Leibak**. On additive generalisation of Voronoï's theory of perfect forms over algebraic number fields. 2006.

57. **Andri Jagomägi**. Photoluminescence of chalcopyrite tellurides. 2006.

58. **Tõnu Martma**. Application of carbon isotopes to the study of the Ordovician and Silurian of the Baltic. 2006.

59. **Marit Kauk**. Chemical composition of CuInSe 2 monograin powders for solar cell application. 2006.

60. **Julia Kois**. Electrochemical deposition of CuInSe2 thin films for photovoltaic

applications. 2006.

61. **Ilona Oja Açik**. Sol-gel deposition of titanium dioxide films. 2007.

62. **Tiia Anmann**. Integrated and organized cellular bioenergetic systems in heart and brain. 2007.

63. **Katrin Trummal**. Purification, characterization and specificity studies of metalloproteinases from *Vipera lebetina* snake venom. 2007.

64. **Gennadi Lessin**. Biochemical definition of coastal zone using numerical modeling and measurement data. 2007.

65. **Enno Pais**. Inverse problems to determine non-homogeneous degenerate memory kernels in heat flow. 2007.

66. **Maria Borissova**. Capillary electrophoresis on alkylimidazolium salts. 2007.

67. **Karin Valmsen**. Prostaglandin synthesis in the coral *Plexaura homomalla*: control of prostaglandin stereochemistry at carbon 15 by cyclooxygenases. 2007.

46. **Sille Ehala**. Development and application of various on- and off-line analytical methods for the analysis of bioactive compounds. 2006.

47. **Maria Kulp**. Capillary electrophoretic monitoring of biochemical reaction kinetics. 2006.

48. **Anu Aaspõllu.** Proteinases from *Vipera lebetina* snake venom affecting hemostasis. 2006.

49. **Lyudmila Chekulayeva**. Photosensitized inactivation of tumor cells by porphyrins and chlorins. 2006.

50. **Merle Uudsemaa**. Quantum-chemical modeling of solvated first row transition metal ions. 2006.

51. **Tagli Pitsi**. Nutrition situation of pre-school children in Estonia from 1995 to 2004. 2006.

52. **Angela Ivask**. Luminescent recombinant sensor bacteria for the analysis of bioavailable heavy metals. 2006.

53. **Tiina Lõugas**. Study on physico-chemical properties and some bioactive compounds of sea buckthorn (*Hippophae rhamnoides* L.). 2006.

54. **Kaja Kasemets**. Effect of changing environmental conditions on the fermentative growth of Saccharomyces cerevisae S288C: auxo-accelerostat study. 2006.

55. **Ildar Nisamedtinov**. Application of 13C and fluorescence labeling in metabolic studies of Saccharomyces spp. 2006.

56. **Alar Leibak**. On additive generalisation of Voronoï's theory of perfect forms over algebraic number fields. 2006.

57. **Andri Jagomägi**. Photoluminescence of chalcopyrite tellurides. 2006.

58. **Tõnu Martma**. Application of carbon isotopes to the study of the Ordovician

and Silurian of the Baltic. 2006.

59. **Marit Kauk**. Chemical composition of CuInSe 2 monograin powders for solar cell application. 2006.

60. **Julia Kois**. Electrochemical deposition of CuInSe2 thin films for photovoltaic applications. 2006.

61. **Ilona Oja Açik**. Sol-gel deposition of titanium dioxide films. 2007.

62. **Tiia Anmann**. Integrated and organized cellular bioenergetic systems in heart and brain. 2007.

63. **Katrin Trummal**. Purification, characterization and specificity studies of metalloproteinases from *Vipera lebetina* snake venom. 2007.

64. **Gennadi Lessin**. Biochemical definition of coastal zone using numerical modeling and measurement data. 2007.

65. **Enno Pais**. Inverse problems to determine non-homogeneous degenerate memory kernels in heat flow. 2007.

66. **Maria Borissova**. Capillary electrophoresis on alkylimidazolium salts. 2007.

67. **Karin Valmsen**. Prostaglandin synthesis in the coral *Plexaura homomalla*: control of prostaglandin stereochemistry at carbon 15 by cyclooxygenases. 2007.

68. **Kristjan Piirimäe**. Long-term changes of nutrient fluxes in the drainage basin of the gulf of Finland – application of the PolFlow model. 2007.

69. **Tatjana Dedova**. Chemical spray pyrolysis deposition of zinc sulfide thin films and zinc oxide nanostructured layers. 2007.

70. **Katrin Tomson**. Production of labelled recombinant proteins in fed-batch systems in *Escherichia coli*. 2007.

71. **Cecilia Sarmiento**. Suppressors of RNA silencing in plants. 2008.

72. **Vilja Mardla**. Inhibition of platelet aggregation with combination of antiplatelet agents. 2008.

73. **Maie Bachmann**. Effect of Modulated microwave radiation on human resting electroencephalographic signal. 2008.

74. **Dan Hüvonen**. Terahertz spectroscopy of low-dimensional spin systems. 2008.

75. **Ly Villo**. Stereoselective chemoenzymatic synthesis of deoxy sugar esters involving *Candida antarctica* lipase B. 2008.

76. **Johan Anton**. Technology of integrated photoelasticity for residual stress measurement in glass articles of axisymmetric shape. 2008.

77. **Olga Volobujeva**. SEM study of selenization of different thin metallic films. 2008.

78. **Artur Jõgi**. Synthesis of 4'-substituted 2,3'-dideoxynucleoside analogues. 2008.

79. **Mario Kadastik**. Doubly charged Higgs boson decays and implications on neutrino physics. 2008.

80. **Fernando Pérez-Caballero**. Carbon aerogels from 5-methylresorcinol-formaldehyde gels. 2008.

81. **Sirje Vaask**. The comparability, reproducibility and validity of Estonian food consumption surveys. 2008.

82. **Anna Menaker**. Electrosynthesized conducting polymers, polypyrrole and poly(3,4-ethylenedioxythiophene), for molecular imprinting. 2009.

83. **Lauri Ilison**. Solitons and solitary waves in hierarchical Korteweg-de Vries type systems. 2009.

84. **Kaia Ernits**. Study of In2S3 and ZnS thin films deposited by ultrasonic spray pyrolysis and chemical deposition. 2009.

85. **Veljo Sinivee**. Portable spectrometer for ionizing radiation "Gammamapper". 2009.

86. **Jüri Virkepu**. On Lagrange formalism for Lie theory and operadic harmonic oscillator in low dimensions. 2009.

87. **Marko Piirsoo**. Deciphering molecular basis of Schwann cell development. 2009.

88. **Kati Helmja**. Determination of phenolic compounds and their antioxidative capability in plant extracts. 2010.

89. **Merike Sõmera**. Sobemoviruses: genomic organization, potential for recombination and necessity of P1 in systemic infection. 2010.

90. **Kristjan Laes**. Preparation and impedance spectroscopy of hybrid structures based on CuIn3Se5 photoabsorber. 2010.

91. **Kristin Lippur**. Asymmetric synthesis of 2,2'-bimorpholine and its 5,5'-substituted derivatives. 2010.

92. **Merike Luman**. Dialysis dose and nutrition assessment by an optical method. 2010.

93. **Mihhail Berezovski**. Numerical simulation of wave propagation in heterogeneous and microstructured materials. 2010.

94. **Tamara Aid-Pavlidis**. Structure and regulation of BDNF gene. 2010.

95. **Olga Bragina**. The role of Sonic Hedgehog pathway in neuro- and tumorigenesis. 2010.

96. **Merle Randrüüt**. Wave propagation in microstructured solids: solitary and periodic waves. 2010.

97. **Marju Laars**. Asymmetric organocatalytic Michael and aldol reactions mediated by cyclic amines. 2010.

98. **Maarja Grossberg**. Optical properties of multinary semiconductor compounds

for photovoltaic applications. 2010.

99. **Alla Maloverjan**. Vertebrate homologues of Drosophila fused kinase and their role in Sonic Hedgehog signalling pathway. 2010.

100. **Priit Pruunsild**. Neuronal Activity-Dependent Transcription Factors and Regulation of Human *BDNF* Gene. 2010.

101. **Tatjana Knjazeva**. New Approaches in Capillary Electrophoresis for Separation and Study of Proteins. 2011.